Colour information in natural scenes: frequency of metamerism and colour gamut

A thesis submitted to the University of Manchester
for the degree of Doctor of Philosophy
in the Faculty of Engineering and Physical Sciences

2013

By
Gaoyang Feng

Sensing, Imaging, and Signal Processing Group
School of Electrical and Electronic Engineering

List of contents

Final word count: 32398

List of figures

List of tables

Abstract

Colour is an important source of information in the natural world. It can be used for distinguishing and identifying surfaces and objects and separating one region from another. For instance, flowers and grasses in a garden can be distinguished by their colours despite a change in illuminant. Intuitively, the identifiability of surfaces in a scene can be described by their volumes of colour gamuts. But is this approximation of the identifiability accurate? On the other hand, the existence of metamerism in natural scenes shows that colour is sometimes unreliable for surfaces identification. Estimating frequency of metamerism normally requires many comparisons between surface colours to determine their distinguishability under different illuminants. Is there a simpler approach to predict the frequency of metamerism in natural scenes? The aim of this thesis was to address these two questions about the identifiability of surfaces in natural scenes.

To answer the first question, the volumes of colour gamuts were estimated over 50 natural scenes under different illuminants. The logarithm of the gamut volume was regressed on the differential entropy of colours. It was found that gamut volume can be an accurate approximation, given a colour difference threshold representing the visual distinguishability within an approximately perceptually uniform colour space.

To answer the second question, the frequency of metamerism was estimated over 50 natural scenes with changes in illuminant; and predictive models were constructed based on different combinations of Shannon differential entropies of colours. There was strong dependence of the frequency of metamerism on the combination of the differential entropy and the conditional differential entropy of colours. It means that the frequency of metamerism can be predicted by the informational quantities of the colours in a scene.

Declaration

No portion of the work referred to in the thesis has been submitted in support of an application for another degree or qualification of this or any other university or other institute of learning.

Copy right statement

i. The author of this thesis (including any appendices and/or schedules to this thesis) owns certain copyright or related rights in it (the "Copyright") and s/he has given The University of Manchester certain rights to use such Copyright, including for administrative purposes.

ii. Copies of this thesis, either in full or in extracts and whether in hard or electronic copy, may be made only in accordance with the Copyright, Designs and Patents Act 1988 (as amended) and regulations issued under it or, where appropriate, in accordance with licensing agreements which the University has from time to time. This page must form part of any such copies made.

iii. The ownership of certain Copyright, patents, designs, trade marks and other intellectual property (the "Intellectual Property") and any reproductions of copyright works in the thesis, for example graphs and tables ("Reproductions"), which may be described in this thesis, may not be owned by the author and may be owned by third parties. Such Intellectual Property and Reproductions cannot and must not be made available for use without the prior written permission of the owner(s) of the relevant Intellectual Property and/or Reproductions.

iv. Further information on the conditions under which disclosure, publication and commercialisation of this thesis, the Copyright and any Intellectual Property and/or Reproductions described in it may take place is available in the University IP Policy (see http://documents.manchester.ac.uk/DocuInfo.aspx?DocID=487), in any relevant Thesis restriction declarations deposited in the University Library, The University Library's regulations (see http://www.manchester.ac.uk/library/aboutus/regulations) and in The University's policy on Presentation of Theses.

Acknowledgements

I am very grateful to my supervisor Prof. David H. Foster for his continuous support, advice and patience over the course of this project. Many thanks to Dr. Iván Marín-Franch for providing codes and discussions on the subject of information theory. Thanks also to Dr. Kinjiro Amano, who has been so extremely helpful since I started this research. Thanks to Dr. Hujun Yin for his advice and examination for my first and second year research reports. My gratitude is also extended to all the people from the Sensing, Imaging, and Signal Processing Group at the University of Manchester. Thanks to EPSRC for works related to hyperspectral images.

Finally, grateful thanks to my parents Jun and Ci'an, wife Xiao and other family member for their support and encouragement.

Chapter 1. Introduction

Colour is an important source of information in our world. Colour can be used for distinguishing and identifying objects, determining the shapes of objects, and predicting the properties of objects. However, to precisely describe colour is another story. For instance, ‘dark red flower’ and ‘pale green leaf ’ are ambiguous descriptions, which do not offer accurate specification of the particular attributes of these colours: the lightness and the hue. The development of colorimetry [1, 2] provides a tool to numerically quantify individual colours, which is able to tell how ‘dark’ the red flower is. Nevertheless, a single flower does not make a garden. The information supplied by colour such as the identifiability of surfaces contained in a garden as a whole cannot be expressed by the specification of individual colours. Obviously, a naive measurement of this kind of colour information is to count the number of surface colours. But is this method accurate?

One should be aware that colour, as an information source, is not always reliable for surface identification. Two fabrics with the same colour in the shop may appear different when viewed outside. For a given observer, if two colour stimuli with different spectral radiant power distributions match in colour, these colour stimuli are referred to as metamers [3]. The phenomenon of metamerism represents a loss of information in which a generally complex spectral distribution describing lights or reflecting surfaces is reduced typically to three numbers, corresponding to the excitations of the three classes of cone receptors of the normal eye. Is there any alternative method that is capable of predicting the occurrence of metamerism in natural scenes?

This thesis aims to address these two fundamental questions about surfaces in natural scenes, namely, predicting their identifiability by their colour despite differences in illumination.

1.1 Colour vision and colorimetry

Colour is one type of visual perception that can be used to distinguish. Colour vision is referred to as the ability to distinguish the visual stimuli based on wavelength composition regardless of radiance [2, 4, 5]. Colorimetry provides a quantitative framework to specify colour and to measure the difference between colours. In order to study the colour distribution and metamerism in natural scenes, it is useful to briefly review the basic elements of colour vision and colorimetry.

1.1.1 Colour vision

Human colour vision in the natural world is the result of the interactions between light sources, objects and the visual system. Light reflected by surfaces is sampled by the retinal cone photoreceptors in the eye, and the transformed signal is sent to the different cortical areas in the brain. An understanding of the anatomy and physiology of human vision is fundamental for the design and application of colorimetry.

1.1.1.1 Structure of the eye

The structure of the eye limits the visual experience of observers. The cornea is the outermost surface of the eye through which light passes. This transparent curved layer provides most of the optical power. The light passes through the pupil whose size is controlled by the iris. Behind the pupil, the lens alters the optical power by changing its shape for viewing objects at different distances. The cornea and lens function together to project an inverted image on the retina. The retina, which covers most of the interior of the eye, serves much the same function as the film or sensory array in a camera. The extent of the retinal image can be measured by the visual angle, that is, the angle subtended by an object at the optical centre of the eye [6]. The retina provides a very wide field of view for the eye, including a small central area subtending 2 – 3 degrees of visual angle

termed fovea. The fovea has the highest visual acuity owing to the high density of cones receptors (see Chapter 1, Section 1.1.1.2). The fovea is covered by macular pigment which serves as a protective filter. The amount of macular pigment varies markedly between individuals, by a factor of 7 [7]. The blind spot is the area where the optic nerve fibres exit the eye, and where it has no sensitivity to light. The optic nerve transmits the signal to the higher levels of the visual system. Interestingly, the ratio between the number of retinal photoreceptors and the number of optic nerve fibres is believed to be larger than 50 [8, 9]. This compression is achieved partly by decorrelation of spatio-temporal information in the retina [10].

The illumination level influences the size of pupil; the optical density of yellow filters of the lens affects the absorption and scattering; and there are differences in the optical density of the macular pigment, even between left and right eyes of one single observer, which play a significant role in inter-observer variability [11]. Yet, the general colour-distinguishability of ordinary observers is surprisingly similar; as evidenced by the utility of the international standards defined by the CIE and traditional clinical colour-vision tests [12].

1.1.1.2 Sensitivities of the receptors of the eye

There are four classes of photoreceptor cells in the retina, three classes of the cones and one class of the rod, whose names are derived from their prototypical shape. At very low illumination levels, only the rods function and give monochromatic vision. If illumination level is higher, the rods are effectively saturated, and only the cones function [13, 14]. Vision served only by the rods is referred to as scotopic vision. Vision served only by the cones is referred to as photopic vision. Vision served by both the rods and the cones is referred to as mesopic vision. The three types of the cones have broad bandwidth over the visible spectrum, and are referred to as long -, middle-, and short-wavelength-sensitive cones respectively, or simply L, M, and S cones [15, 16]. Figure 1.1 illustrates the spectral sensitivities of the cones [17]. The overlapping spectral

sensitivities of the cones (especially between long- and middle-wavelength-sensitive cones) results in high correlation between cone responses [18].

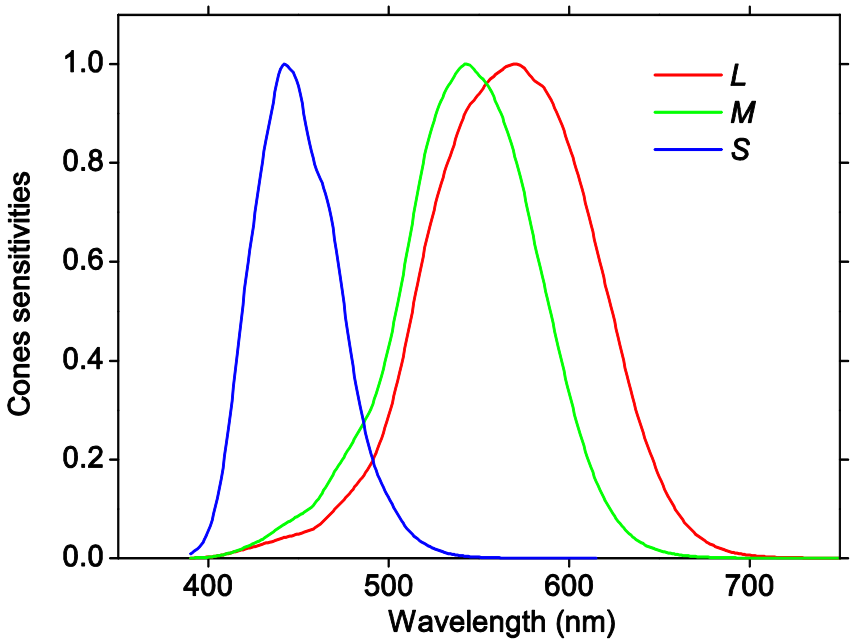

Figure 1.1: Spectral sensitivities of the long-, middle-, and short-wavelength cones, data from [17].

In order to convert radiometric measures, such as radiance, to perceptually relevant quantities, such as luminance, the CIE established two luminous efficiency functions, $V(\lambda)$ for photopic vision and $V'(\lambda)$ for scotopic vision. The luminous efficiency functions are relative weighting functions which define visual 'effectiveness' over wavelength [19, 20]. The function $V'(\lambda)$ is used at low illumination levels for scotopic vision. The function $V(\lambda)$ represents overall sensitivity of the three types of the cone for photopic vision. Figure 1.2 illustrates the CIE luminous efficiency functions $V(\lambda)$ and $V'(\lambda)$ [3] for the standard two degree observer (see Chapter 1, Section 1.1.4.2).

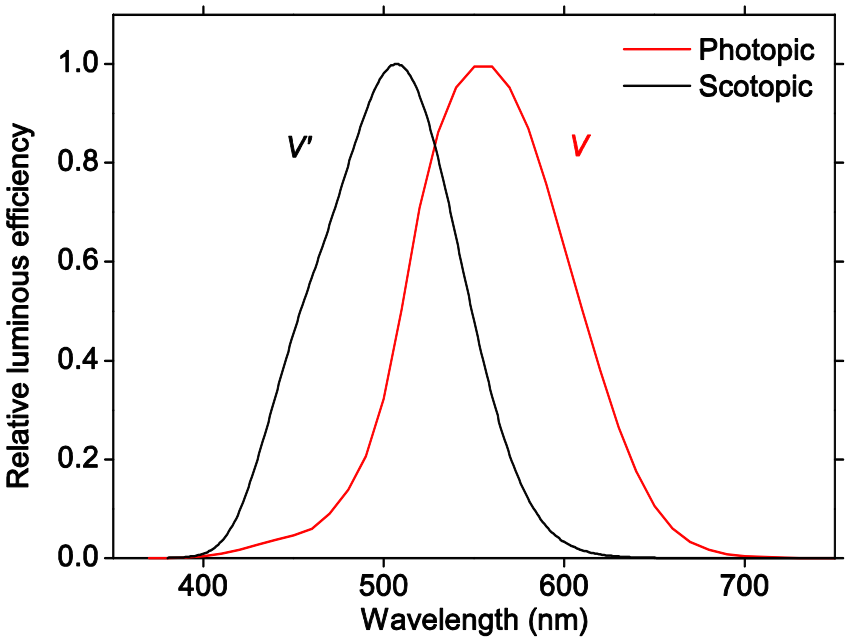

Figure 1.2: The CIE spectral luminous efficiency functions for scotopic $V'(\lambda)$ and photopic $V(\lambda)$ vision, data from [17].

1.1.1.3 Theories of colour vision

In order to explain the function of colour vision, several theories were developed in history.

Trichromatic theory was supported by psychophysical experiments. The assumption of trichromacy was that there are three independent cone types, and the cone signals are transmitted to the brain to generate colour sensations [3, 21]. As shown in Equation 1.1 to 1.3, the responses of the cones are obtained by the integration of the power distribution $\Phi(\lambda)$ of incident light weighted by $\bar{l}(\lambda)$, $\bar{m}(\lambda)$, and $\bar{s}(\lambda)$, the sensitivities of L, M, and S cones over the wavelength range.

$$L = \int_{\lambda} \Phi(\lambda)\bar{l}(\lambda)\mathrm{d}(\lambda), \qquad 1.1$$

$$M = \int_{\lambda} \Phi(\lambda)\bar{m}(\lambda)\mathrm{d}(\lambda), \qquad 1.2$$

$$S = \int_{\lambda} \Phi(\lambda)\bar{s}(\lambda)\mathrm{d}(\lambda). \qquad 1.3$$

This transformation reduces the degrees of freedom of dimension from infinity to three, which leads to a loss of spectral information. The reduction of the degrees of freedom of dimension means that the spectral information can only be retrieved by analysing the responses of the cones. Historically, trichromatic theory was often credited to Young and Helmohltz in the 19th century [3, 22]. And later in 1964, Marks, Dobelle and MacNichol used microspectrophotometry to reveal that there are three classes of the receptors responding maximally to different wavelengths of light [23], confirming the earlier assumption about the existence of the three types of the cones.

Although the trichromatic theory explains the process of distinguishing the spectral stimuli, it cannot explain colour appearance, such as hue, an important perceptual attribute in colour vision. This is because trichromacy only explains the visual coding process at the receptoral level without considering the post-receptor processing. The information from the cones is carried by optic fibres before it reaches the post-receptoral level. As mentioned earlier, the number of photoreceptors is at least 50 times larger than the number of optic nerve fibres. And the overlapping sensitivities of L and M cones results in high correlation between the responses of the cones. The encoding of information in optic fibres is very efficient owing to the decorrelation process [10]. The existence of colour opponent retino-geniculate channels provides the physiological confirmation to opponent and non-opponent coding [4, 24-26]. These opponent channels were also inferred from psychophysical and experiments [27, 28]. The transformation from the cone responses to the opponent colour signals can be modelled by the orthogonal vector model based on electrophysiological studies [28].

Figure 1.3 illustrates the basic processing organisation of colour vision [29]. At the receptoral stage, the light is absorbed by the three classes of cone photoreceptors. For a fixed visual angle and time, the responses of the cones are

univariate, and independent of wavelength. At the post-receptoral stage, the inputs are cone responses, and the outputs can be treated as weighted combination of cone responses. Approximately, the achromatic channel, which is often referred to as the luminance channel, adds the responses from L and M cones. The second channel, which is often referred to as the red-green channel, obtains the difference between weighted responses from L and M cones. And the third channel, which is often referred to as the yellow-blue channel, obtains the difference between weighted responses from S cone and sum of weighted responses from L and M cones [21, 29].

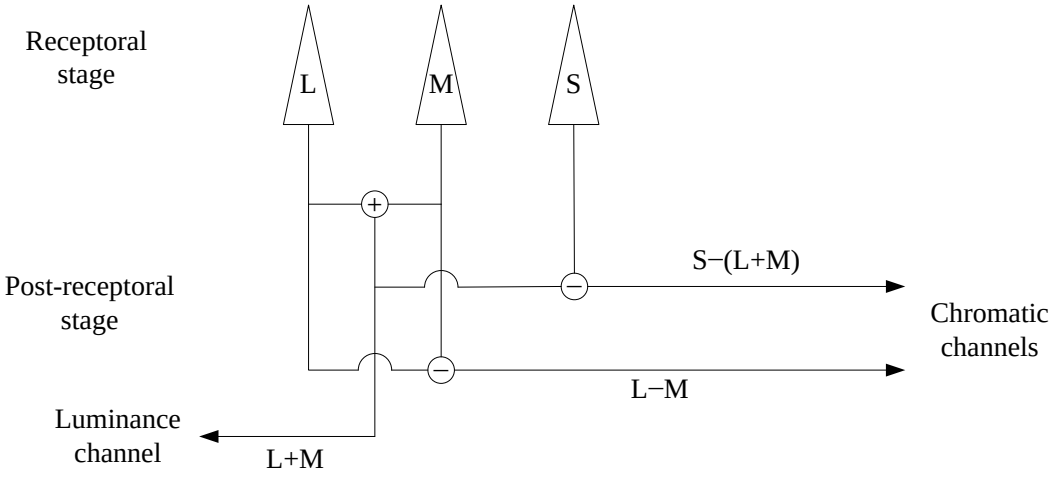

Figure 1.3: Basic illustration of two stage colour coding in human visual system, adapted and modified from [28, 29].

1.1.2 Adaptation mechanisms

The human vision system is not just a static transformation. The dynamic of human vision system allows chromatic and achromatic visual discrimination over a large range of illumination levels, with a ratio of intensities between daily visual extreme over 10^9 [21, 30, 31]. It was also found that the colour distribution in viewing environment can be a potent stimulus for adaptation [32]. The time course of adaptation ranges from milliseconds to weeks, or perhaps even years [33]. The adaptation mechanisms are able to optimize the visual response to the

particular viewing environment by regulating the sensitivities of the photoreceptors.

1.1.2.1 Dark Adaptation

Dark adaptation is caused by the variation of visual sensitivities when the dominant level of illumination immediately decreases. The rods need to improve their sensitivities to outperform the cones after the transition from an extremely high illumination level to complete darkness. It takes on the order of 30 minutes [3, 34] for the rods to reach the maximum sensitivity.

1.1.2.2 Light Adaptation

On the contrary, light adaptation is the opposite process of dark adaptation. Nevertheless, compared to the time of dark adaptation, it only takes approximately 5 minutes for the visual system to reduce the sensitivities to produce clear perceptions. The dynamic range of neurons is nowhere near the wide range of illumination levels. Fortunately, it is very rare to view the entire range of illumination levels at the same time. In any given situation, light adaptation changes the operating range of output range in order to obtain the best possible visual perception.

1.1.2.3 Chromatic Adaptation

The human visual system is capable of remaining preserving the colour appearance against varying illumination [35]. This ability is often referred to as chromatic adaptation which is closely related to colour constancy [36]. An understanding of the mechanisms of chromatic adaptation is essential for the design and applications of colour appearance model (see Chapter 1, Section 1.1.4.6). Chromatic adaptation can be interpreted as largely independent regulating the sensitivities of the cones. It is assumed that there may exist at least two stages of chromatic adaptation: a faster one is about several seconds, a slower one is about one minute. And the chromatic adaptation was believed to be completed within 2 minutes [35, 37].

Generally, the function of the adaptation mechanisms is to make observer less sensitive to the greater change of physical intensities of the stimulus.

1.1.3 Psychophysics of colour vision

Psychophysics is the quantitative study of the relations between physical stimuli and psychological sensations and perceptions that those stimuli evoke. It is the foundation of colorimetry (see Chapter 1, Section 1.1.4). Psychophysical tools allow quantitative measurements of perception and performance which hitherto were often considered subjective.

In psychophysical experiments, decisions of observers are recorded. Basically, there are two types of decision tasks: judgments and adjustments [38]. The idea of threshold and matching in judgments tasks plays an important role in visual experiments. Threshold experiments are used to investigate visual sensitivities to small changes in stimuli which are referred to as a just-noticeable difference. And there are two types of matching experiments: Class A and Class B. Class A observation can be expressed as the identity or non-identity of two sensations. Class B observation only requires responses of a particular aspects of stimuli, generally with additional conditions. For example, the observers might be asked to match the brightness of two patches with different colours [39]. However, it was pointed out that the results of Class B observations are less secure than results of Class A observations [40]. The Class A matching experiments, which determine whether two stimuli are perceptually the same, are the basic tools to investigate the properties of metameric reproduction in a tristimulus system such as CIE (International Commission on Illumination) colorimetry (see Chapter 1, Section 1.1.4).

1.1.4 Colorimetry

Colorimetry offers the numerical specification of the colour of a physically defined visual stimulus [3]. Basic colorimetry predicts colour matching of two visual stimuli in certain viewing conditions. Advanced colorimetry is concerned with colour appearance in various viewing conditions, including colour differences and chromatic adaptation. The CIE colorimetric system is the most

widely used international standard which compromises several metrics. It provides the mathematical foundation for answering the questions raised in this thesis.

1.1.4.1 Trichromatic generalization and tristimulus colour spaces

An empirical generalization of the experimental law of colour matching is referred to as the trichromatic generalization. It states that if there are three fixed primary stimuli whose radiant powers can be adjusted by the observer to suitable levels and none of them can be matched in colour by a mixture of the other two, some colour stimuli can be matched in colour by a mixture of the three fixed primary stimuli; some colour stimuli mixed with one of the primary stimuli can be matched in colour by a mixture of the other two primary stimuli; other colour stimuli mixed with two primary stimuli can be matched in colour by the remaining primary stimulus [3]. The tristimulus values of a colour stimulus are the intensities of the three primary stimuli to match it. Tristimulus space is one of the colour spaces which are based on the trichromatic generalization in order to describe colour stimuli. If the primary stimuli (red, green and blue) of unit amounts are represented by uppercase letters *R*, *G*, and *B*, a colour stimuli match can be achieved under the same conditions in terms of the amounts of three additive primaries as illustrated in Equation 1.4.

$$C \equiv R_C(R) + G_C(G) + B_C(B), \qquad 1.4$$

where the scalar multipliers R_C, G_C and B_C measured in terms of the assigned respective units of the given primary stimuli *R*, *G* and *B* are called the tristimulus values of *C*. As a result, a given colour stimulus defined by a spectral power distribution can be specified by an additive mixture of three primaries [3].

Figure 1.4 illustrates a set of spectral tristimulus values for monochromatic primaries of wavelengths 645 nm, 526 nm, and 444 nm based on data from Stiles and Burch [3]. The tristimulus values over the whole defined spectrum are named ‘colour matching functions’. If other primaries had been used instead, the colour-matching functions obtained would have been different, but linearly related to those of Stiles and Burch [41]. The negative tristimulus values in

Figure 1.4 means the negative contribution of *R* primaries. Adding the primary to the monochromatic light can desaturate it, which leads to a negative tristimulus value.

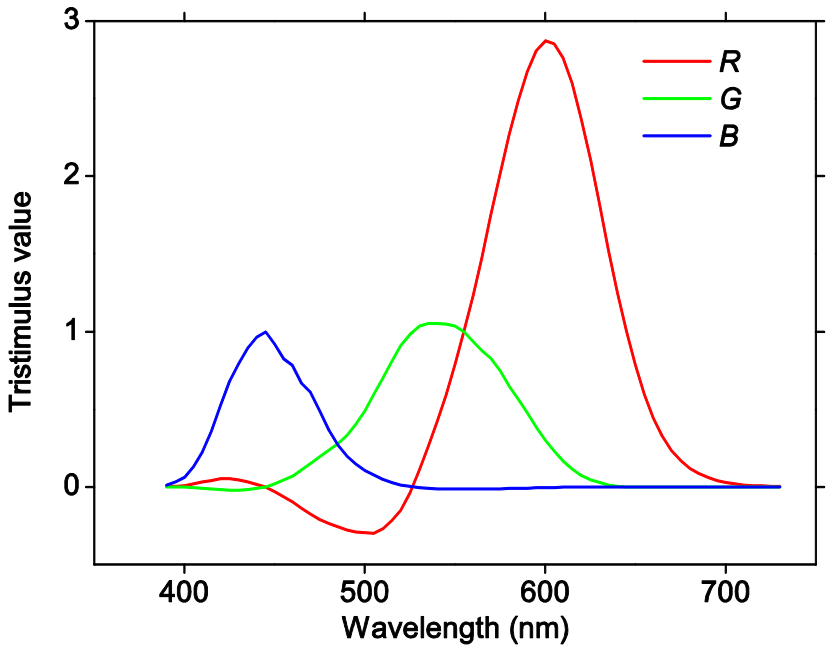

Figure 1.4: Spectral tristimulus values for the CIE RGB system of colorimetry with monochromatic primaries at 645, 526, and 444 nm, data from Stiles and Burch [41].

In a stronger from of the trichromatic generalization, the results of colour matching are assumed to obey linearity laws of additivity and proportionality. Thus, the tristimulus values of a colour stimulus can be obtained by multiplying the colour matching functions by a certain amount of energy in the stimulus at each wavelength and integrating across the spectrum [3]. Given a stimulus with spectral power distribution $\Phi(\lambda)$, the tristimulus values can be calculated from Equations 1.5 to 1.7, where $\bar{r}(\lambda)$, $\bar{g}(\lambda)$ and $\bar{b}(\lambda)$ are the colour matching functions.

$$R = \int_{\lambda} \Phi(\lambda)\bar{r}(\lambda)\mathrm{d}(\lambda), \qquad 1.5$$

$$G = \int_{\lambda} \Phi(\lambda)\bar{g}(\lambda)\mathrm{d}(\lambda), \qquad 1.6$$

$$B = \int_{\lambda} \Phi(\lambda)\bar{b}(\lambda)\mathrm{d}(\lambda). \qquad 1.7$$

The equations for calculating tristimulus values actually show the cause of a common colour phenomenon called metamerism (see Chapter 2 and Chapter 1, Section 1.3). Since two colour stimuli with different spectral power distributions will match if they have equal *R*, *G* and *B* values. Once the spectral power distribution changes, it is likely that the sets of tristimulus values of two stimuli become different.

1.1.4.2 CIE standard observers

Because of the physiological differences among the observers, the colour matching functions of different observers are not the same. It is essential for practical applications to build average colour matching functions of the observers with normal vision. The CIE decided to set standard colour matching functions based on the mean results of the Wright [42] and Guild [43] experiments, with primaries located at 700.0, 546.1 and 435.8 nm. These adopted primaries were accurately reproducible during that time, because wavelengths 546.1 and 435.8 nm are mercury excitation lines and 700.0 nm is the location where the change in wavelength barely affects the hue of spectral lights [44]. In order to achieve convenience with non-negative computation and coherence with the CIE 1924 photopic luminous efficiency function $V(\lambda)$, the CIE issued a linearly transformed set of primaries, the so-called XYZ primaries. These imaginary tristimulus values and the corresponding colour matching functions were standardized in the CIE 1931 Standard Colorimetric Observer [12]. The original colour matching functions were defined in the wavelength range λ = 380 to 780 nm at intervals of $\Delta\lambda$ = 5 nm. In 1971, the CIE complemented the CIE 1931 Standard Colorimetric Observer with interpolated values at 1 nm intervals and range λ = 360 to 830 nm, illustrated in Figure 1.5.

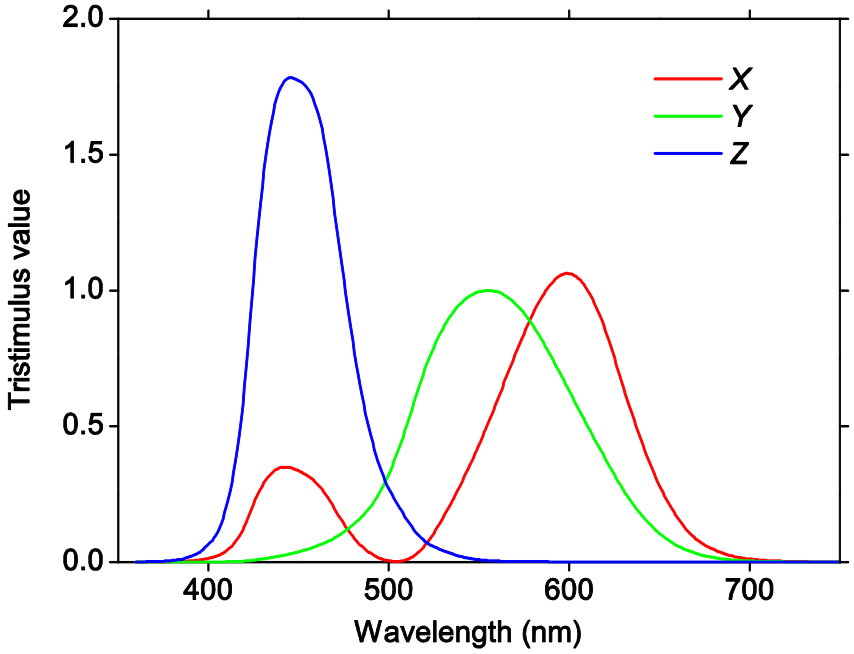

Figure 1.5: Spectral tristimulus values of the CIE 1931 standard two degree colorimetric observer.

In order to eliminate the influence of rod vision, the colour-matching experiments for standard observers were obtained with matching fields of two degrees angular subtense [3]. The colour matching functions (Equations 1.8 to 1.10) of CIEXYZ system follow the same form as those of RGB system, where $\bar{x}(\lambda)$, $\bar{y}(\lambda)$, and $\bar{z}(\lambda)$ are colour matching functions; k is a constant which is chosen for computational convenience according to the different application.

$$X = k\int_{\lambda} \Phi(\lambda)\bar{x}(\lambda)\mathrm{d}(\lambda), \qquad 1.8$$

$$Y = k\int_{\lambda} \Phi(\lambda)\bar{y}(\lambda)\mathrm{d}(\lambda), \qquad 1.9$$

$$Z = k\int_{\lambda} \Phi(\lambda)\bar{z}(\lambda)\mathrm{d}(\lambda), \qquad 1.10$$

In 1964, new supplement colour-matching functions were recommended by the CIE (illustrated in Figure 1.6). These functions are used when colour matching experiments are conducted with fields of 10 degrees which is named as the CIE 1964 Supplementary Standard Colorimetric Observer [3].

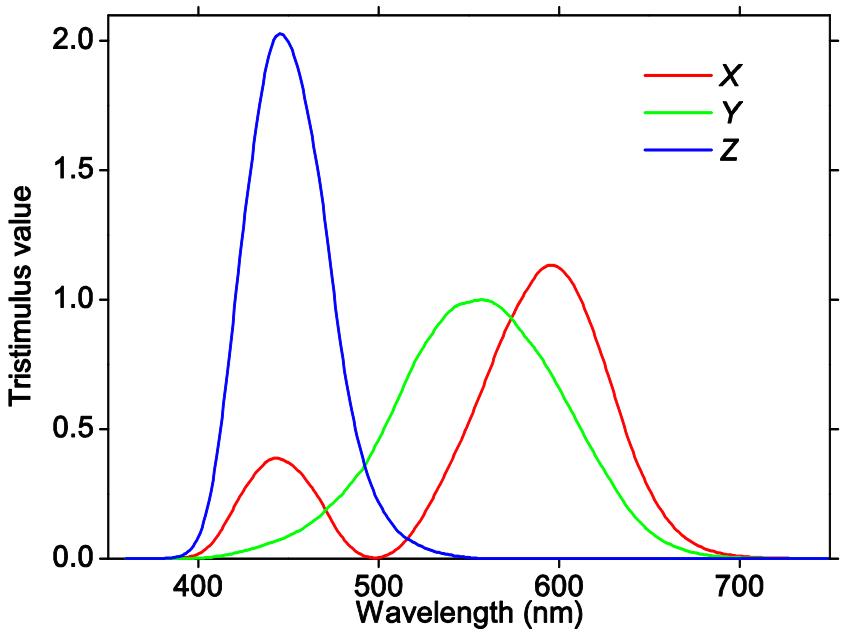

Figure 1.6: Spectral tristimulus values of the CIE 1931 standard ten-degree colorimetric observer.

It should be emphasized that the most recent version of the CIEXYZ colour matching functions [45] are a linear transformation of the human cone spectral sensitivities measured by Stockman, Sharpe and Fach [15, 16]. Stockman, Sharpe and Fach measured the short-wavelength cone spectral sensitivity by measuring S-cone thresholds centrally and peripherally in five trichromats and three blue-cone monochromats (who lack functioning L- and M- cones) [16]. Subsequently, Stockman and Sharpe measured the spectral sensitivities of L- and M-cones by testing dichromats of known genotype: M-cone sensitivities in nine protanopes (who are missing L-cone function), and L-cone sensitivities in 20 deuteranopes (who are missing M-cone function) [15]. These measurements and re-analysis of

the original 10 degrees Stiles and Birch data, were later incorporated by the CIE into the CIE colour-matching functions [45].

1.1.4.3 CIE standard illuminants

There would be no colour at all without light. The CIE specified the light with two terms: light source and illuminant. A source refers to a physical emitter of radiant power and an illuminant refers to a specific spectral radiant power distribution incident on the object viewed by the observer [3]. The CIE standardized illuminants and sources can be identified by using correlated colour temperature (CCT). Correlated colour temperature is defined as the absolute temperature of a Planckian radiator whose chromaticity is located nearest to the chromaticity of the given spectral distribution. Because of the importance of daylights in natural scenes, different phases of daylights were simulated in this thesis by using the CIE standard daylight illuminants D. The relative spectral power distribution of the CIE daylight illuminant D65 over the visual spectrum is shown in Figure 1.7, which is intended to represent the average daylight.

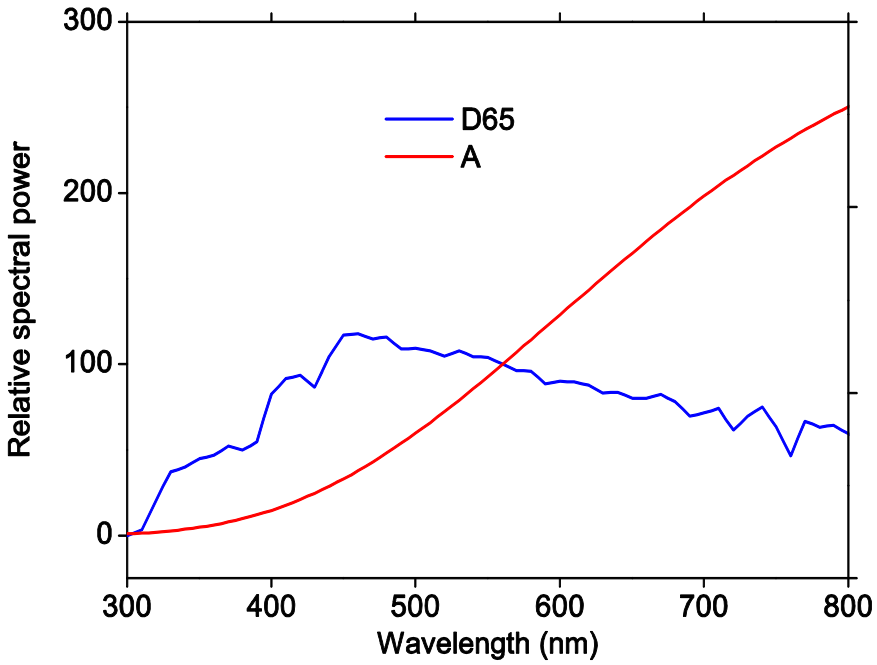

Figure 1.7: Relative spectral power distributions of the CIE standard illuminants D65 and A (tungsten-filament lighting) [3, 46].

1.1.4.4 Chromatic-adaptation models

The human visual system is able to adapt to moderate changes in the spectrum of the illumination, so that the colour appearance remains approximately constant. This phenomenon is generally referred to as colour constancy [36]. The mechanisms of chromatic adaptation may be the most likely source for discounting the changes in the illumination. The mechanisms of chromatic adaptation can be classified as two types: sensory and cognitive [35, 47]. And most theories and models of sensory mechanisms are based on the work of von Kries [3].

The hypotheses of Johannes von Kries [3] are interpreted nowadays that three types of cone responses adapt independently and linearly, as expressed in Equation 1.11.

$$\begin{bmatrix} L_{\mathrm{a}} \\ M_{\mathrm{a}} \\ S_{\mathrm{a}} \end{bmatrix} = \begin{bmatrix} K_L & 0 & 0 \\ 0 & K_M & 0 \\ 0 & 0 & K_S \end{bmatrix} \begin{bmatrix} L \\ M \\ S \end{bmatrix}, \qquad 1.11$$

where L, M and S represent the original cone responses; K_L, K_M and K_S are the scaling coefficients; L_{a}, M_{a} and S_{a} represent the post-adaptation cone responses. In practice, the scaling coefficients are generally taken to be the inverse of the white or the maximum stimuli value of L, M and S responses, respectively. Despite their simplicity, these hypotheses are still capable of explaining the majority of chromatic-adaptation effects. Indeed, independent adjustment of multiplicative coefficients is a feature of most theories of colour constancy [48, 49]. The sensor transformations developed by Finlayson et al., which narrow the band of sensitivities of receptor over the wavelengths, improved the performance of colour constancy [50, 51]. An enhanced version of the von Kries model is the Retinex Theory, which takes the spatial distribution into consideration [48, 49]. The non-linear Nayatani model is able to predict the state of incomplete adaptation [52]. And this model can also predict several additional effects such as the Hunt effect, Steven effect and Helson-Judd effect [53].

1.1.4.5 Colour differences and uniform colour spaces

The aim of basic colorimetry is to predict the match between two colour stimuli. If two colours are different, what is the magnitude of the difference? The CIELAB system was initially designed to be a perceptually uniform colour space [54], which means that the colour difference between two stimuli located anywhere in the space is measured by the Euclidean distance between them. The full transformation from CIEXYZ to CIELAB is given in Equations 1.12 to 1.14, where X, Y and Z are the set of tristimulus values of one colour stimulus and X_n, Y_n and Z_n represent the reference white.

$$L^* = 116\, f(Y / Y_n) - 16, \qquad 1.12$$

$$a^* = 500[\, f(X / X_n) - f(Y / Y_n)], \qquad 1.13$$

$$b^* = 200[\, f(Y / Y_n) - f(Z / Z_n)], \qquad 1.14$$

where

$$f(\omega) = \left\{ \begin{array}{c} (\omega)^{1/3}, \, if\, \omega > (24/116)^{1/3} \\ (841/108)(\omega) + 16/116, \, if\, \omega < (24/116)^{1/3} \end{array} \right\}. \qquad 1.15$$

One should be aware that CIELAB does not include real von Kries scaling, because the CIEXYZ tristimulus values are not transformed to cone responses at any stage. This modified version of von Kries scaling results in a failure of prediction of colour appearance (e.g. gemstone tanzanite upon changes of illumination [55]). The poor blue constancy within CIELAB colour space has also been of concern [56]. As shown in Figure 1.8, the lines of constant hue of OSA uniform colour scales [57, 58] shift from blue to purple when the chroma is decreased.

In order to improve the perceptual uniformity available with CIELAB [59], additional colour difference equations such as CMC(l:c) [60] and BFD(l:c) [61, 62] were introduced in place of the Euclidean distance. The CIE recommended

CIE94 [63] and CIEDE2000 [64] for industrial use. The CIEDE2000 colour difference equation is given in Equation 1.16.

$$\Delta E_{00} = \sqrt{(\frac{\Delta L'}{k_L S_L})^2 + (\frac{\Delta C'}{k_C S_C})^2 + (\frac{\Delta H'}{k_H S_H})^2 + R_T(\frac{\Delta C'}{k_C S_C})^2(\frac{\Delta H'}{k_H S_H})^2}, \quad 1.16$$

where $\Delta L'$, $\Delta C'$ and $\Delta H'$ are referred to as the lightness, chroma, and hue differences, respectively; k_L, k_C, k_H are parametric factors based on different applications; S_L, S_C, S_H are lightness-, chroma-, and hue-dependent weighting functions, respectively; and R_T is an additional function that improves the performance of fitting chromatic differences in blue region [64].

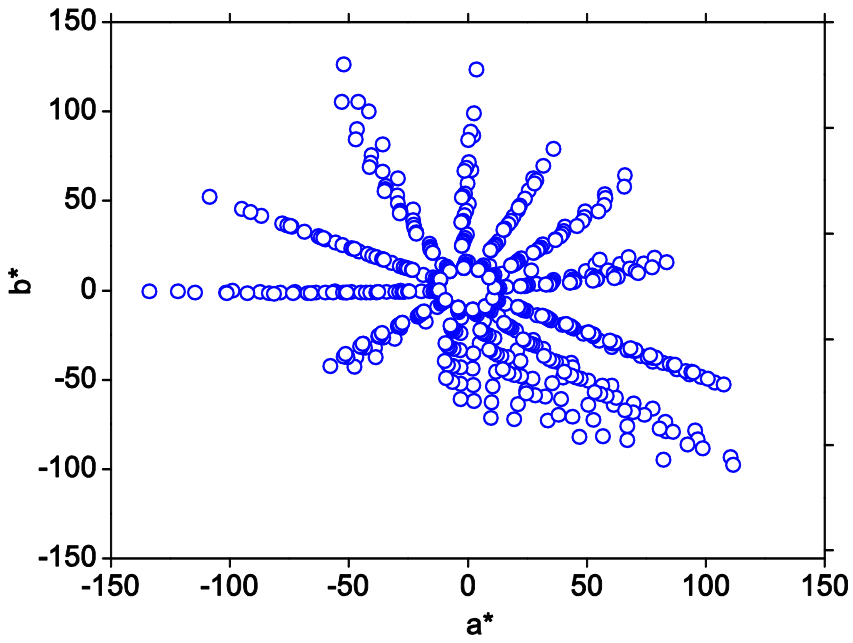

Figure 1.8: Radial sampling of OSA uniform colour scales within the CIELAB.

1.1.4.6 Colour-appearance models

Colour-appearance models offer a more comprehensive description of colour stimuli, including the prediction of lightness, chroma and hue, and effects of chromatic adaptation. CIECAM02 [65] is a colour-appearance model recommended by CIE after CIECAM97s [66]. Unlike CIECAM97s, a von Kries-

type chromatic-adaptation transform (Equations 1.20 to 1.22) is incorporated in CIECAM02, which can be compared with Equation 1.11. CIECAM02 simplifies the computation and allows for an analytical inverse model. The forward model which transforms CIECXYZ tristimulus values to colour-appearance attributes in CIECAM02 is given as follows [65].

Step 1: Convert CIEXYZ tristimulus values to long, middle and short-wavelength space.

$$\begin{bmatrix} R \\ G \\ B \end{bmatrix} = \mathbf{M}_{\text{CAT02}} \begin{bmatrix} X \\ Y \\ Z \end{bmatrix}, \tag{1.17}$$

where

$$\mathbf{M}_{\text{CAT02}} = \begin{bmatrix} 0.7328 & 0.4296 & -0.1624 \\ -0.7036 & 1.6975 & 0.0061 \\ 0.0030 & 0.0136 & 0.9834 \end{bmatrix}. \tag{1.18}$$

Step 2: Decide degree of adaptation and apply it to chromatic adaptation.

$$D = F\left[1 - (\frac{1}{3.6})e^{(\frac{-(L_{\text{A}}+42)}{92})}\right], \tag{1.19}$$

where L_{A} is the luminance of adapting field,

$$R_{\text{C}} = [(Y_{\text{W}} D / R_{\text{W}}) + (1 - D)]R, \tag{1.20}$$

$$G_{\text{C}} = [(Y_{\text{W}} D / G_{\text{W}}) + (1 - D)]G, \tag{1.21}$$

$$B_{\text{C}} = [(Y_{\text{W}} D / B_{\text{W}}) + (1 - D)]B, \tag{1.22}$$

where R_{W}, G_{W} and B_{W} are the cone responses of adapting white reference [67]; and Y_{W} is the Y tristimulus value of white reference, which is normally 100 if white reference is a perfect reflecting diffuser.

Step3: Compute parameters of viewing conditions

$$k = 1/(5L_{\mathrm{A}} + 1), \tag{1.23}$$

$$F_{\mathrm{L}} = 0.2k^4(5L_{\mathrm{A}}) + 0.1(1 - k^4)^2(5L_{\mathrm{A}})^{1/3}, \tag{1.24}$$

$$n = Y_{\mathrm{b}} / Y_{\mathrm{w}}, \tag{1.25}$$

where Y_{b} is background luminance,

$$N_{\mathrm{bb}} = N_{\mathrm{cb}} = 0.725(1/n)^{0.2}, \tag{1.26}$$

$$z = 1.48 + \sqrt{n}. \tag{1.27}$$

Step4: Convert to Hunt-Pointer-Estevez space, which is closer to cone sensitivities.

$$\begin{bmatrix} R' \\ G' \\ B' \end{bmatrix} = \mathbf{M}_{\mathrm{HPE}} \mathbf{M}_{\mathrm{CAT02}}^{-1} \begin{bmatrix} R_{\mathrm{C}} \\ G_{\mathrm{C}} \\ B_{\mathrm{C}} \end{bmatrix}, \tag{1.28}$$

where

$$\mathbf{M}_{\mathrm{HPE}} = \begin{bmatrix} 0.38971 & 0.68898 & -0.07868 \\ -0.22981 & 1.18340 & 0.04641 \\ 0.00000 & 0.00000 & 1.00000 \end{bmatrix}, \tag{1.29}$$

$$\mathbf{M}_{\mathrm{CAT02}}^{-1} = \begin{bmatrix} 1.096124 & -0.278869 & 0.182745 \\ 0.454369 & 0.473533 & 0.072098 \\ -0.009628 & -0.005698 & 1.015326 \end{bmatrix}. \tag{1.30}$$

Step5: Apply post-adaptation non-linear compression

$$R'_{\mathrm{a}} = \frac{400(F_{\mathrm{L}} R'/100)^{0.42}}{27.13 + (F_{\mathrm{L}} R'/100)^{0.42}} + 0.1, \tag{1.31}$$

$$G'_{\mathrm{a}} = \frac{400(F_{\mathrm{L}} G'/100)^{0.42}}{27.13 + (F_{\mathrm{L}} G'/100)^{0.42}} + 0.1, \tag{1.32}$$

$$B'_{\mathrm{a}} = \frac{400(F_{\mathrm{L}} B'/100)^{0.42}}{27.13 + (F_{\mathrm{L}} B'/100)^{0.42}} + 0.1. \tag{1.33}$$

If any of R', G' or B' is negative, then the corresponding absolute values must be used, and then the quotient term must be multiplied by −1.

Step6: Create opponent-colour responses.

$$a = R'_{\mathrm{a}} - 12G'_{\mathrm{a}}/11 + B'_{\mathrm{a}}/11, \tag{1.34}$$

$$b = (1/9)(R'_{\mathrm{a}} + G'_{\mathrm{a}} - 2B'_{\mathrm{a}}). \tag{1.35}$$

Step7: Calculate the attributes.

Hue

$$h = \tan^{-1}(b/a). \tag{1.36}$$

Eccentricity factor

$$e_{\mathrm{t}} = \frac{1}{4}[\cos(h\frac{\pi}{180} + 2) + 3.8]. \tag{1.37}$$

Achromatic response

$$A = [2R'_{\mathrm{a}} + G'_{\mathrm{a}} + (1/20)B'_{\mathrm{a}} - 0.305]N_{\mathrm{bb}}. \tag{1.38}$$

Lightness

$$J = 100(A/A_{\mathrm{W}})^{cz}, \tag{1.39}$$

where c is the surround factor.

Brightness

$$Q = (4/c)\sqrt{J/100}(A_{\mathrm{W}} + 4)F_{\mathrm{L}}^{\ 0.25}. \tag{1.40}$$

Chroma

$$C = t^{0.9}\sqrt{J/100}(1.64 - 0.29^{n})^{0.73}, \tag{1.41}$$

where

$$t = \frac{(50000/13) N_{cb} N_{bb} e_t \sqrt{a^2 + b^2}}{R'_a + G'_a + (21/20) B'_a}. \quad 1.42$$

Colourfulness

$$M = C F_L^{0.25}. \quad 1.43$$

Saturation

$$s = 100\sqrt{M/Q}. \quad 1.44$$

Cartesian coordinates

$$a_C = C\cos(h), \quad 1.45$$

$$b_C = C\sin(h), \quad 1.46$$

$$a_M = M\cos(h), \quad 1.47$$

$$b_M = M\sin(h), \quad 1.48$$

$$a_S = S\cos(h), \quad 1.49$$

$$a_S = S\sin(h). \quad 1.50$$

CIECAM02 includes a more comprehensive description of the viewing conditions than colour spaces such as CIELAB and CIELUV. It can also predict certain luminance-dependent effects and incomplete adaptation. Although the colour uniformity is not the specified objective of CIECAM02, Moroney and Zeng showed the significant improvement of hue uniformity for CIECAM02 relative to CIELAB, especially for blue hues [68]. CIECAM02 also performs reasonably [69] compared to other uniform colour spaces such as DIN99 [70].

1.2 Hyperspectral imaging

1.2.1 Hyperspectral image acquisition

Hyperspectral imaging systems have higher spectral resolution over the spectrum than conventional three-sensory RGB colour camera. As mentioned earlier, colour in natural scenes is a result of the interaction between light sources, objects and vision systems. The spectrally fine-grained hyperspectral images allow a more accurate estimation of spectral reflectances of object surfaces. In order to investigate colour distribution and metamerism of object surfaces in natural scenes, a dataset of 50 hyperspectral images [71, 72] was used for most simulations in this thesis.

The hyperspectral images were acquired with a low-noise Peltier-cooled digital camera with spatial resolution of 1344 × 1024 pixels. A fast tuneable liquid-crystal filter was mounted in front of the lens with an infrared blocking filter in order to select specific wavelengths of light. The exposure time at each wavelength was chosen by software so that maximum pixel output was within 86% to 90% of the saturation value of CCD (charge-coupled device). The raw images were corrected for dark noise, spatial non-uniformities, stray light, and any wavelength-dependent variations in magnification or translation. The spectrum of light reflected from a small reference surface (Munsell N5 or N7) in the scene was recorded with a telespectroradiometer. The estimated effective spectral reflectance at each pixel was obtained by normalizing the corrected signal against the signal reflected from the reference surface. The line-spread function of the hyperspectral imaging system was close to Gaussian with standard deviation of ≈ 1.3 pixels at 550 nm. In order to exclude the trivial correlation between pixels, adjacent pixels were discarded in the samples. Thus, hyperspectral images used in the simulations were within a size of 672 x 512 pixels after the down-sampling [71].

In total, there were 29 scenes categorized as predominantly vegetated, and 21 scenes categorized as predominantly non-vegetated [73, 74]. All visible sky and other self-luminous regions or objects were excluded. Each hyperspectral image

of one scene had spectral range from 400 nm to 720 nm sampled at 10 nm intervals.

1.2.2 Conversion of hyperspectral images to tristimulus images

The CIEXYZ tristimulus values can be calculated by integrating spectral power data with colour-matching functions as weighting functions [75]. Given a certain observer and an illuminant, the tristimulus values can be calculated from Equation 1.51 to 1.53.

$$X = \int \bar{x}(\lambda) e(\lambda) r(\lambda; x, y) \, \mathrm{d}\lambda, \tag{1.51}$$

$$Y = \int \bar{y}(\lambda) e(\lambda) r(\lambda; x, y) \, \mathrm{d}\lambda, \tag{1.52}$$

$$Z = \int \bar{z}(\lambda) e(\lambda) r(\lambda; x, y) \, \mathrm{d}\lambda. \tag{1.53}$$

where $r(\lambda)$ is the reflectance of the surface; $\bar{x}(\lambda)$, $\bar{y}(\lambda)$ and $\bar{z}(\lambda)$ are the colour-matching functions of the observer; and $e(\lambda)$ is the illuminant spectrum on the reflected surface. Compared with Equation 1.8 to 1.10, the spectral power distribution $\Phi(\lambda)$ of a stimulus is replaced by a product of spectral reflectance $r(\lambda)$ and illuminant $e(\lambda)$.

1.3 Metamerism

Physically, a colour stimulus has complex spectral power distribution over the whole visible wavelength. But the eye only has three classes of the cone receptors. The reduction in dimensions makes it possible for two colour stimuli with different spectral power distributions to match each other in colour. If two colours with different spectral power distributions match each other, they are metamers [3, 75]. Metamerism in natural scenes is of interest since this phenomenon suggests the failure of surfaces identification by using colours in real world. Given two illuminants, the frequency of metamerism in each scene

under these two illuminants is defined by the ratio between the number of metameric pairs and the number of all possible pairs. With the same situation, the relative frequency of metamerism is defined by the ratio between the number of metameric pairs and the number of indistinguishable pairs under one of the given illuminants. More technical details will be given in Chapter 2.

1.4 Why information theory?

Thanks to colorimetry, within colour spaces the numeric specification of colours makes it possible to further measure the colour gamut of surface colours in natural scenes and to determine the metamers. Nevertheless, the questions raised at the beginning of this thesis are still unanswered.

Information theory supplies a mechanism to measure information objectively and quantitatively. Quantities derived from information theory such as entropy, relative entropy, and mutual information [76] are defined as functionals of probability distributions [77]. Entropy can be used as a measure of relative amount of trichromatic information of a image, which is obtained from a scene under a particular illuminant. Relative entropy and mutual information can detect general dependency between trichromatic images obtained from the same scene but under different illuminants.

Colour gamut sometimes were used to describe the volume of colour content of an image obtained from a natural scene, but the distribution of surface colours was ignored when using this method. To compare the colour information of different images by using the corresponding colour gamut is not mathematically justifiable. In a perceptually uniform colour space, this comparison can be justified by using the entropy of trichromatic images.

From an engineering point of view, the process of colour coding in colour vision can be treated as a type of communication. Thus, metamerism (see Chapter 2) can be interpreted as a mismatch between senders and receivers in a communication network. Indeed, the phenomenon of metamerism represents a loss of information, as explained in Chapter 6.

The definition of entropy, relative entropy and mutual information of discrete random variables are given in this section. More details of differential entropy and mutual information and their application on trichromatic images will be revealed in Chapter 3.

1.4.1 Entropy

The entropy of a discrete random variable *X*, which is a measure of the uncertainty of the random variable *X*, is defined as

$$H(X) = -\sum_{x \in X} p(x) \log p(x). \qquad 1.54$$

where $p(x)$ is the probability mass function. Entropy is expressed in bits if the logarithm is to the base 2, and in nats if the logarithm is to the base e. Note the convention is that $0 \log 0 = 0$, which is justified by continuity because $x \log x \to 0$ as $x \to 0$ [77]. If a pair of discrete random variables (*X*, *Y*) is considered to be a single vector random variable with a joint distribution $p(x, y)$, the joint entropy can be defined as

$$H(X,Y) = -\sum_{x \in X} \sum_{y \in Y} p(x, y) \log p(x, y). \qquad 1.55$$

Similarly, the conditional entropy of a random variable *Y* given another random variable *X* is defined as,

$$H(Y \mid X) = -\sum_{x \in X} \sum_{y \in Y} p(x, y) \log p(y \mid x). \qquad 1.56$$

1.4.2 Mutual information

The joint entropy of a pair of random variables is a measure of the amount of information required on average to describe the pair of random variables. On the other hand, the relative entropy is a measure of the relationship between the two distributions. The relative entropy [77] between two probability mass functions $p(x)$ and $q(x)$ is defined as

$$D(p \| q) = \sum_{x \in X} p(x) \log \frac{p(x)}{q(x)}. \qquad 1.57$$

Mutual information [77] between random variable X and Y, can be defined as $D((p(x,y) \| p(x)p(y))$, the relative entropy between the joint distribution $p(x,y)$ and the product distribution $p(x)p(y)$:

$$I(X;Y) = \sum_{x \in X} \sum_{y \in Y} p(x,y) \log \frac{p(x,y)}{p(x)p(y)}. \qquad 1.58$$

Mutual information [77] between random variables X and Y, is the reduction in the uncertainty of one random variable caused by knowing the other variable, which can also be defined as

$$I(X;Y) = H(X) - H(X \mid Y) = H(Y) - H(Y \mid X). \qquad 1.59$$

The relationship between entropy, relative entropy, and mutual information may be illustrated in a Venn diagram [77].

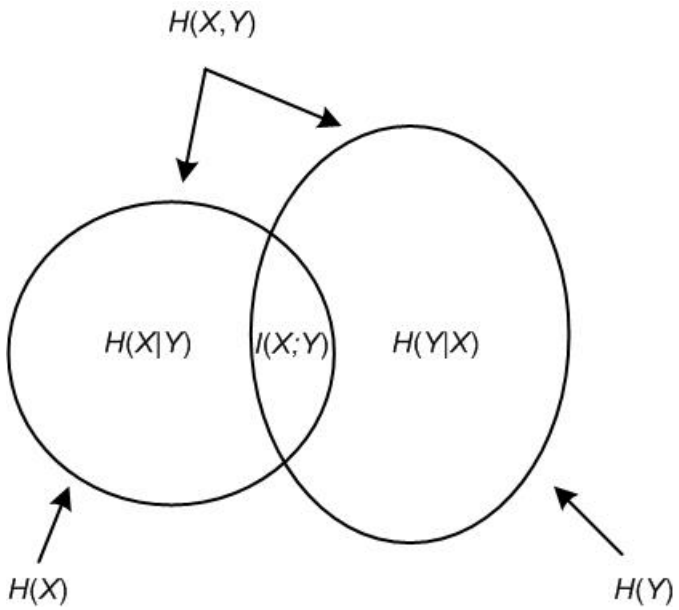

Figure 1.9 Relationship between entropy and mutual information, adapted from [77].

1.5 Objectives

The objectives of this thesis are as follows:

- To construct models for predicting the frequency/conditional frequency of metamerism in natural scenes by information-theoretic measurements.

- To determine whether colour gamut is a good description of the distribution of surface colours in natural scenes.

- To determine the number of basis functions to represent the spectral reflectances of surfaces in natural scenes, and to explore spectral features of observed metamers in natural scenes.

1.6 Thesis structure

The remainder of this thesis is organized as follows.

Chapter 2 Metamerism and frequency of metamerism. A further review of previous work on metamerism and frequency of metamerism is reviewed here, including the terminology of metamerism, the CIE indices of metamerism, and previous research on frequency of metamerism.

Chapter 3 Information-theoretic measurements of colours. To quantify the information content of colours is not straightforward. The literature on estimating differential entropy with limited number of samples is considered at first. Second, the method to obtain entropy and mutual information from trichromatic images is revealed. Last, the robustness of this method is examined.

Chapter 4 Measurements of colour gamut of natural scenes. The volume of the colour gamut of natural scenes may be treated as an approximate description of the information content of colours. Convex hull algorithms and cube-counting algorithms were used to measure the volume of the colour gamut. It turned out

that given certain colour difference thresholds, volumes measured by a cube-counting algorithm within the colour space CIECAM02 is a quite good description information content.

Chapter 5 Exploratory analysis of reflectances in natural scenes. Spectral reflectance, rather than colour, is a reliable property for identifying surfaces. The statistical properties of spectral reflectances in natural scenes are analyzed in this chapter. Reflectances of metamers are analyzed for both synthetic and real surfaces data.

Chapter 6 Predicting frequency of metamerism. Estimating the frequency of metamerism usually requires numerous comparisons between the colour appearance of surfaces under different illuminants. Information-theoretic measurements were used instead to predict the frequency of metamerism over 50 natural scenes under two different illuminants.

Chapter 7 Conclusion. Salient results and contribution are recalled in this chapter with potential research on different subjects suggested.

Chapter 8 Appendix. Technical details of the simulations and analysis are set out in this chapter including the parameters of transformations from CIEXYZ colour space to CIELAB colour space and CIECAM02 colour space.

Chapter 2. Metamerism and frequency of metamerism

The phenomenon of metamerism is of importance in practice because the match between metameric colours could disappear if one of the viewing conditions is changed [54]. Metameric matches can be upset by a change in illuminant, a change in field size, and a change in observer. Metamerism associated with reflecting surfaces is particularly important [75], not least because it concerns the foundations of camouflage [78] and the relationship between visual and material identity in the natural world [71]. The existence of metamerism means that surface colours may be unreliable for identifying objects. A mismatch between metameric colours affects colour reproduction in industries such as printing, dyeing, photography and digital imaging.

In this chapter, the technical terms of metamerism are reviewed, followed by an application of the method of estimating the relative frequency of metamerism that was first described in [71].

2.1 Definitions of metamerism

By definition, metameric stimuli appear the same in colour although they have different spectral power distributions [3]. In colorimetric terms, spectral power distributions of metameric stimuli produce the same tristimulus values when weighted by the CIE colour matching functions (See Equations 1.8 to 1.10 in Chapter 1, Section 1.1.4.2) [75].

2.1.1 Terminology

There are several different interpretations of metamerism in the literature, which are not all endorsed by the CIE. In order to clarify, the explanations of these terms are given as follows.

1. Metameric colour stimuli, metamers
   Colour stimuli with different spectral power distributions that have the equal tristimulus values. The corresponding concept is metamerism. The practical problem is that as the representation of physical quantities, tristimulus values are never likely to coincide exactly.
2. Perceived metameric colour stimuli, perceived metamers
   Colour stimuli with different spectral power distributions that match each other visually for a particular real observer under specified viewing conditions. This interpretation circumvents the problem described in (1), but a threshold level or statistical equivalent needs also to be defined.
3. Parameric colour stimuli, paramers
   Colour stimuli with different spectral power distributions that have nearly the same tristimulus values. The corresponding concept is paramerism. Technically, there is no difference between paramerism and perceived metamerism. The word ‘parameric’ is often used for parameric correction [79].

As a practical approach to the problem defined in (1), that is, because it is not very often that two colours have the same tristimulus values, a visual match between colour stimuli with different spectral composition (perceived metamerism) were often referred to as metamers if the meaning from context is clear.

2.1.2 Metameric black

In order to study the frequency of metamerism and the features of metameric reflectances in natural scenes, it is helpful to understand some methods of generating metamers at first. Indeed, the process of colour reproduction involves generation of metamers since the duplicates of colours showed on papers, photos and monitors are generated by the mixture of pigments. One of the methods used for generating metameric object-stimuli is named as metameric black method [3]. For a given illuminant and a given observer, if the tristimulus values generated by the reflectance functions are equal to zero as there is no light at all, these reflectance functions are metameric blacks [80]. Because the spectral reflectance functions of all metameric blacks necessarily have negative values at some wavelengths unless the reflectances are all zero over the visible spectrum, no metameric black exists physically in natural scenes. Given a object surface with spectral reflectance function $\rho_1(\lambda)$, a corresponding metameric colour stimulus with spectral reflectance function $\rho_2(\lambda)$ can be obtained by

$$\rho_2(\lambda) = \rho_1(\lambda) + \rho_b(\lambda), \qquad 2.1$$

where $\rho_b(\lambda)$ is the spectral reflectances of a metameric black. If the physical condition of real objects $0 \le \rho_2(\lambda) \le 1$ is not met, further scaling procedure by multiplying $\rho_b(\lambda)$ before adding it to $\rho_1(\lambda)$ will be needed. Indeed, the metameric black space is orthogonal to the space consisted of colour matching functions [81]. This is the reason that the scaling procedure applied on a metameric black reflectance does not alter the tristimulus values.

Theoretical approaches to reproducing metameric colours such as the metameric black method are useful for theoretical study of generation of metamers. Nevertheless, these numerical methods can tell neither the frequency of metamers nor the features of metameric reflectances in natural scenes.

2.2 CIE indices of metamerism

As mentioned earlier, a metameric match can be upset due to a change in environment. When a mismatch happens, how should one quantify the degree of metamerism? In most cases, for a metameric pair, the greater the differences between spectral compositions, the greater the perceptual differences with a change in illuminant or observer. Nevertheless, because the phenomenon of metamerism is not solely determined by spectral compositions, it is impractical to quantify the degree of metamerism only on spectra. The CIE recommended special indices of metamerism for changes in illuminant or observer to quantify the degree of metamerism [54]. These indices are based on the colour differences between metameric pairs after a change in illuminant or observer.

The procedure of quantify the degree of metamerism recommended by the CIE is described as follows. For a pair of metameric object colours, of which the tristimulus values under the reference illuminant are $X_{1,r}$, $Y_{1,r}$, $Z_{1,r}$ and $X_{2,r}$, $Y_{2,r}$, $Z_{2,r}$ respectively, the metamerism index is calculated by the corresponding colour difference between tristimulus values $X_{1,t}$, $Y_{1,t}$, $Z_{1,t}$ and $X_{2,t}$, $Y_{2,t}$, $Z_{2,t}$ under the test illuminant. The choice of colour difference equation should be noted if the colour difference equation other than CIELAB is used. The choice of the reference illuminant should also be noted if any illuminant other than the standard illuminant D65 is used as reference. The other suitable test illuminants include CIE standard illuminant A (tungsten light) and the FL (fluorescent lamps) and HP (high pressure discharge lamps) illuminants [54].

In practice, one should be aware that the perceptual non-uniformity of a colour space such as CIELAB reduces the quantitative power of the index of metamerism [82]. In addition, even the most advanced colour difference equation CIEDE200 [83], which corrects the non-uniformity of CIELAB for small colour differences under reference conditions, may not accurately represent the colour differences under other illuminants. In addition, there is no chromatic adaptation factor incorporated into the index of metamerism for change in illuminant.

The index of metamerism for change in observer is analogous to the index for change in illuminant. The tristimulus values are obtained by substituting the

colour matching functions of the reference observer for those of the test observer. The test observer can be the CIE standard deviate observer, who is classified as normal and not colour deficient [54].

In order to offers quantitative measurements of the degree of a mismatch between metamers, the CIE made the special metamerism index: change in illumiant. But it is unsuitable for the estimating the frequency of metamerism in natural scenes because of two underlying reasons. First, the special metamerism index requires the same tristimulus values between surfaces under a certain illuminant, which makes the probability of finding such surfaces in natural scenes very small. Second, it is more relevant to vision in natural scenes if two surfaces are visually indistinguishable rather than having the same tristimulus values. Although the notes of the special metamerism indices (Section 9.2.2.3 in [54]) supplies a multiplicative adjustment method if the tristimulus values are not exactly equal, the allowance of this adjustment is not specified.

Another index, the CMC 2002 colour inconstancy index [84], which is intended to predict colour constancy for the reflectance spectrum of a single surface, is also unsuitable for estimating the frequency of metamerism in natural scenes because metamerism is associated with the distinguishability of two surfaces. Alternative method should be used for estimating the frequency of metamerism in natural scenes rather than these indices.

2.3 Metamerism in natural scenes

According to the definition [3], metamers shall have numerically equal tristimulus values given certain viewing conditions. As noted earlier, the probability to find metamers with exactly equal tristimulus values in natural scenes is vanishingly small. Taking the limit of visual sensitivity into consideration, it is more pragmatic to count the number of perceived metamers in natural scenes. In other words, metameric surfaces are visually indistinguishable under a illuminant, but become distinguishable when the illuminant changes. Given a certain threshold colour difference for visual distinguishability,

metameric pairs can be determined if the colour difference between them is subthreshold under one illuminant and suprathreshold under another illuminant [71].

2.3.1 Metamerism due to changes in illuminant

Change in illuminant is a major cause of metamerism associated with surface in natural scenes. In order to study the frequency of metamerism in natural scenes, it is essential to build a model which simulates illumination changes upon natural scenes. The choice of simulated illuminants depends on two criteria. First, illuminants must be relevant to human vision in natural scenes. Second, changes in illuminant must be sufficiently large to reveal the visual difference between metameric pairs. Therefore, daylights were used for the simulation in [71], which include average daylight with correlated colour temperature (CCT) of 6500 K and the extremes with CCTs of 4000 K and 25,000 K, characteristic of the sun and sky at different times of the day [3, 85]. On a reciprocal colour-temperature scale, the distance from 4000 K to 6500 K is approximately equal to the distance from 25,000 K to 6500 K. These simulated daylights were assumed to be direct, global and constant [71]. The spectra of these daylights were generated according to the CIE [54] which is described as follows.

Step1: Determine the chromaticity of the correlated colour temperature *T* of D-illuminants.

i. The *x*-coordinates of chromaticity of D-illuminants with CCT approximately from 4000 K to 7000 K is calculated by

$$x = \frac{-4.6070\times10^{9}}{T^{3}} + \frac{2.9678\times10^{6}}{T^{2}} + \frac{0.0911\times10^{3}}{T} + 0.244063. \quad 2.2$$

ii. The *x*-coordinates of chromaticity of the D-illuminants with CCT from greater than 7000 K to approximately 25000 K is calculated by

$$x = \frac{-2.0064\times10^{9}}{T^{3}} + \frac{1.9018\times10^{6}}{T^{2}} + \frac{0.24748\times10^{3}}{T} + 0.237040. \quad 2.3$$

The *y*-coordinates of chromaticity is given by

$$y = -3.000x^2 + 2.870x - 0.275. \quad 2.4$$

Step2: Compute the relative spectral power distribution of D-illuminants by using a linear combination of a mean distribution $S_0(\lambda)$ and two distributions $S_1(\lambda)$ and $S_2(\lambda)$ which represents the two most important eigenvectors of the dataset of daylights distributions [3].

$$S(\lambda) = S_0(\lambda) + M_1 S_1(\lambda) + M_2 S_2(\lambda), \quad 2.5$$

where the two factors M_1 and M_2 are determined by the chromaticity coordinates.

$$M_1 = \frac{-1.3515 - 1.7703x + 5.9114y}{0.0241 + 0.2562x - 0.7341y}, \quad 2.6$$

$$M_2 = \frac{0.0300 - 31.4424x + 30.0717y}{0.0241 + 0.2562x - 0.7341y}, \quad 2.7$$

As mentioned in Chapter 1, Section 1.2.2, given a certain observer and an illuminant the tristimulus values of reflecting surfaces can be computed by using Equations 1.51 to 1.53. Two metameric surfaces were selected from the same natural scene. The tristimulus values of these two surfaces were obtained under the daylights with CCT of 4,000 K and 25,000 K, with or without chromatic adaptation to the daylight with CCT of 6,500 K, respectively. After transforming to the sRGB colour space [86], the colour perception of surfaces can be displayed on monitors. Figure 2.1 illustrates the visual differences between two surfaces with different reflectances in a real scene when illumination changes. In Figure 2.1 (a), it shows that if the eye is not chromatically adapted, the two surfaces cannot be distinguished by the eye. In Figure 2.1(b), if the eye is allowed to chromatically adapt to the daylight with CCT of 6,500 K, the surfaces are still indistinguishable. However, after changing the illuminant to a daylight with CCT of 25,000 K showed in Figure 2.1(c), if the eye is not chromatically adapted, the surfaces are noticeably different. The surfaces are still visually different even if the eye is chromatically adapted to the daylight with CCT of 6,500 K, with the surface on the left appearing more neutral than the surface on the right.

(a) Two surfaces under daylight (4,000 K)

(b) Two surfaces under daylight (4,000 K), adapted to daylight (6,500 K)

(c) Two surfaces under daylight (25,000 K)

(d) Two surfaces under daylight (25,000 K), adapted to daylight (6,500 K)

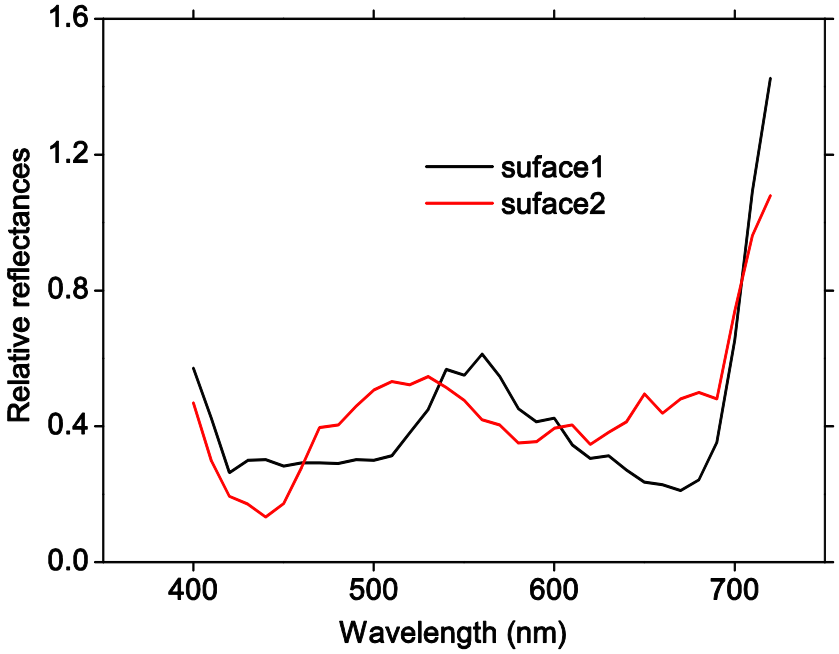

(e) Reflectances of two metameric surfaces

Figure 2.1: Illustration of metameric pairs under different illumination.

The general procedure described in this section shows that technically how to obtain colour representations of natural scenes with changing illumination. It means that given a certain threshold colour difference for visual distinguishability, metamerism in natural scenes can be determined.

2.3.2 Method of estimating frequency of metamerism

In order to estimate the frequency of metameric surfaces, the spatial resolution of the eye must be taken into consideration because it decides whether or not the spectral reflectances of surfaces in a scene are unmixed. The 50 hyperspectral images used in this thesis [71, 87] were obtained at least with the spatial resolution of the eye.

A threshold-based method was established in previous research [71] to answer the question that how often the metamerism happens in natural scenes. The illuminants upon natural scenes were assumed to be direct, global and constant

[71]. In order to capture the properties of the scene as a whole, a subset of N pixels was chosen at random without replacement according to a spatially uniform distribution. This sampling scheme is neutral to scene contents, and a previous analysis has shown that there was little effect on estimating the relative frequency of metamerism with different numbers of pixels within the subset [71, 88]. The word "relative" means that the frequency was estimated from a set of N samples in one scene rather than the whole scene. If all the surfaces in this subset are unique, the total number of unique pairs for this subset of surfaces is $N(N-1)/2$. Let the number of unique pairs with colour differences less than threshold ΔE^{thr} under one illuminant be N_0. And from this subset of N_0 pairs, the number of pairs whose colour difference is greater than a certain multiple n = 1, … , 4 of the threshold ΔE^{thr} under another illuminant be N_1, say. The multiple n is defined as the criterion degree of metamerism. The estimate of the relative frequency of metamerism in this scene is N_1 / N, and the estimate of the conditional relative frequency of metamerism is $(N_1 / N) / (N_0 / N) = N_1 / N_0$ [71]. The conditional relative frequency of metamerism is the probability of the indistinguishable surfaces of pairs under one illuminant becoming distinguishable when the illuminant changes.

The nominal threshold ΔE^{thr} for visual distinguishability, can be quantified according to a colour difference formula, such as the CIEDE2000 [64] in CIELAB or the Euclidean distance in CIECAM02 [65]. In principle, psychometric functions could have been used instead of these nominal threshold values ΔE^{thr}, but the increased complexity of analysis is unnecessary for estimating the frequency of metamerism because the variation of the frequency of metamerism introduced by psychometric functions is small. In addition, neither the performance of observer nor the level of physical stimulus is particular concerned in the present application. The value of nominal thresholds ΔE^{thr} was chosen to encompass possible visual just-noticeable-differences in different colour spaces [70, 89, 90].

In summary, given a colour difference threshold for visual distinguishability, two illuminants with known spectral power distribution, the reflectances of surfaces,

and colour matching functions of an observer, the frequency of metamerism can be estimated by this threshold-based method.

2.4 Discussion

Metamerism associated with surfaces is a phenomenon that shows that colour is unreliable for material identification occasionally. It is of great importance to understand the frequency of metamerism in natural scenes. Since exact metamerism is rare in natural scenes, it is more practical to use a visually relevant approach to estimate the occurrence of metamerism in natural scene.

There are many factors that can affect the estimates of the relative frequency of metamerism in natural scenes, such as the spectral reflectances of surfaces, the spectral power distributions of illumination, the sensitivities of the individual cone classes, the threshold of distinguishability, the choice of colour difference equation, and the choice of colour spaces. In this thesis, daylights were chosen as the simulated illumination because of the relevance to vision in natural scenes. In order to study metamerism associated with surfaces rather than observers, the CIE 1931 and 1964 standard colorimetric observers were chosen to represent an average observer and eliminate the variation of sensitivities from different observers [71]. Because the distinguishability of surfaces is quantified by the threshold, the colour difference formula used for this quantification should provide approximately perceptual uniformity in a corresponding colour space. This approximately perceptual uniformity can be achieved by using CIEDE2000 [64, 83, 91] in CIELAB or the Euclidean distance in CIECAM02 [65]. Unfortunately, there is no consensus about the threshold of colour difference for distinguishability in CIELAB or CIECAM02. Further research including the threshold of colour difference appropriate for metamerism estimates and the difference between the two metrics will be discussed is discussed in Chapter 6.

There are also other technical considerations to do with the method of estimating the frequency of metamerism [71]. It has been confirmed that the assumption of effective global illuminant has negligible effect on estimates of the relative

frequency of metamerism, which means that the effects of shadow is negligible. Increasing the number of samples randomly selected from the scene from 3,000 to 6,000 or changing the colour matching functions of standard observer did not affect the results significantly as well.

In this chapter, an established method of estimating the frequency of metamerism [71] is reviewed. The incorporation of nominal threshold in this method allows the inclusion of visual distinguishability in natural scenes. This method is applied in this thesis for estimating the frequency of metamerism in later chapters.

Chapter 3. Information-theoretic measurements of colours

In natural world, colour supplies the information about reflected lights from surfaces. Thanks to the tools offered by colorimetry, a colour of physically defined visual stimulus can be numerically specified [3]. Nevertheless, the colour information such as identifiability of surfaces contained in a whole scene cannot be expressed by these individual specifications. Theoretically, if the spatial information of a scene is ignored, the numerical specifications of colours can be treated as random variables. Thus, the quantities derived from information theory such as Shannon's entropy and mutual information [77] can be used to measure the colour information contained in a scene. Thus, the entropy of colours describes the average uncertainty of the colour appearance at a random point in a scene, and mutual information of colours quantifies the dependency between the two different sets of colours under two different illuminants in a scene. Because these informational quantities are determined by the probability functions of random variables, technical difficulties arise when the estimates of these quantities are based on the necessarily limited colour samples drawn from natural scenes.

This chapter starts with the definitions of differential entropy and mutual information of continuous random variables, then continues with information measures for trichromatic representations of surface colours in natural scenes, and ends with a discussion of the application and robustness of asymptotically bias-free estimators of differential entropy for surface colours in natural scenes.

3.1 Informational quantities of continuous random variables

Differential entropy and mutual information of continuous random variables are defined by analogy with the entropy and mutual information of discrete random variables (see Chapter 1, Section 1.4). If X is a continuous random variable with the probability density function $f(x)$, the differential entropy [77] is defined as

$$h(X) = -\int_S f(x) \log f(x) \mathrm{d}x, \tag{3.1}$$

where S is the support set of the random variable. The differential entropy is quantified in bits if the logarithm is to the base 2, and in nats if it is based on the natural logarithm.

If X and Y are continuous random variables with density functions $f(x)$ and $f(y)$, and a joint density function $f(x, y)$, the conditional differential entropy can be expressed as

$$h(X \mid Y) = -\int f(x, y) \log f(x \mid y) \mathrm{d}x\mathrm{d}y. \tag{3.2}$$

Additionally, the mutual information $I(X;Y)$ between two random variables is defined as

$$I(X;Y) = \int f(x, y) \log \frac{f(x, y)}{f(x) f(y)} \mathrm{d}x\mathrm{d}y. \tag{3.3}$$

From these definitions, if all the differential entropies are finite, it can be proved that

$$h(X \mid Y) = h(X, Y) - h(Y), \tag{3.4}$$

and

$$\begin{aligned} I(X;Y) &= h(X) - h(X \mid Y) \\ &= h(Y) - h(Y \mid X) \\ &= h(X) + h(Y) - h(X, Y). \end{aligned} \tag{3.5}$$

3.1.1 Difference between differential entropy and discrete entropy

Differential entropy of continuous random variables can be related to the entropy of discrete random variables. Assume there is a continuous random variable *X* with a discrete density after quantization, as illustrated in Figure 3.1 [77]. There then exists a value x_i within each bin of width Δ such that

$$f(x_i)\Delta = \int_{i\Delta}^{(i+1)\Delta} f(x)\mathrm{d}x. \tag{3.6}$$

If the quantized random variable X^Δ is defined as

$$X^\Delta = x_i, \text{ if } i\Delta \le X \le (i+1)\Delta, \tag{3.7}$$

then the probability that $X^\Delta = x_i$ is

$$p_i = \int_{i\Delta}^{(i+1)\Delta} f(x)dx = f(x_i)\Delta. \tag{3.8}$$

Thus, the entropy of the quantized variable is

$$\begin{aligned} H(X^\Delta) &= -\sum_{-\infty}^{\infty} p_i \log p_i \\ &= -\sum_{-\infty}^{\infty} f(x_i)\Delta \log(f(x_i)\Delta) \\ &= -\sum \Delta f(x_i)\log f(x_i) - \sum f(x_i)\Delta \log\Delta \\ &= -\sum \Delta f(x_i)\log f(x_i) - \log\Delta. \end{aligned} \tag{3.9}$$

If the density $f(x)$ is Riemann integrable, then as $\Delta \to 0$,

$$H(X^\Delta) + \log\Delta \to h(f) = h(X). \tag{3.10}$$

Thus the entropy of a continuous random variable *X* after *n*-bit quantization is approximately $h(X) + n$ [77].

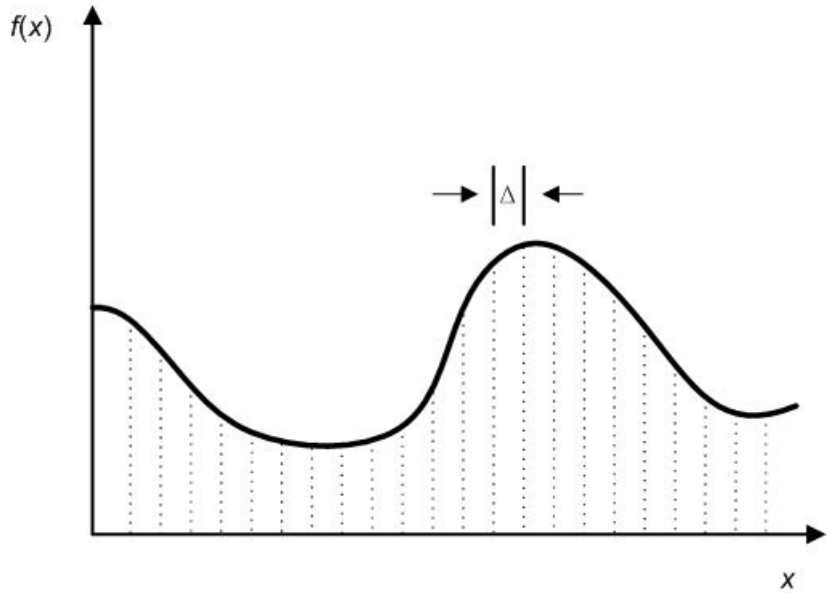

Figure 3.1: Quantization of a continuous random variable with bin width Δ, adapted from [77].

Discrete entropy is invariant to both translation and scaling of the random variable, but differential entropy is only invariant to translation not scaling, as shown in Equation 3.11 and 3.12.

$$h(X+c)=h(X). \tag{3.11}$$

$$h(aX)=h(X)+\log|a|. \tag{3.12}$$

Correspondingly, if a random continuous variable is scaled by an invertible transformation with matrix **M**, the entropy can be expressed as

$$h(\mathbf{M}X)=h(X)+\log|\mathbf{M}|, \tag{3.13}$$

where |**M**| is the determinant of **M**.

3.2 Information measures for trichromatic representations

In order to measure the colour information of natural scenes, the first step is to establish trichromatic representations of surface colours in natural scenes, which allows colours to be treated as continuous random variables. The second step is to define the entropy and mutual information of these trichromatic representations.

3.2.1 Trichromatic representations

Consider that there is a global illuminant with spatially uniform incident spectral radiance $e(\lambda)$ upon a scene, where wavelength λ ranges over the visible spectrum. If a random point (x, y) has an effective spectral reflectance $r(\lambda; x, y)$, the corresponding long-, medium-, and short-wavelength-sensitive cone responses, l, m, and s, are given by

$$l(x, y) = \int \bar{l}(\lambda) e(\lambda) r(\lambda; x, y) \mathrm{d}\lambda, \tag{3.14}$$

$$m(x, y) = \int \bar{m}(\lambda) e(\lambda) r(\lambda; x, y) \mathrm{d}\lambda, \tag{3.15}$$

$$s(x, y) = \int \bar{s}(\lambda) e(\lambda) r(\lambda; x, y) \mathrm{d}\lambda, \tag{3.16}$$

where $\bar{l}(\lambda)$, $\bar{m}(\lambda)$, and $\bar{s}(\lambda)$ are cone spectral sensitivities and the integrals are evaluated over the visible spectrum [92]. This set of equations provides a numerical specification of the colour at each point (x, y) in a scene. Indeed, because there are an infinite number of possible values of colour specification, any triplet of values for colour specification may be treated as values of a trivariate continuous random variable [93], such as (L, M, S) for cone responses, (X, Y, Z) for tristimulus values, (L^*, a^*, b^*) for coordinates in CIELAB colour spaces and (J, a_C, b_C) for coordinates in the CIECAM02 colour appearance model.

Figure 3.2 is an image of a natural scene under daylight with CCT of 6,500 K. The marginal histograms of the corresponding long-, medium- and short-wavelength cone responses are illustrated in Figure 3.3. These histograms provide a one-dimensional uniform binning approach to estimating entropy, which will be discussed in Chapter 3, Section 3.3.

Figure 3.2: A natural scene under daylight with CCT of 6,500 K [87].

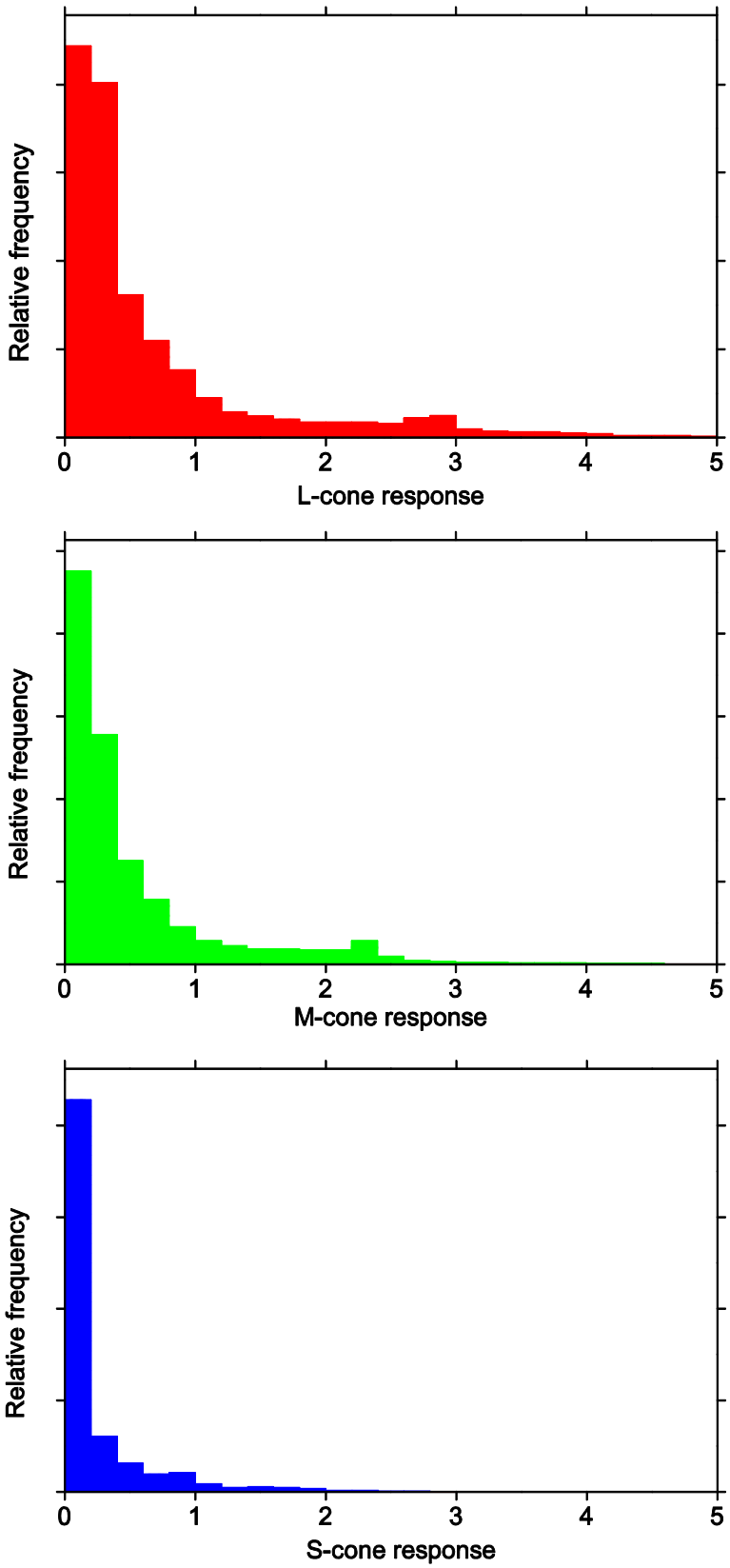

Figure 3.3: Marginal distributions of L-, M-, and S-cone excitations, obtained from the same scene as Figure 3.2 under a daylight with CCT of 6,500 K.

3.2.2 Differential entropy and mutual information of colours

If colour specification is treated as instances u, of a trivariate continuous random variable U, with a probability density function (pdf) f_U, the differential entropy of $h(U)$ of U can be defined by Equation 3.1. The differential entropy of colours describes the average uncertainty of colour appearance at a random point in scene.

Similarly, suppose that a scene is illuminated by two different illuminants in turn. The differential entropies of surface colours are denoted by $h(U_1)$ and $h(U_2)$ respectively, and the conditional differential entropy of colours is denoted by $h(U_2|U_1)$. The conditional differential entropy $h(U_2|U_1)$ of U_2 given U_1, may be defined as in Equation 3.2. But because generally $f(u_2 \mid u_1) = f(u_1, u_2) / f(u_1)$, it is more useful to calculate the conditional differential entropy of colours by Equation 3.4, for computational convenience.

Mutual information of colours represents the reduction of uncertainty of colour appearance under one illuminant due to known colour appearance under another illuminant. The mutual information between different sets of colours in the same scene under two different illuminants can be obtained by Equation 3.5.

The calculation of the differential entropy and mutual information of colours treated as continuous random variables is not straightforward. It is susceptible to bias if the estimators used for calculating informational quantities are based on binning [94]. It has been argued that because statistical fluctuations tend to make the distribution less uniform, the estimates obtained from histogram-based binning may leads to an underestimation of entropy [95]. With a limited number of samples obtained from natural scenes, it is important to achieve minimal bias for accurate estimates of colour information.

3.3 Asymptomatically bias-free information estimator

As mentioned in Chapter 1, Section 1.2.1, the spatial resolution of the hyperspectral imaging system is 1344 × 1024 pixels, sub-sampling algorithm was

applied to exclude the trivial correlation between adjacent pixels. These technical limitations mean that information measurements of colours must obtained from limited samples.

Compared to binning, given a sufficiently large number of samples, an estimate based on adaptive partitioning [96] can be asymptomatically bias-free. But it still depends on the choice of origin and bin width, and it may lack smoothness. Kernel smoothing [97, 98] can overcome some of the difficulties mentioned earlier but still relies on the choice of window width. A *k*th-nearest neighbour method has been developed to estimate the differential entropy and mutual information without knowing the probability density function [94]. This advantage makes it possible to accurately estimate the colour information if insufficient samples were obtained from natural scenes.

3.3.1 Kozachenko-Leonenko estimator

Kozachenko and Leonenko proposed an entropy estimator of multi-dimensional continuous random variable without estimating the density function [99]. It was further generalized by Goria etal. to a class of estimators based on *k*th-nearest neighbour [100].

Consider in a *m*-dimensional Euclidean space R^m, the Euclidean distance

$$\rho(x,y)=\sqrt{\sum_{j}^{m}(x_j-y_j)^2}, \qquad 3.17$$

where $x=(x_1,...,x_m)\in R^m$, $y=(y_1,...,y_m)\in R^m$ and $m\geq 1$. Suppose there is a ball $v(y,r)$ of radius *r* with centre $y\in R^m$, that is,
$v(y,r)=\{x\in R^m:\rho(x,y)<r\}$. Let the volume of the ball be $|v(y,r)|=r^m c_1(m)$, where

$$c_1(m)=\frac{2\pi^{m/2}}{m\Gamma(m/2)}, \qquad 3.18$$

and Γ denotes the gamma function. For a *m*-dimensional random variable *X*, a fixed point x_i and fixed *k*, where $1 \le i \le N$ and $0 < k < N$, let $\rho_{i,k}$ be the Euclidean distance between x_i and its *k*th-nearest neighbour. Denote the geometric mean of the random variables $\rho_{i,k}$ by $\bar{\rho}_k$; that is,

$$\bar{\rho}_k = \left(\prod_i^N \rho_{i,k} \right)^{1/N}. \qquad 3.19$$

Then, the estimate of differential entropy, expressed in nats, is given by

$$\hat{h}_{\mathrm{KL}}(X;N) = m\ln(\bar{\rho}_k) + \ln(N-1) - \psi(k) + \ln(c_1(m)), \qquad 3.20$$

where $c_1(m)$ is the volume of the ball given by Equation 3.18 and ψ is the digamma function. Thus, the estimated mutual information, in nats, is given by

$$\hat{I}_{\mathrm{KL}}(X;Y;N) = \hat{h}_{\mathrm{KL}}(X;N) + \hat{h}_{\mathrm{KL}}(Y;N) - \hat{h}_{\mathrm{KL}}(X,Y;N). \qquad 3.21$$

It has been shown that when $N \to \infty$, the estimates of differential entropy is asymptotical bias free and consistent under very weak conditions on the density function [99, 100]. Obviously, the estimate of mutual information in Equation 3.21 is also asymptotical unbiased and consistent under the same condition.

3.3.2 Offset version of the mutual information estimator

Surface colours tend to appear similarly to the chromatic adapted eye when the illumination varies. This phenomenon means that the colour information is highly correlated. This property makes it possible to improve the estimator of mutual information between colours obtained from the same scene under different illuminants [101].

Let U_1 and U_2 be trivariate random vectors representing colour signals under two illuminants. Set $U_1^* = (\mathrm{var}\,U_1)^{-1/2}U_1$, $U_2^* = (\mathrm{var}\,U_2)^{-1/2}U_2$, and $(U_1,U_2)^* = (\mathrm{var}(U_1,U_2))^{-1/2}(U_1,U_2)$. Because the covariance matrix is an

invertible square matrix, the differential entropy of U_1 can be calculated by Equation 3.13; that is,

$$h(U_1) = h(U_1^*) - \log\left|(\operatorname{var} U_1)^{-1/2}\right|. \tag{3.22}$$

Furthermore, the mutual information between U_1 and U_2 is given by

$$\begin{aligned} I(U_1;U_2) = {} & h(U_1^*) + h(U_2^*) - h((U_1,U_2)^*) \\ & - \log\left|\operatorname{var}(U_1)^{-1/2}\right| - \log\left|\operatorname{var}(U_2)^{-1/2}\right| \\ & + \log\left|(\operatorname{var}(U_1,U_2))^{-1/2}\right|. \end{aligned} \tag{3.23}$$

Let V_1 and V_2 be the two Gaussian vectors with the same covariance matrix as U_1 and U_2. Then the mutual information between V_1 and V_2 is given by [77]

$$\begin{aligned} I(V_1,V_2) &= \frac{1}{2}\log\left(\frac{\left|\operatorname{var} V_1\right|\left|\operatorname{var} V_2\right|}{\left|\operatorname{var}(V_1,V_2)\right|}\right) \\ &= \frac{1}{2}\log\left(\frac{\left|\operatorname{var} U_1\right|\left|\operatorname{var} U_2\right|}{\left|\operatorname{var}(U_1,U_2)\right|}\right). \end{aligned} \tag{3.24}$$

The mutual information $I(V_1,V_2)$ is referred to as the mutual information of the equivalent Gaussian I_{EG} [101]. Then Equation 3.23 can be rewritten

$$I(U_1;U_2) = h(U_1^*) + h(U_2^*) - h((U_1,U_2)^*) + I_{\mathrm{EG}}, \tag{3.25}$$

where I_{EG} is obtained by calculating the variance of the samples.

The improved estimator of the differential entropy and mutual information can be obtained with the aid of the Kozachenko-Leonenko algorithm, [101]

$$\hat{h}_{\mathrm{KLo}}(U_1) = \hat{h}_{\mathrm{KL}}(U_1^*) + \frac{1}{2}\log\left|\operatorname{var} U_1\right|, \tag{3.26}$$

$$\hat{I}_{\mathrm{KLo}}(U_1;U_2) = \hat{h}_{\mathrm{KLo}}(U_1) + \hat{h}_{\mathrm{KLo}}(U_2) - \hat{h}_{\mathrm{KLo}}(U_1,U_2). \tag{3.27}$$

By partitioning U_1 into Gaussian and non-Gaussian components, the mutual information converges to the true value more quickly for highly correlated continuous random variables [101].

3.3.3 Robustness of estimators

Because the estimators based on *k*th-nearest neighbour are only asymptotically bias-free, they will still have an unacceptable bias if the size of the samples is too small. Unfortunately, it is impractical to tell how many samples are sufficient even if a certain threshold of error has been determined because the true values of entropy and mutual information of colours is not known. But it is sensible to test the robustness of the estimators by examining how quickly the estimates converge to the true value with a known distribution.

The values estimated by the Kozachenko-Leonenko differential entropy estimator were compared with analytical results for some classical distributions in order to test the convergence of the estimator. The trivariate Gaussian distributions, which has the maximum differential entropy within the support set without any constraints, and the multivariate uniform distributions, which has the maximum differential entropy over the other distributions with a given covariance matrix, were used as test distributions.

3.3.3.1 Behaviour of KL estimator on the trivariate Gaussian distributions

The analytical expression of differential entropy of random variables with a multivariate Gaussian distribution [77] is

$$h(X_1, X_2, ..., X_n) = \frac{1}{2}\log(2\pi e)^n |K|, \qquad 3.28$$

where n is the dimension and $|K|$ denotes the determinant of the covariance matrix. Since the mean of a multivariate Gaussian distribution does not affect the differential entropy, only the covariance matrix needs to be considered. Two different covariance matrices were obtained from the perceptual attributes J, a_C and b_C within CIECAM02 under the daylight 6,500 K with default chromatic adaptation in two natural scenes, one predominantly vegetated (roses) and another predominantly non-vegetated (urban buildings).

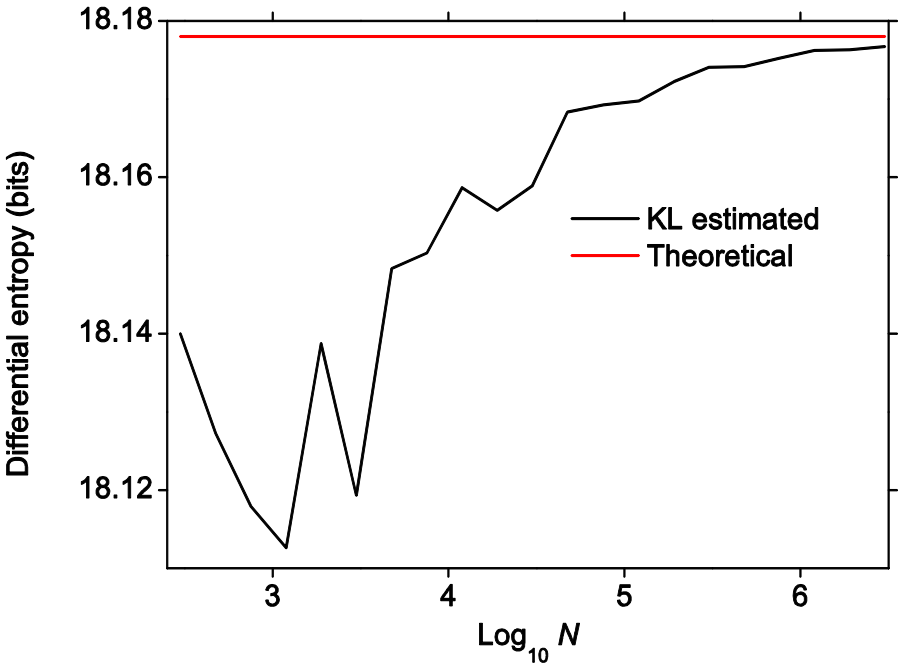

(a)

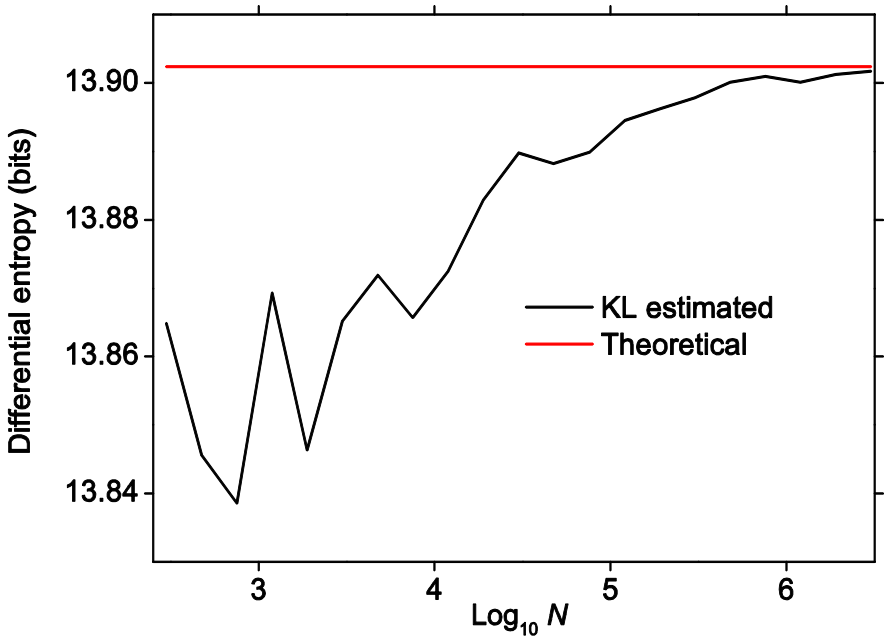

(b)

Figure 3.4: Differential entropy of a random variable with a trivariate Gaussian distribution, calculated by Equation 3.28 (red line), and by Kozachenko-Leonenko estimator (black line). (a) Covariance matrix from vegetated scene. (b) Covariance matrix from non-vegetated scene. The results are the means taken over 100 runs.

Consider a random variable with a trivariate Gaussian distribution of with covariance matrix obtained from the real samples in natural scenes. There were N samples ($3\times10^2 \le N \le 3\times10^6$) randomly selected from a three-dimensional space. The differential entropy estimated by Kozachenko-Leonenko estimator is illustrated in Figure 3.4.

As expected, the difference in differential entropy between estimated and theoretical values diminished as the number of samples increased. The spatial resolution of the hyperspectral images used here is 1344 × 1024 pixels. Even sub-sampled by a factor of 2 at each dimension, the number of pixels is larger than 2.5×10^5. If colours in one natural scene are treated as a trivariate random variable, the total number of down-sampled colour responses is still more than $3 \times 2.5 \times 10^5$. The error of the estimated differential entropy of a trivariate Gaussian distribution is about 0.004 and 0.001 with 3×10^5 samples and with 3×10^6 samples respectively, which is much smaller than 1% of the magnitude of the theoretical values of the differential entropy of a variable with trivariate Gaussian distribution. It means that the error of differential entropy estimated by Kozachenko-Leonenko estimator for this particular application is negligible.

3.3.3.2 Behaviour of KL estimator on the multivariate uniform distributions

In principle, the Kozachenko-Leonenko differential entropy estimator is unstable for application of discontinuous functions [99]. But it is useful to know the extent of the bias if the estimator is applied on discontinuous functions, because it is possible that colours in a natural scene are uniformly distributed in a certain colour space.

Uniform distribution has maximum differential entropy within the support set without any constraints [77]. Within the support colour set, if any colour appears more than others, the entropy will decrease. For instances, if the ‘red’ pattern appear multiple times in a colour system, the uncertainty of colour appearance will be reduced.

Consider a random variable with uniform distribution on the interval [*a*, *b*], so that the probability density function is

$$f(x)=\begin{cases}\dfrac{1}{b-a}, & x\in[a,b],\\ 0, & \text{elsewhere.}\end{cases} \tag{3.29}$$

The differential entropy [77] of the distribution is

$$h(x)=-\int_a^b \frac{1}{b-a}\log\frac{1}{b-a}\,\mathrm{d}x. \tag{3.30}$$

Note that if $b-a<1$, the differential entropy will be negative. The negative value makes it difficult to interpret physically the differential entropy of colours. But all the analysis regarding to differential entropy in this research were used as relative comparison involved within specified colour spaces.

The differential entropy of a multivariate random variable with multivariate uniform distribution is

$$h(x)=\int_{a_1}^{b_1}\int_{a_2}^{b_2}\cdots\int_{a_n}^{b_n}\frac{1}{(b_1-a_1)}\frac{1}{(b_2-a_2)}\cdots\frac{1}{(b_n-a_n)}\mathrm{d}x_1\mathrm{d}x_2\ldots\mathrm{d}x_n, \tag{3.31}$$

where *n* is the number of dimensions.

For colour coordinates *L**, within CIELAB and *J*, within CIECAM02, the values *L** and *J* range from 0 to 100. To illustrate some of the properties of colours in these coordinate systems, a multivariate random variable was constructed with a multivariate uniform distribution on the interval [0, 100] at each of *n* dimensions. The differential entropy of this multivariate random variable is

$$h(x)=n\log 100. \tag{3.32}$$

Suppose there is a *m*-dimensional ($1\le m\le 6$) multivariate random variable with *N* samples ($10^2\le N\le 10^6$) randomly selected at each dimension. The difference between differential entropy calculated from analytical expression and differential entropy estimated by Kozachenko-Leonenko estimator is summarized in Table 3.1.

Table 3.1: Difference[b] between differential entropy calculated from analytical expression and estimated by Kozachenko-Leonenko estimator with various dimension and number of samples at each dimension.

	N, Number of sample at each dimension[a,b]					Theoretic values
M	10^6	10^5	10^4	10^3	10^2	
1	0.20	0.02	0.00	0.00	0.00	6.64
2	0.00	0.00	0.01	0.02	0.09	13.29
3	0.01	0.03	0.06	0.12	0.24	19.93
4	0.05	0.09	0.16	0.28	0.55	26.58
5	0.12	0.19	0.31	0.50	0.84	33.22
6	0.23	0.34	0.51	0.79	1.18	39.86

[a] The number of samples for each test equalled to $N \times m$ in total.

[b] All results showed are the means taken over 100 runs.

As mentioned in Chapter 3, Section 3.3.3.1, if colours in one natural scene are treated as a trivariate random variable, the total number of pixels in hyperspectral images is larger than $3 \times 2.5 \times 10^5$. The error of the estimated differential entropy of a three-dimensional uniform distribution with 3×10^5 samples is about 0.03, which is less than 2% of the magnitude of the differential entropy of a variable with trivariate uniform distribution defined on the same domain. However, it should be noted that for a one-dimensional random variable, there was 0.20 difference on average for the test with 10^6 samples. With smaller numbers of samples, although the mean of difference was close to 0, there were still variations between individual tests.

Figure 3.5 illustrates the relationship between estimated differential entropy and the theoretical value of a trivariate uniform distribution. The difference between estimation and theoretical values becomes smaller as the number of samples increases. Despite the discontinuity, the error of the application of Kozachenko-Leonenko estimator on uniform distributions is acceptable.

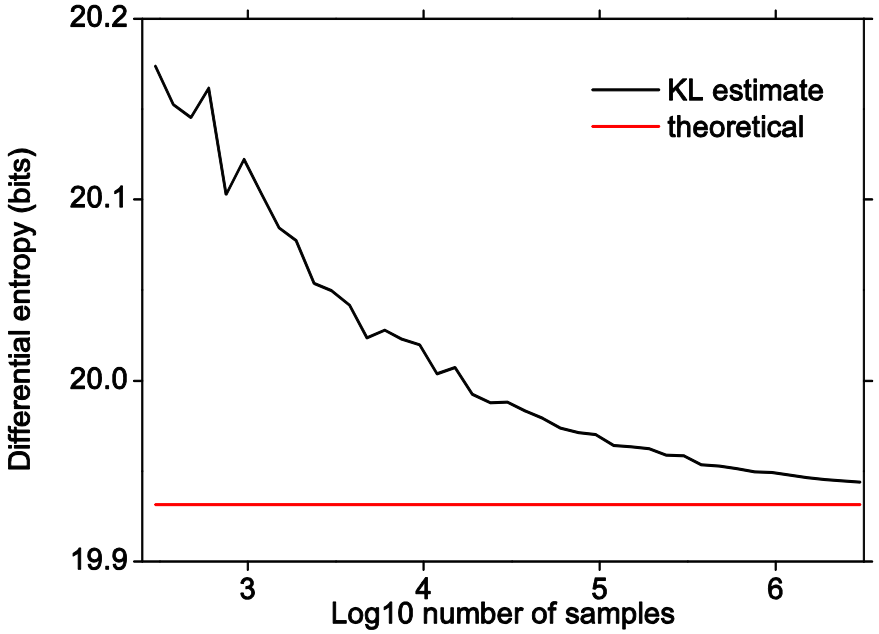

Figure 3.5: Differential entropy a continuous random variable with a trivariate uniform distribution with interval [0, 100] at each of three dimensions. Theoretical values calculated from Equation 3.32 are shown in red line and the estimates is shown in black line. The results are the means taken over 100 runs.

3.4 Discussion

Differential entropy and mutual information, which are derived from information theory, were used in this chapter to measure the colour information in natural scenes. But these theoretical quantities cannot be directly applied on numerical specifications of colours because the definitions of these quantities are based on the known probability density of continuous random variables, as mentioned at the beginning of Chapter 3, Section 3.3.

The Kozachenko-Leonenko estimator does not requires either pre-defined parameter or known probability density to estimate differential entropy. It has already been shown that this estimator can reach convergence quicker and close to analytical value of the highly correlated Gaussian variables [101]. One technical concern about the behaviour of this estimator is the error when the

estimator is applied on the insufficient number of samples. In Chapter 3, Section 3.3.3, the robustness of the estimator was tested on the multivariate Gaussian and uniform distributions, which posses certain similar statistical properties as colour distribution in natural scenes.

Note that all the estimated informational quantities were only interpreted as a relative measurement within specified colour space without any physical meaning in this thesis.

Chapter 4. Measurements of colour gamut of natural scenes

The colour gamut of natural scenes is a subset of all possible colours in a colour space. Because there are certain limitations on the spectral power distribution of daylights and the spectral reflectance of surfaces in natural scenes, some theoretical colour samples may never appear in natural scenes. For instance, the optimal colours [102] were not found in the 50 hyperspectral images [71, 87]. Indeed, colour stimuli in natural scenes are very constrained compared with the theoretical limits [103].

In principle, the volume of the colour gamut in real scenes may represent an approximate description of the colour information contained in a scene. For instance, to anticipate a later analysis, the estimated volume of the colour gamut of Figure 4.1 is larger than the one of Figure 4.2 (see Chapter 4, Section 4.2). Correspondingly, there are many distinguishable colours that can be identified in Figure 4.1, but only a few distinguishable colours in Figure 4.2.

Figure 4.1: A natural scene with many colours under daylight (6,500 K).

Figure 4.2: A natural scene with few colours under daylight (6,500 K).

This image has been intentionally brightened by using different gamma correction.

If surface colours in natural scenes were distributed in a similar way to the colour samples in the Musell colour system [104], the volume of the colour gamut within the Munsell colour system would certainly be good description of colour information such as identifiablity. In other words, the bigger the gamut, the more identifiable the colours. But colours in natural scenes are not distributed in this way: some colours can appear more frequently than others in natural scenes. In addition, there are many colours in natural scenes which are not included in the Munsell colour system. The question is then to what extent or under what circumstances, the volume of the colour gamut can be a good description of the colour information in natural scenes.

Two different methods are available to estimate the volumes of the colour gamut of natural scenes. First method is based on convex hull algorithms, which relies on the assumption that the colour gamut of natural scenes is a convex hull in a three-dimensional colour space. Another method is based on a cube-counting algorithm, which counts the number of colours in the gamut by segmenting the colour space into 'colour cubes'. Each colour cube represents one colour in a scene. This chapter demonstrates that given a reasonable colour difference threshold for the colour cubes, the volumes of the colour gamut of natural scenes calculated by a cube-counting algorithm is a good description of the uncertainty of colour appearance in natural scenes.

4.1 Gamut measured by convex hull algorithms

Convex hull algorithms are often used for gamut mapping in the colour reproduction industry [105]. Because different colour reproduction devices have different colour gamuts, gamut mapping is necessary to make sure that all the colours are located inside of the new gamut after the transformation of gamut between different devices. The method of gamut mapping is applied here to calculate the volume of the colour gamuts of natural scenes.

4.1.1 Preliminary convex-hull measurements

In principle, within a perceptually uniform colour space, the volume of the colour gamut is more likely to be a good description of colour information of a scene than within a non-uniform colour space. Thus, the attributes of a colour such as L^*, a^* and b^* within CIELAB and J, a_C and b_C within CIECAM02 were chosen as coordinates in a three-dimensional Euclidean space to measure the volume of the colour gamut. In the simulations reported here, natural scenes were illuminated by daylights with CCTs of 4,000 K, 6,500 K and 25,000 K, and all the illuminants were assumed to be constant, direct and global. The volumes of the colour gamut of the natural scenes under the daylights were initially estimated by the Matlab function 'convhull' (Matlab version: 2010a). The means and standard deviations of the estimates of the volumes within CIELAB and within CIECAM02 are given in Table 4.1 and Table 4.2, respectively. Within CIELAB, both full chromatic adaptation and no chromatic adaptation were applied. In Table 4.1, the second and third columns show the results obtained without chromatic adaptation and the fourth and fifth columns show the results obtained after full adaptation (degree 1 in CMCCAT2000 [106]). CMCCAT2000 is a chromatic adaptation transform which can predict the corresponding colour appearance under different illuminants. Within CIECAM02, different degrees of chromatic adaptation were applied. In Table 4.2, the second and third columns show the results obtained after full adaptation (degree 1 in CAT02 [65]) and the fourth and fifth columns show the results obtained after the default degree of adaptation (degree 0.92 in CAT02 [65]); the technical parameters are detailed in Chapter 8 Section 8.1.

Table 4.1: Means and SDs of the volume of colour gamut of natural scenes within CIELAB, estimated by convex-hull algorithm

CCT of daylights	No adaptation		Adaptation to 6,500 K	
	Mean	SD	Mean	SD
4,000 K	8.90×10^4	5.44×10^4	8.78×10^4	5.35×10^4
6,500 K	8.49×10^4	5.21×10^4	Not applicable	Not applicable
25,000 K	7.59×10^4	4.68×10^4	8.26×10^4	5.07×10^4

Table 4.2: Means and SDs of the volumes of the colour gamut of natural scenes within CIECAM02, estimated by convex-hull algorithm

CCT of daylights	Fully adapted at 6,500 K		Default adapted at 6,500 K	
	Mean	SD	Mean	SD
4,000 K	7.77×10^4	5.14×10^4	10.30×10^4	6.76×10^4
6,500 K	9.23×10^4	5.88×10^4	12.41×10^4	7.82×10^4
25,000 K	11.00×10^4	6.40×10^4	14.86×10^4	8.66×10^4

As Table 4.1 and Table 4.2 show, with the same degree of adaptation, the standard deviations of the estimated volumes of colour gamuts of natural scenes under each of the three daylights are fairly large, larger than the half of the average volume. These large standard deviations reflect the large variations of the colour gamuts between different scenes (see earlier examples in Figure 4.1 and Figure 4.2).

Table 4.1 shows that the effect of different degrees of chromatic adaptation on the estimated volumes of the colour gamuts within CIELAB is small. Within CIELAB, the differences between full and no chromatic adaptation in average volumes are 1194 and 6644, and the differences in standard deviation are 864 and 3886, with the daylight with CCT of 4,000 K and 25,000 K respectively. But the effect of different degrees of chromatic adaptation on the volumes within CIECAM02 is very large, especially taking the small difference between degrees of adaptation into consideration. As shown in Table 4.2, the differences between full and no chromatic adaptation in average volumes are 2.53×10^4, 3.19×10^4 and 3.87×10^4, and the differences in standard deviation are 1.61×10^4, 1.94×10^4, and 2.26×10^4, with the daylight with CCT of 4,000 K, 6,500 K and 25,000 K respectively.

One area of concern with convex-hull estimates is that the colour gamut of natural scenes is not always convex. In order to obtain a more accurate estimate and test the robustness of the convex hull algorithm, a modified convex hull algorithm was introduced, as described in next section.

4.1.2 Modified convex-hull measurements

One consequence of the colour gamut not being convex is that a convex-hull algorithm will give an inflated estimate. There are, however, several modified convex-hull algorithms which are designed to reduce over estimation [105, 107, 108]. The fundamental idea of the widely used modified convex-hull algorithm introduced in [108] is to increase the probability of finding correct vertices on the surfaces of a hull by inflating the hull. The volume can then be calculated like a polyhedron. If the idea is feasible for the estimation of the volume of the colour gamut of natural scenes, the volume of the colour gamut should be approximately equal to the sum of the volumes in sub-spaces. For instance, within CIECAM02, if a three-dimensional Euclidean space whose coordinates are J, a_C, and b_C is divided into eight octants with the centre at [50, 0 ,0], then the sum of the volumes located in eight divisions should be approximately equal to the volume calculated as a whole. But as Table 4.3 shows, there is a very large difference between the volume as a whole and the sum of the volumes of its eight parts. In addition, the volumes estimated by the modified convex-hull algorithm were even larger than the results given in Table 4.2. The large disparity of the volumes calculated by two methods and the more inflated volumes calculated by the modified convex-hull algorithm mean that the modified convex-hull algorithm designed for the gamut mapping cannot eliminate the effect of over estimation of the colour gamuts of natural scenes.

Table 4.3: Comparison between the volumes of the colour gamuts of natural scenes within CIECAM02, estimated by the modified convex hull algorithm

CCT of daylights	Whole volume		Sum of volumes of eight parts	
	Mean	SD	Mean	SD
4,000 K[a]	9.64E+04	6.39E+04	7.25E+04	5.12E+04
6,500 K	1.17E+05	7.45E+04	8.74E+04	5.70E+04
25,000 K	1.39E+05	8.17E+04	1.06E+05	6.01E+04

[a]All CIECAM02 attributes were obtained with chromatic adaptation to a daylight with CCT of 6,500 K. Default values were used for the CIECAM02 specification.

It is clear that both the conventional and modified convex hull algorithms are not capable of accurately estimating the volume of the colour gamut of natural scenes. To accurately estimate the volumes of colour gamut of natural scenes, an alternative method is needed.

4.2 Gamut measured by cube-counting algorithm

As indicated at the beginning of this chapter, the volume of a colour gamut can be estimated by segmenting the colour space into unit cubes [103]. This method does not require a assumption of the convexity of the colour distribution in colour space. The perceptual attributes L^*, a^*, and b^* within CIELAB and J, a_C, and b_C within CIECAM02 can be used as coordinates in a three-dimensional Euclidean space to calculate the volumes of the colour gamut, as illustrated in Figure 4.3. The number of colours is counted as the number of cubes that contain at least one colour sample. The volume of the colour gamut is the product of the number of colours and the volume of a unit cube, which defines the smallest distinguishable colour region. This method is robust against the choice of the starting point in the specified coordinate system [103]. But a major disadvantage of this method is that it is difficult to determine the appropriate colour difference threshold defining the unit cube. To compare the effect of variations in threshold, seven different thresholds within CIECAM02 were used in measurements of the volumes of the colour gamuts of natural scenes. As a control, the volumes of the colour gamuts within CIELAB were also evaluated.

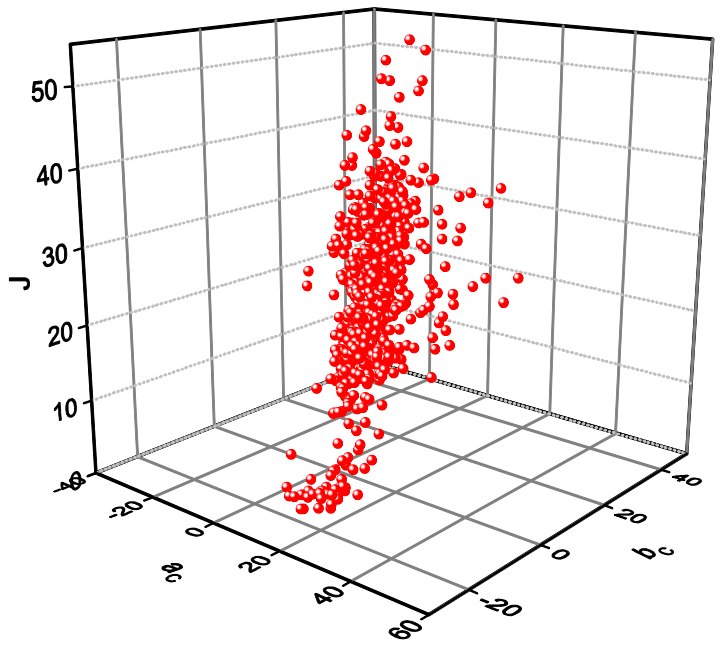

Figure 4.3: Representation of colour samples of a natural scene within the colour space CIECAM02. The samples of colour were spatially down-sampled by factor 20 along with each spatial axis of the image.

4.2.1 Relationship between volume of colour gamut and colour difference threshold

To understand the relationship between the gamut volumes and colour difference threshold, it is helpful to consider their variation with a known colour distribution. Suppose that there is a scene with 10^5 pixels distributed uniformly within a three-dimensional colour space, and that each pixel has a different colour. Suppose also that the range of the perceptual attributes of colours is 0 to 100 in each dimension. Let the colour difference threshold ΔE^{thr} range from 0.1 to 2 with 0.1 interval. The volume of a unit cube is $(\Delta E^{\text{thr}})^3$. The results are shown in Figure 4.4: if the cube is small enough so that it contains only one colour, the volume of the colour gamut increases linearly as the volume of the cube increases, but as each cube contains more and more one colours, the gradient decreases.

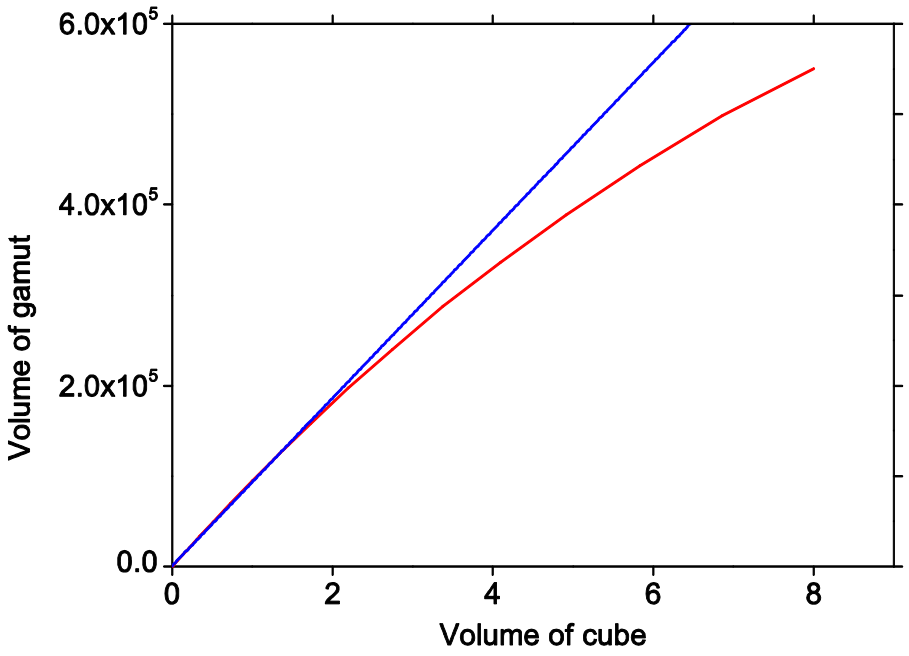

Figure 4.4: Relationship between the volume of the colour gamut and the volume of the unit cube with colours uniformly distributed in colour space. The linear part is shown in blue.

Notice that the colour distributions obtained from natural scenes under daylights are different from the uniform distribution considered here. There may be many samples concentrated in a small region of space with just a few samples sporadically distributed over other parts of colour space.

4.2.2 Estimated gamut volume within CIECAM02

As noted earlier, the estimated gamut volumes are affected by the choice of the colour difference threshold of the cube. To encompass typical thresholds within CIECAM02 [70, 89, 90], initially the threshold ΔE^{thr} was set, in turn, to 0.5, 0.6 and 1. But for theoretical study, the extreme colour difference threshold ΔE^{thr} that ranged from 0.1 to 0.4 with interval of 0.1 was also tested. Table 4.4 shows the results of the estimated volumes of the colour gamuts within CIECAM02 with the default chromatic adaptation, whereas Table 4.5 shows the results of

volumes of the colour gamuts with the full chromatic adaptation (parametric setting detailed in Chapter 8, Section 8.1).

Table 4.4: Colour gamuts of the 50 natural scenes under daylights within CIECAM02 with the default chromatic adaptation to a daylight with CCT of 6,500 K. Entries show estimated average colour-gamut volumes of colour gamut.

CCT of daylights	ΔE^{thr}						
	0.1	0.2	0.3	0.4	0.5	0.6	1
4,000 K	304	1767	4065	6645	9266	11831	21403
6,500 K	313	1902	4516	7516	10587	13611	24931
25,000 K	318	2033	5067	8738	12590	16424	30800

Table 4.5: Colour gamuts of the 50 natural scenes under daylights within CIECAM02 with the full chromatic adaptation to a daylight with CCT of 6,500 K. Entries show estimated average colour-gamut volumes of colour gamut.

CCT of daylights	ΔE^{thr}			
	0.3	0.5	0.6	1
4,000 K	3510	7692	9740	21183
6,500 K	3888	8696	11069	24748
25,000 K	4421	10417	13414	30528

Unless the colour difference threshold represents the discriminable colour difference for observers [103, 109], the actual values of the gamut volumes do not have any physical meaning. But as a relative quantity, is the gamut volume a good description of the colour information contained in a natural scene under a certain illuminant?

4.2.3 Gamut volume and colour entropy within CIECAM02

As noted in Chapter 3, the colour information of natural scenes under certain illuminants can be quantified by the differential entropy and mutual information. If the volume of the colour gamut of natural scenes is a good description of the

colour information, the volume should have a strong dependence on some of these informational quantities. To give a more intuitive example, with an appropriate colour difference threshold, the estimated volumes of the colour gamuts of Figure 4.1 and Figure 4.2 within CIECAM02 shown in Table 4.6 should be a good relative quantity to estimate the colour information contained in the images. The question then is what the appropriate colour difference threshold is.

Table 4.6: Volumes of the colour gamut within CIECAM02 of Figure 4.1 and Figure 4.2 with different colour difference thresholds. Entries show estimated volumes of the colour gamut.

	ΔE^{thr}						
	0.1	0.2	0.3	0.4	0.5	0.6	1
Figure 4.1	336	2469	7083	13754	21881	30840	70293
Figure 4.2	268	1338	2935	4754	6637	8505	15298

To answer this question, a simple linear model was constructed of the relationship between the gamut volumes and the entropy of colours. The logarithm of the volume of the colour gamut was linearly regressed on the estimated differential entropy within CIECAM02 with the default or full degree of chromatic adaptation under a daylight with CCT of 6,500 K, as shown in Table 4.7 and Table 4.8. All values of R^2 were adjusted for the degrees of freedom associated with different numbers of regressor variables [110]. As shown in Table 4.7, when $\Delta E^{thr} = 0.3$, the regression of the logarithm of the volume of colour gamut on the estimated differential entropy of colours was the strongest within CIECAM02 with the default degree of chromatic adaptation. The maximum adjusted value of R^2 was 0.94, independent of the CCT of the illuminant.

Table 4.7: Linear regression over 50 natural scenes of the logarithm of the volume of the colour gamut on the estimated differential entropy within CIECAM02 with default chromatic adaptation under a daylight with CCT of 6,500 K. Entries show adjusted values of R^2.

CCT of daylights	ΔE^{thr}						
	0.1	0.2	0.3	0.4	0.5	0.6	1
4,000 K	0.75	0.92	0.94	0.91	0.87	0.83	0.74
6,500 K	0.72	0.90	0.94	0.92	0.89	0.85	0.76
25,000 K	0.70	0.90	0.94	0.92	0.88	0.85	0.73

Table 4.8: Linear regression over 50 natural scenes of the logarithm of the volume of the colour gamut on the estimated differential entropy within CIECAM02 with full chromatic adaptation under a daylight with CCT of 6,500 K. Entries show adjusted values of R^2.

CCT of daylights	ΔE^{thr}			
	0.3	0.5	0.6	1
4,000 K	0.92	0.85	0.82	0.73
6,500 K	0.93	0.87	0.83	0.75
25,000 K	0.93	0.86	0.82	0.72

In the following, the number of colours in a gamut is taken to be the number of samples obtained by sampling with a given threshold, and the sampling is referred to as ‘colour sampling’. Although there was strong correlations between the gamut volume and entropy of colours for $\Delta E^{thr} = 0.3$, this strong dependence must not be over interpreted.

To understand the conditions that make this strong dependence possible, it is useful to consider a simplified version of this correspondence. The number of colours can be treated as an ill-defined version of the discrete distribution that has equal probability over the usually discontinuous support set, since the bin width (colour difference threshold) is arbitrary. Consider the colour specified by just one parameter, luminance. Let the number of colours be q; then the discrete entropy of the colours after the colour sampling will be $\log q$. On the other hand,

the differential entropy is determined by the range of support set and the distribution within this range. For some small thresholds, the ill-defined discrete entropy may have strong dependence on the corresponding differential entropy, which means that the logarithm of the number of colours will have strong linear regression on the differential entropy. But if the threshold is too small, the number of colours will be simply equal to the number of pixels in the scene, and the strong dependence will disappear. The situation in a three-dimensional space is more complicated, but the simulations show that a strong regression is still possible for certain ΔE^{thr}.

4.2.4 Gamut volumes and colour entropy within CIELAB

The relationship between gamut volumes and colour entropy within CIELAB was also examined as a comparison. The colour space CIELAB is also an approximate perceptually uniform colour space, but it is less uniform than CIECAM02, especially for very small colour difference when $\Delta E^{thr} \leq 1$ [111]. The unit Euclidean distance was used as one of the colour difference threshold within CIELAB, since it was originally designed to represent the just noticeable difference (JND). Table 4.9 summarizes the linear regressions over 50 natural scenes of the logarithm of the volume of the colour gamut on the estimated differential entropy of colours within CIELAB without chromatic adaptation.

Table 4.9: Linear regression over 50 natural scenes of the logarithm of the volume of the colour gamut on the estimated differential entropy within CIELAB, with different colour difference thresholds. Entries show adjusted values of R^2.

CCT of daylights	ΔE^{thr}				
	1	0.5	0.3	0.1	0.05
4,000 K	0.45	0.60	0.71	0.76	0.59
6,500 K	0.46	0.61	0.72	0.77	0.59
25,000 K	0.47	0.61	0.72	0.78	0.59

Compared with the results within CIECAM02, the linear regression of the gamut volume on the estimated differential entropy is weaker within CIELAB. The

perceptual non-uniformity within CIELAB may be the major cause of the weaker dependence of gamut volume on the uncertainty of colour appearance in natural scenes.

4.2.5 Colour distribution and flat entropy

The density of the colour distribution in a colour space is not taken into consideration when the volumes of the colour gamuts are calculated by the cube-counting algorithm. If one cube is treated as one colour, then the colour distribution after the colour sampling will be flatter than the natural colour distribution in natural scenes. Is the gamut volume still a good description of the uncertainty of these colours after the colour sampling? In other words, if a colour only appears once in a scene, can the gamut volume represent the uncertainty of the colour appearance? The differential entropy of colours obtained after the sampling is referred to as 'flat entropy' in the following discussion.

Colour sampling is a procedure for selection, and the samples that are selected to represent unit colour cubes inevitably affect the values of the flat entropy. The differences between the flat entropies calculated by two different selection seeds were calculated.

Table 4.10 shows that compared with the flat entropies which are always larger than 10 bits given the colour difference thresholds used in this section, the variation caused by the colour sampling procedure on the flat entropy is negligible. Another area of concern of with accuracy of flat entropy is that the number of samples decreases after colour sampling. The colour difference thresholds used here, however, were constrained to be sufficiently small that most sets still had more than 10^4 samples, which is unlikely to result in a significant bias.

Table 4.10: Mean of the differences between flat entropies calculated from two sets of samples with different selection seeds. Entries show the mean of the differences.

CCT of daylights	ΔE^{thr}			
	0.3	0.5	0.6	1
4,000 K	4.16×10^{-3}	6.91×10^{-3}	9.50×10^{-3}	13.3×10^{-3}
6,500 K	3.40×10^{-3}	5.12×10^{-3}	6.66×10^{-3}	15.5×10^{-3}
25,000 K	4.04×10^{-3}	5.46×10^{-3}	6.95×10^{-3}	10.7×10^{-3}

The flat entropies calculated here can be treated as the lower bound of the true value of the entropy of the colours after sampling. Table 4.11 shows the linear dependence of the logarithm volume of the colour gamut on the estimated flat entropy within CIECAM02. For colour thresholds ranging from $\Delta E^{thr} = 0.4$ to 1, the correlation is extremely strong. However, when the colour difference became smaller, the correlation becomes weaker. The results in Table 4.11 mean that when $1 \geq \Delta E^{thr} \geq 0.4$, the logarithm volume of the colour gamut can be a good description of uncertainty of colours after the colour sampling; that is, each distinguishable colour only appear once in a scene.

Table 4.11: Linear regression over 50 natural scenes of the logarithm of the volume of the colour gamut on the estimated flat entropy within CIECAM02 with default chromatic adaptation. Entries show adjusted values of R^2.

CCT of daylights	ΔE^{thr}						
	0.1	0.2	0.3	0.4	0.5	0.6	1
4,000 K	0.56	0.75	0.85	0.91	0.94	0.95	0.97
6,500 K	0.53	0.82	0.82	0.89	0.92	0.95	0.97
25,000 K	0.50	0.81	0.81	0.87	0.92	0.94	0.97

Compared with the regression of the gamut volume on the differential entropy, to interpret the regression of the gamut volume on the flat entropy is more difficult since the flat entropy changes along with the change of the colour difference threshold. There is no analytical expression to describe the changes of the distribution. The strong dependence only means that over 50 natural scenes, for

certain colour difference thresholds, the number of colours can be a good description of the uncertainty of themselves.

4.3 Summary

This chapter is to answer to what extent or under what circumstances, the volume of the colour gamut can be a good description of the colour information in natural scenes. The dependence between the gamut volume and differential entropy was used to test how good the description is.

Both the conventional and modified convex-hull algorithms are not suited to estimating the volumes of the colour gamuts because these algorithms ignore the fact that colour distributions within a colour space of a natural scene can be concave. On the other hand, given an appropriate colour difference threshold, the logarithm volumes of the colour gamuts calculated by the cube-counting algorithm showed very strong linear dependence on the estimated differential entropy over 50 natural scenes for certain colour difference thresholds. The volume calculated by the cube-counting algorithm is the product of the number of colours and the volume of a unit cube. Because the volume of a unit cube is a constant, the strong linear dependence still holds if the number of colours was regressed on the differential entropy. It suggests that if the distinguishable colour difference ΔE^{thr} within CIECAM02 is between 0.2 and 0.6, the volume of colour gamut or the number of distinguisbale colours can be a good description of the uncertainty of the colour appearance in natural scenes.

This strong dependence is affected by three factors. First is the uniformity of colour space. That is the reason that the dependence within CIECAM02 is much stronger than the dependence within CIELAB. Second is the choice of the colour difference threshold. The strong dependence only exists for certain thresholds within CIECAM02 and CIELAB, as shown in Table 4.7, Table 4.8 and Table 4.9. Third is the colour distribution in natural scenes. Imagine that images captured by a camera with the spatial resolution that is much better than the eye, it is unlikely that the gamut volumes of these kind of images have strong dependence

on the entropy of colours. The colour distribution related to the human vision in natural scenes makes it possible to model the uncertainty of colour appearance on the gamut volumes.

Chapter 5. Exploratory analysis of reflectances in natural scenes

As noted earlier, colour is often used for surface identification. But the phenomenon of metamerism means that sometimes colour is an unreliable signal, because colour appearance may change when the illumination or observer changes. On the other hand, the spectral reflectances of surfaces are physical properties of surfaces, and they do not change when the illumination or observer changes.

Despite the much analysis of the reflectances of Munsell colours and selected colour patterns [112-118], only limited research has been focused on reflectances of the surfaces with relevance to human vision in natural scenes [90, 119]. The aim of this chapter is to address three questions about these reflectances. First, how many basis functions of spectral reflectances are needed for an accurate approximation of spectral reflectances in natural scenes? Second, does any basis function represent the feature of a real pigment? Third, what are the features of the spectral reflectances of perceived metamerism?

5.1 Analysis of reflectances in natural scenes

To analyze the spectral reflectances of natural scenes, 50 hyperspectral images [71] as described in Chapter 1, Section 1.2, were used in the work reported in this chapter. The estimated effective spectral reflectances at each pixel were obtained by dividing the spectral radiance by the spectral radiance of a neutral reference surface [71]. Nevertheless, because some surfaces oriented at an angle to the camera may reflect more light than vertical surfaces, their effective spectral reflectances may exceed unity [71]. For computational convenience and consistency, if this maximum value was larger than unity, the spectral reflectances of the whole scene were normalized against the maximum value of spectral reflectance over all the measured wavelengths. For the purpose of this analysis, the spectral reflectances at extreme visible spectrum (400 nm, 410 nm,

710 nm, and 720 nm) were discarded owing to the low signal-to-noise ratios at these wavelengths.

In accordance with previous research [112, 113, 115, 116, 118-121], as a first step, principal component analysis (PCA) was applied to the set of spectral reflectances in natural scenes. Alternative decomposition techniques were then used because of their technical advantages over PCA.

5.1.1 PCA on spectral reflectances in natural scenes

Principal component analysis (PCA) uses orthogonal transformation to decompose data into basis functions and their respective weights. To answer the first question raised at the beginning of this chapter, reflectances were approximated by using certain number of basis functions, and then the approximations were compared with the original reflectances according to two different criteria [113, 121]. One criterion is based on the mathematic accuracy of the approximations, such as variance and goodness of fit; the other criterion is based on the colorimetric quality of the approximations. To answer the second question, the basis functions of spectral reflectances were compared with the reflectances of real pigments.

One should be aware that there are two different types of covariance matrix used in PCA: zero-centred [122] and mean-centred [85], as discussed in [123]. The difference between the two methods is that for the mean-centred matrix, the mean spectrum is subtracted from the original data. If the subtracted mean spectrum is not treated as one of the principal components, the mean-centred method will give the better fit to original data for a given number of principal components. In the following part of this section, mean-centred PCA was used to obtain basis functions as principal components from each individual natural scene.

5.1.1.1 Mathematical accuracy of approximations

One property of PCA is that the first principal component accounts for the largest variability in the data. For both the Munsell colour chips [121] and the natural scenes [119], 95% and 99% of variance of the spectral reflectances can be accounted by a linear model with two and three basis functions, respectively [113].

For the 50 natural scenes used here [71], on average, the first two basis functions accounted for more than 95% of the variance of the spectral reflectances in natural scenes, as shown in Table 5.1. But on average, three basis functions were not able to account for 99% of the variance of the spectral reflectances. In addition, more basis functions were needed to account for the same percentage of the variance from the predominantly vegetated scenes than the predominantly non-vegetated scenes. It is because that the first basis functions of the spectral reflectances in predominantly non-vegetated scenes may account for higher percentage of variance owing to possibly more uncorrelated spectra information. On the other hand, there are many surfaces such as leaves and grasses in the predominantly vegetated scenes that have subtle differences in spectral reflectance within the same group. As a result, the majority of variation cannot be described by one basis function.

Table 5.1: Number of the basis functions accounting for the variance of spectral reflectances in 50 natural scenes. Entries show means (SDs) of the number of basis functions accounting for the percentage of variance.

Percentage	All scenes	Non-vegetated	Vegetated
95	1.74 (0.60)	1.43(0.51)	1.97 (0.57)
99	3.54 (1.90)	2.43 (0.75)	4.34 (2.07)

Another mathematical quantity to measure the accuracy of the approximated spectral reflectances is goodness of fit. But some basis functions obtained from PCA have negative values, which may leads to negative reflectances. There were some approximated reflectances that exceed unity as well. The pixels with these physically unrealistic reflectances were subsequently discarded. Table 5.2 shows the number and percentage of these discarded pixels over 50 natural scenes.

Table 5.2: The number and percentage of pixels which posses unrealistic spectral reflectances after reproduction by PCA

		Number of basis functions					
		3	4	5	6	7	8
Negative	Number	1062649	982169	925237	933829	923370	914410
	Percentage[a]	6.24%	5.76%	5.43%	5.48%	5.42%	5.37%
Exceed unity	Number	17	7	8	6	6	6
	Percentage	0.00%	0.00%	0.00%	0.00%	0.00%	0.00%

[a]The total number of pixels in the 50 natural scenes is 17037540.

To calculate the goodness of fit of the approximations, the approximated spectral reflectances for each pixel were regressed on the original reflectances with only one explanatory variable, which excludes the constant. The R^2 of the linear regressions are shown in Table 5.3.

Table 5.3: Simple linear regression of reproduced reflectances on original reflectances in 50 natural scenes. Entries show values of R^2.

	Number of basis functions					
	3	4	5	6	7	8
Mean	0.86	0.90	0.92	0.93	0.94	0.95
SD	0.08	0.06	0.05	0.04	0.04	0.03

It is difficult to determine the minimum number of basis functions for accurate approximations, which depend on the specific requirements defining accuracy in different applications. But the simulation in this section shows the relationship between the number of basis functions of the spectral reflectances in natural scenes and the accuracy of approximations based on mathematic quantities. In next section, a vision-related approach will be introduced to measure the colorimetric quality of the approximated spectral reflectances.

5.1.1.2 Colorimetric quality of approximations

To quantify the colorimetric quality of the approximated spectral reflectances, the colour difference between the colour signal reflected from the original and the approximated reflectances were used as measurements. But unlike the previous studies, which used chromaticity [121] or the Euclidean distance within CIELAB [90, 124], the Euclidean distance within CIECAM02 was used in this section because of its better perceptual uniformity.

The illuminant on both types of reflectances was assumed to be a global, direct and uniform daylight with a CCT of 6,500 K. The CIE 1931 standard observer was used as the observer, who was assumed to be chromatically adapted to the illuminant. The parametric specifications of CIECAM02 used here are detailed in Chapter 8, Section 8.1.

Table 5.4 shows that, as expected, the colour difference ΔE decreases as the number of basis functions used for approximations increases. On average, under the daylight of CCT of 6,500 K, the colour differences between the colour signals reflected from the original and the approximated reflectances in the predominantly non-vegetated scenes were smaller than those in the predominantly vegetated scenes. If the distinguishable colour difference threshold within CIECAM02 is 0.6, on average at least 8 basis functions are needed to accurately reproduce the spectral reflectance in natural scenes. This finding is consistent with [90].

Table 5.4: Colorimetric quality of approximated spectral reflectances in natural scenes. Entries show the means and SDs of colour differences within CIECAM02.

		Number of basis functions					
		3	4	5	6	7	8
All scenes	Mean	2.40	1.45	1.05	0.82	0.66	0.52
	SD	1.29	0.70	0.44	0.34	0.30	0.27
Non-vegetated	Mean	1.72	1.16	0.89	0.69	0.54	0.38
	SD	0.77	0.54	0.36	0.24	0.21	0.15
Vegetated	Mean	2.90	1.66	1.18	0.91	0.75	0.62
	SD	1.37	0.73	0.45	0.37	0.33	0.30

Technically speaking, PCA does not guarantee the minimal visual difference between the lights reflected from the original and approximated spectral reflectances. Thus, the results here only mean that for a linear model, if the distinguishable colour difference is set to 0.6 within CIECAM02, it needs at least 8 principal components to reproduce a spectral reflectance that is visually indistinguishable under a daylight with CCT of 6,500 K.

5.1.1.3 Interpretation of basis functions

For the spectral reflectances of the 50 natural scenes [71], the curves of the first basis functions were relatively flat, as shown in Figure 5.1. This indicates that the variation of reflectances in natural scenes were relatively uniform distributed over wavelengths. If the reflectances were therefore approximated with only one basis function, the corresponding images under daylights would be monochrome. It indicates that the largest variation in colour signals reflected from the surfaces are the achromatic signals, i.e., luminance, as mentioned in [125]. But the second and third basis functions were quite different over different scenes. Indeed, even for predominantly vegetative scenes that contain largely green colours, the second and third basis functions did neither share much similarity over different scenes, nor resemble the peaks of reflectances curves of chlorophyll [126, 127].

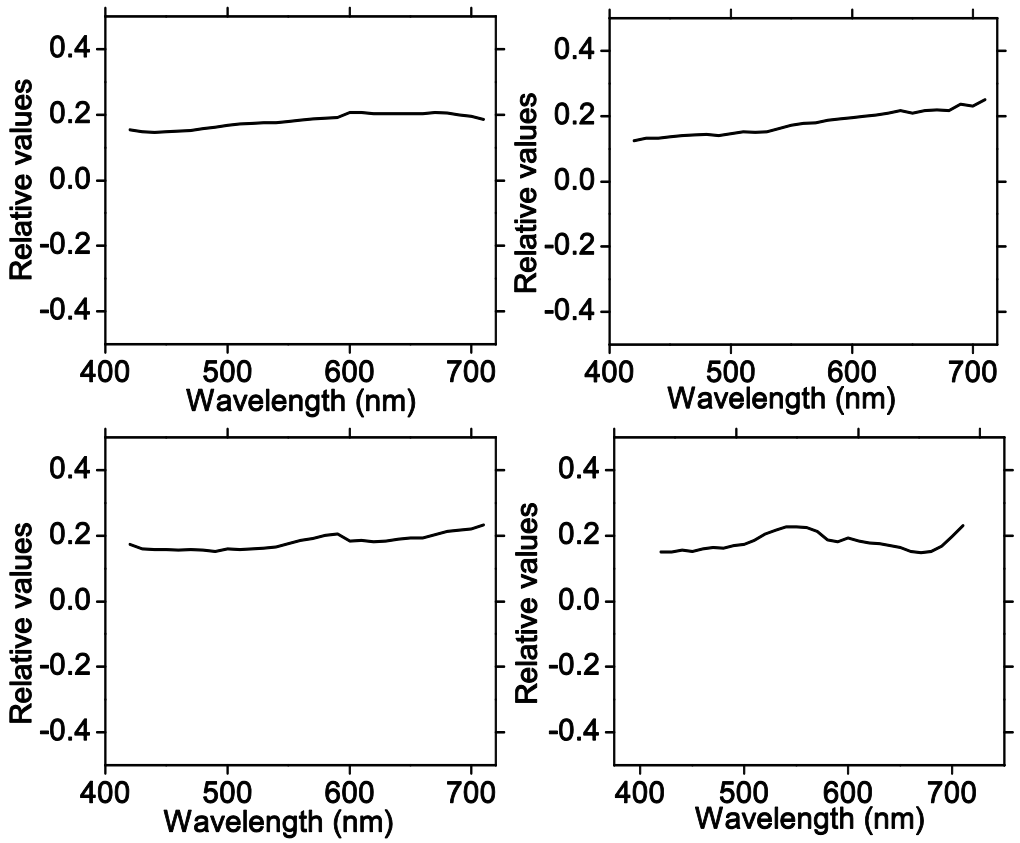

Figure 5.1: The first basis functions of the sets of spectral reflectances from four natural scenes.

5.1.2 Alternative methods of reflectance analysis

5.1.2.1 Independent component analysis

PCA helps quantify the importance of each dimension in accounting for the variance of the data. It requires, however, that each dimension must be orthogonal to the previous. This stringent limitation does not benefit some datasets arranged along non-orthogonal axes. To address this problem, one solution is to impose a more general statistical definition of dependency within a dataset, namely within the framework of independent component analysis (ICA) [128].

Statistical independence means that the joint probability density function of variables can be factorized into individual marginal probability density functions. The success of ICA depends on the maximization of non-gaussianity and

minimization of mutual information [128]. The FastICA algorithm [128] can be used to analyse the spectral reflectances of both the Munsell colour chips [129] and natural scenes. Nevertheless, it needs an additional criterion to determine the order of the independent components [130, 131]. Because of the complexity of the different selection criteria, this approach was not taken further.

5.1.2.2 Non-negative matrix factorization

The spectral reflectances in natural scenes are non-negative. Non-negative matrix factorization (NNMF) [132, 133] is an option to decompose spectral reflectances into all positive components and their respective weights. This makes it possible for basis functions to represent some physical pigment spectra such as chlorophyll in predominantly vegetated scenes.

Previously, it was suggested that NNMF can reveal colour names based on the basis functions obtained from spectral reflectances of the Munsell colour chips [134]. It is an interative optimization algorithm which is guaranteed to find a locally optimal solution to matrix factorization [132, 133]. The NNMF algorithm introduced in [135] was used here. One concern with the NNMF to spectral reflectances, however, is the inconsistency of the basis functions caused by the different number of iterations. When the number of repetitions of the factorisation was set to 50, the basis functions of a set of 1269 spectrophotometer-measured Munsell colour were similar to the results shown in [134] and Figure 5.2. When the number of repetitions of the factorization was increased to 200, the basis functions changed little, as shown in Figure 5.2. This shows that the number of iterations of NNMF has limited influence on the basis functions of the spectral reflectances of the Munsell colour chips.

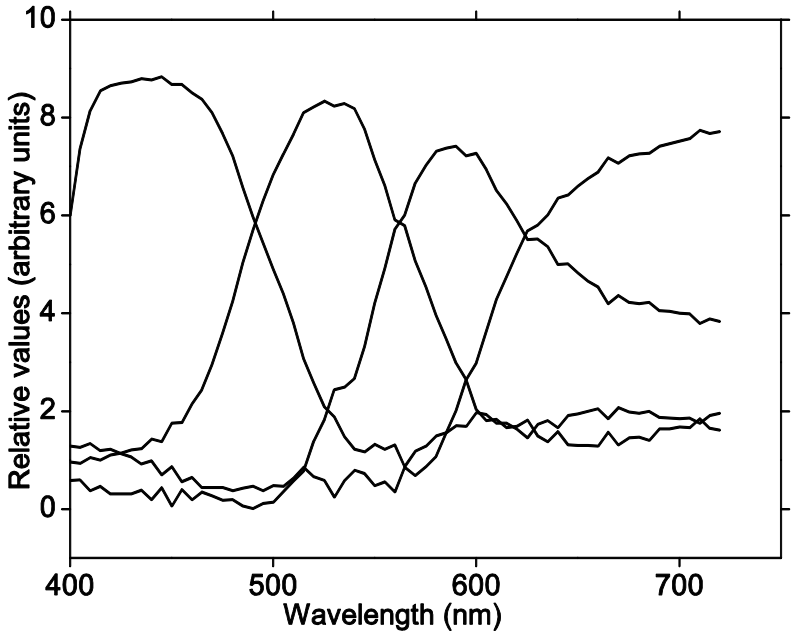

(a)

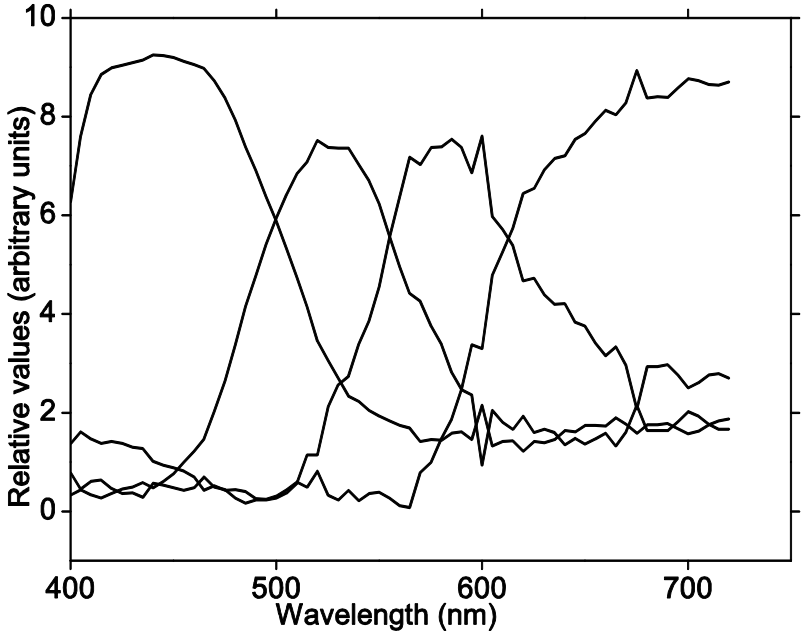

(b)

Figure 5.2: Four basis functions computed by NNMF with different number of iterations of the update rules for the spectral reflectances of a set of 1269 Munsell colour chips. The ordinates are in arbitrary scale. (a) 50 times iterations, (b) 200 times iterations.

Another concern of the colour naming based on Munsell colours [134] is that the spectral reflectances of Munsell colours are smooth functions of wavelength as opposed to the reflectances of surfaces in natural surfaces, where small-scale surface structure can cause complicated variations in the reflected light [72, 87]. In addition, the Munsell collection does not take the frequency of colour appearance in the real world into consideration.

To test the capacity of colour naming based on NNMF in natural scenes, eight predominantly vegetated scenes were selected for analysis. The four basis functions computed by NNMF for the spectral reflectances of one natural scene were shown in Figure 5.3. The basis functions do not have narrow-banded peaks, which mean that the colour names in natural scenes cannot be revealed by NNMF. Indeed, according to [134], three basis functions are enough to categorize the three dominant colours, red, green and blue. But for predominantly vegetated scenes, it is hard to find basis functions which can represent green consistently over different natural scenes. Despite the non-negativity offered by NNMF, it failed to categorize colours based on the spectral reflectances in natural scenes.

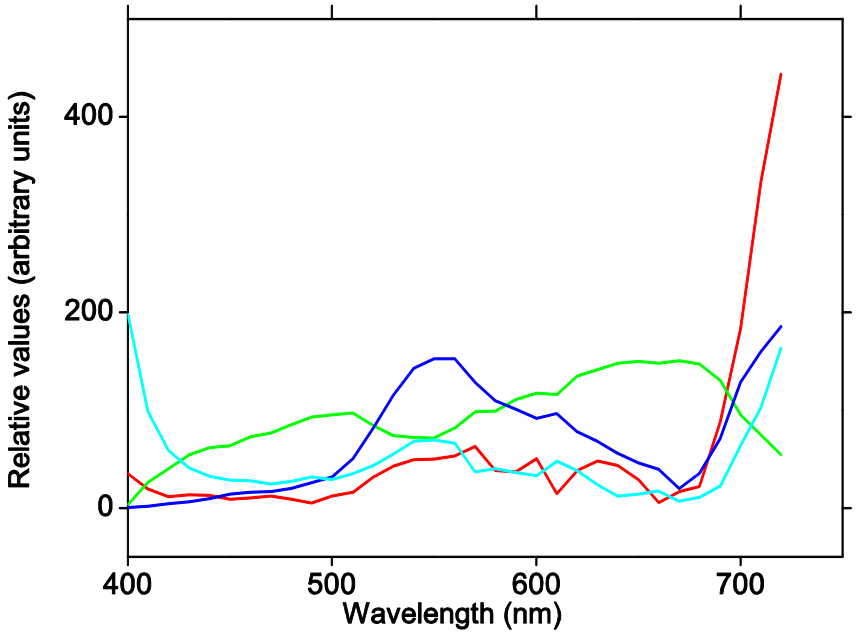

(a)

(b)

Figure 5.3: (a) Four basis functions computed by NNMF for spectral reflectances of one predominantly vegetated natural scene. (b) The image obtained of the corresponding natural scene under the daylight with CCT of 6,500 K

5.1.3 Discussion

Spectral reflectances are physical properties of the surfaces of objects, which are continuous functions of wavelength. But the colour signals perceived by the eye are often defined by three parameters. Despite the reduction in the freedom of dimension, the human visual system is still able to recover most of the spectral information available, even with changes in illuminants [92]. To explain this capability, it was assumed that spectral reflectances can be approximated by a low-dimensional linear model [113, 118, 119, 121, 122, 136]. This assumption has been treated as an explanation of the physical possibility of colour constancy [114], but the constraints are rarely satisfied [47]. From a colorimetric point of view, the minimum number of basis functions needed to approximate the spectral reflectances in natural scenes is larger than three, despite about 95% of the variance of spectral reflectances being accounted for by two basis functions. Nevertheless, it does not necessarily mean that three dimensions is insufficient for recovering most of the spectral information in natural scenes. It just showed that a three-dimensional linear model is highly unlikely to suffice.

As shown here, it is difficult to relate any of the basis functions revealed by PCA to real pigments. This is because PCA is intended to explain the largest global variance. It does not guarantee that the second and third basis functions represent the largest variance in the reflectances of a particular pigment or mixture of pigments. In addition, if all the spectral reflectances were obtained from the same type of surfaces, the second and third basis functions might represent similar features. But in natural scenes, the variety of surfaces is very large. PCA did not extract any features of one particular pigment from the natural scenes used here.

By contrast with PCA, ICA does not require orthogonality between basis functions, but it needs further criteria for ranking the significance of basis functions. NNMF posses some advantages over PCA in spectral reconstruction [137], but it seems unreliable for the colour naming of surfaces in natural scenes. Colour appearance is also affected by the receptor spectral sensitivities of visual system and the power distribution of illumination. If these two factors are not

taken into consideration, it is difficult to relate the basis functions to real pigments.

5.2 Spectral reflectances and metamers

As explained in Chapter 2, Section 2.1, two reflecting surfaces are metameric if they have the same tristimulus values under a certain illuminant but have different spectral reflectances. The large literature on metameric spectral reflectances has been focused on the theoretical reproduction of the spectral reflectances of exact metamers [80, 138-142]. The general procedure is to generate metameric reflectances that have the same tristimulus values given a certain illuminant and an observer. But neither the effect of complexity of spectral reflectances on metamerism nor the metameric reflectances found in natural scenes can be revealed by these methods because the spectral reflectances of a metamer set are generated for a pre-assigned triplet of tristimulus values.

To take a more general approach, two methods were devised to study the spectral reflectances of perceived metamers (See Chapter 2, Section 2.1.1). The first examined the relationship between the complexity of the synthesized spectral reflectances and the frequency of metamerism. The second examined the features of the spectral reflectances of perceived metamers (see Chapter 2, Section 2.3) in natural scenes.

5.2.1 Complexity of spectral reflectances and metamerism

For two exact metamers (see Chapter 2, Section 2.1.1), given an illuminant and an observer, it has been shown that the curve of the spectral reflectances of two metamers should have at least three intersections [3, 143]. Previous research showed the number of intersections and the location of the intersections. But the question remains that if the spectral reflectances of surfaces have more intersections, will there be more perceived metamers [143, 144]?

Synthesized spectral reflectances were generated to examine the relationship between the complexity of the spectral reflectances and the frequency of metamerism (see Chapter 2, Section 2.3.2). Gaussian functions were used to generate reflectances because they have been used for modelling both reflectance and absorption spectra before [145, 146]. With the physical limits of reflectances, i.e. $0 \le \rho(\lambda) \le 1$, the reflectances were obtained by summing different numbers of Gaussian functions. To increase the complexity of the reflectances, the centre of each Gaussian distribution was kept from the neighbouring Gaussian distribution by a distance at least equal to the standard deviation, and the standard deviation was kept small, as illustrated in Figure 5.4. These constraints mean that in most cases, the number of intersections between reflectances of different surfaces increases as the number of Gaussian distributions is increased. The spatial resolution of the synthesized reflectance was 400 × 400, and the reflectances were assumed to be represented by discrete samples over wavelength from 400 nm to 720 nm at 10 nm intervals.

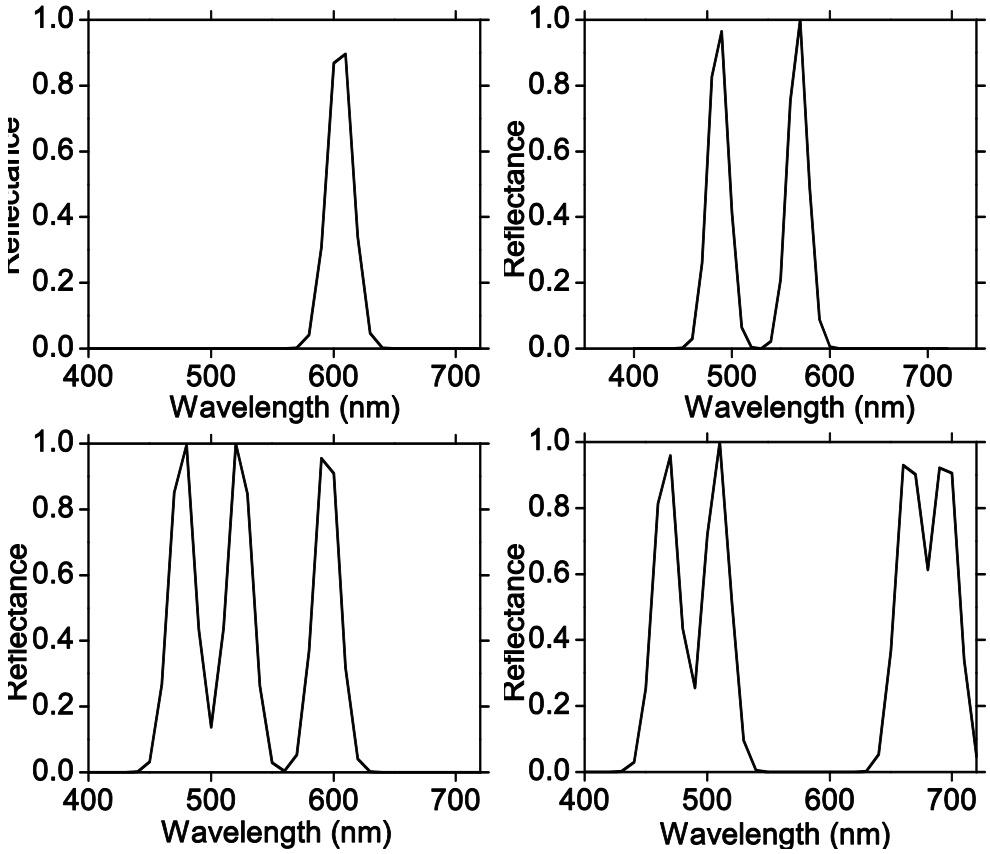

Figure 5.4: Examples of synthesized reflectances.

All the synthesized scenes were assumed to be illuminated by the daylights with CCTs of 4,000 K, 6,500 K and 25,000 K. The illuminant was assumed to be global, direct and uniform. For each synthesized scene, the relative frequency of metamerism and the conditional relative frequency of metamerism were calculated as mentioned in Chapter 2, Section 2.3.2. A set of 50,000 spectrally unique pixels were chosen at random according to a spatial uniform distribution for calculation, which means that there are 1249975000 unique pairs. Within CIECAM02, the colour difference threshold was set to 0.5, which was within the range of typical thresholds [70, 89, 90], and the criterion degree of metamerism was set to 1.

Table 5.5: The number of indistinguishable pairs N_0 and metamers N_1 from 50000 samples randomly selected from a synthesized scene.

Number of Gaussian functions	Daylights					
	4,000 K to 6,500 K		4,000 K to 25,000 K		6,500 K to 25,000 K	
	N_0	N_1	N_0	N_1	N_0	N_1
1	2339209	102396	2335992	191908	2313532	88028
2	58563	11757	57712	15512	64049	9051
3	3997	2304	3980	2587	4399	1912
4	1293	1185	1307	1231	1082	953
5	1261	1243	1230	1221	997	977
6	1504	1499	1472	1470	1098	1092
7	2036	2031	2031	2029	1528	1520
8	2699	2687	2681	2679	1928	1921
9	3655	3637	3623	3616	2542	2532
10	4733	4710	4804	4800	3212	3193

As shown in Table 5.5, the reflectances generated with a smaller number of Gaussian functions result in more indistinguishable colours and more metamers. But with a larger number of Gaussian functions, most of the indistinguishable pairs become distinguishable after a change in illuminant. In other words, the surfaces with more complex reflectances have the lower relative frequency of

metamerism but the higher conditional relative frequency of metamerism. To some extent, if more narrow-banded peaks are located at the wavelengths with the maximum spectral sensitivities, there will be more distinguishable colours under daylights. That is why when the number of Gaussian functions is 1, the numbers of indistinguishable pairs are significantly larger than the others. But when the number of Gaussian functions is larger than 7, there is only a slight increase of the number of indistinguishable pairs, because some peaks are located at the wavelengths with small spectral sensitivities.

Table 5.5 reveals a relationship between the complexity of spectral reflectance and metamerism, but it does not tell us the features of the spectral reflectances of real perceived metamers in natural scenes. In next section, the real spectral reflectances of perceived metamers in natural scene are examined.

5.2.2 Spectral reflectances of metamers in natural scenes

The structures of the spectral reflectances of metamers have been often discussed theoretically, but the reflectances of metamerism in natural scenes are quite different. First, exact metamers in natural scenes are very rare. Second, some synthesized reflectances (either generated for a pre-assigned tristimulus values or by the method introduced in Chapter 5, Section 5.2.1) do not exist in natural scenes. To understand the features of the spectral reflectances of metamers in natural scenes, several real metameric sets were selected from the 50 natural scenes [71].

Metamerism was determined within CIECAM02, and the colour difference threshold was set to 0.5 with the criterion degree of metamerism of 1, as used in Chapter 5, Section 5.2.1. To study the reflectances of metameric set with large samples, only the sets with more than 100 metameric surfaces were selected. For each metameric set, there was a reference surface, and all the other surfaces were metameric to this reference surface. Figure 5.5 illustrates the spectral reflectances of four metameric sets in natural scenes, in which the red lines represent the

spectral reflectance of the reference surface, and blue lines represent the subsets of the spectral reflectance of metameric surfaces. In order to fit the range of the spectral reflectances, the vertical axes were scaled accordingly.

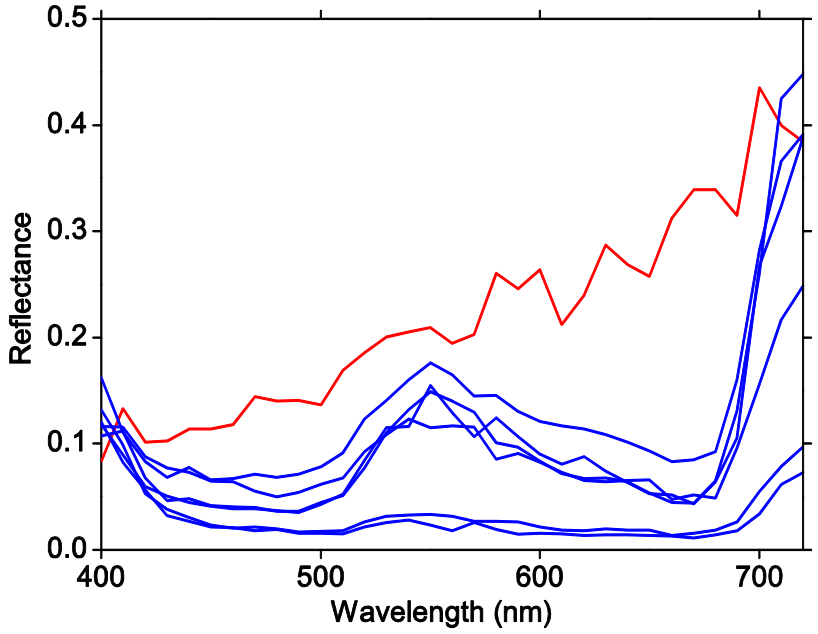

(a)

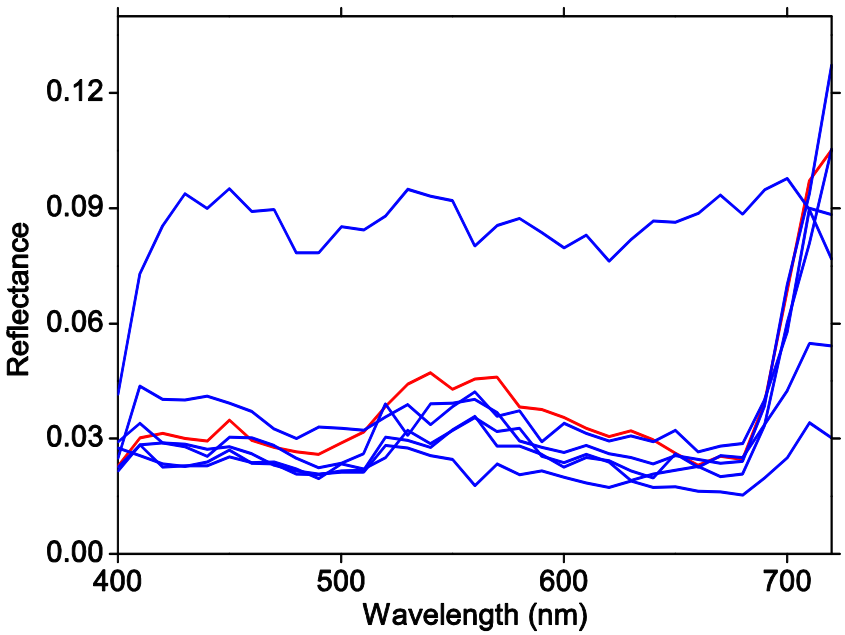

(b)

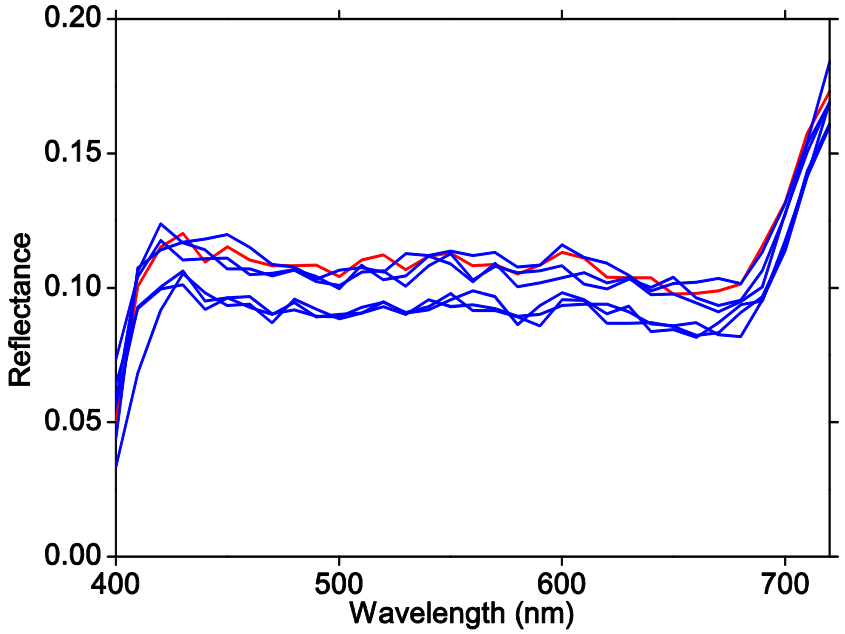

(c)

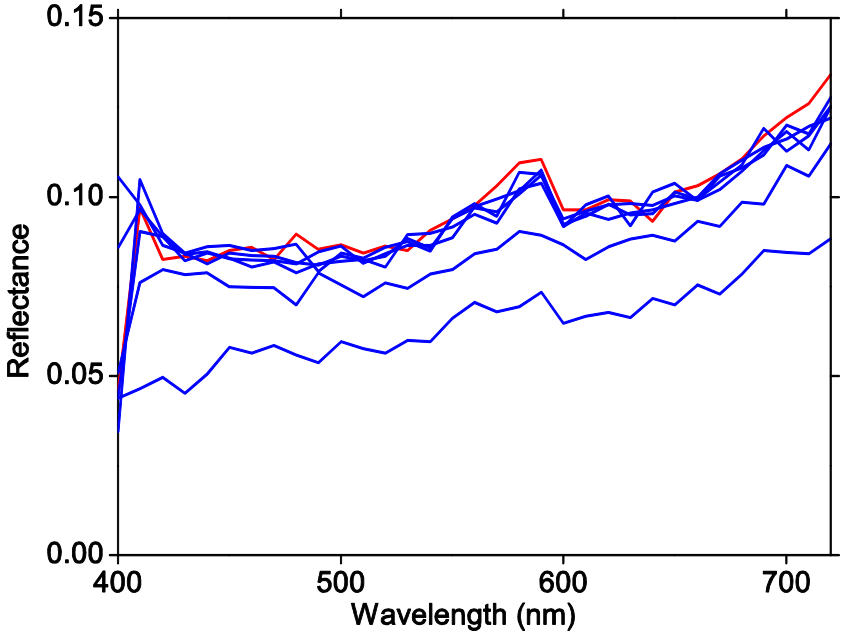

(d)

Figure 5.5: Subsets of the spectral reflectances of four metameric sets in natural scenes. The red line represents the reflectance of the reference surface, and the blue lines represent the reflectances of the corresponding metameric surfaces. The metamers were determined within CIECAM02. Colour difference threshold $\Delta E^{thr} = 0.5$ and the criterion degree of metamerism was set to 1.

Because there is some allowance of colour difference for metamerism, some of the spectral reflectances shown in Figure 5.5 do not have any intersections. As mentioned in [144], if the requirement of exact metamerism is relaxed, the number of intersections may be reduced. Most of the spectral reflectances of metamers are similar to those of the reference surfaces in Figure 5.5 (b), (c) and (d). This is because these metameric surfaces may belong to the same group of objects, such as leaves or grasses. On the other hand, in Figure 5.5 (a), some spectral reflectances of metameric surfaces are different from the reflectances of the reference surface. It may suggest that certain metameric surfaces are also from different group of objects.

5.2.3 Discussion

The aim of Section 5.2 is to address the third question raised at the beginning of the chapter: what are the features of the spectral reflectances of metamers? Although these experiments are illustrative rather than comprehensive, they provide an approach to studying the relationship between reflectance and metamerism.

The method used in Section 5.2.1 to generate synthesized reflectances is more general than the methods used in previous work which used pre-assigned tristimulus values [80, 138-142]. The experiment confirmed that if the requirement for exact metamerism is relaxed, the number of intersections of reflectances can be fewer than three. It was also shown that for two indistinguishable surfaces, the more complex their reflectances, the higher probability that they become distinguishable after a change in illuminant. It might be argued that there are other methods to generate the synthesized reflectances, but the objective of this experiment is to study the effect of the complexity of reflectances on the frequency of metamerism.

Unlike some of the synthesized reflectances generated in Chapter 5, Section 5.2.1, the reflectances of surfaces in natural scenes do not have so many peaks. In addition, most of the reflectances of metamers shown in Section 5.2.2 are very

similar. These similarities may indicate that the majority of metamerism in natural scenes comes from surfaces which consist of the same material, such as grasses and leaves, and which exhibit the expected biological variation from sample to sample.

Chapter 6. Predicting frequency of metamerism

The method of estimating the frequency of metamerism, which was mentioned in Chapter 2, Section 2.3.2, requires a large computation of the comparisons between surface colours under different illuminants. On the other hand, the colour information contained in a scene under a certain illuminant can be estimated by the quantities derived from information theory, such as differential entropy and mutual information. Is there a simpler approach based on these informational quantities for estimating the frequency of metamerism in natural scenes?

This chapter begins with the estimation of the relative frequency of metamerism and the conditional relative frequency of metamerism in natural scenes, then continues with models of predicting the frequencies, and ends with the a discussion of the predictive power of informational quantities.

6.1 Metamerism in natural scenes

The treatment here follows that in [71, 87]. Spectral-reflectances were taken from 50 hyperspectral images (0, Section 1.2.1) [147, 148]. The colour signals under different illuminants were represented by the tristimulus values, and the observer was assumed to be the CIE 1931 standard observer. These tristimulus values were then transformed into the corresponding coordinates within CIECAM02 [149]and CIELAB [150] with respect to D65, respectively.

The metamers were determined within colour spaces CIECAM02 and CIELAB, and a nominal colour-difference threshold value ΔE^{thr} was chosen to represent the corresponding distinguishable colour difference within each colour space.

The nominal threshold ΔE^{thr} was set, in turn, to 0.5 and 1.0 for both colour spaces, in order to encompass typical thresholds for the two spaces [70, 151, 152].

As in Chapter 2, Section 2.3.2, let the number of the indistinguishable pairs under one illuminant be N_0, and from this subset, let the number of the distinguishable pairs under another illuminant be N_1. If the number of total pairs is N, the estimate of the relative frequency of metamerism in this scene is N_1 / N , and the estimate of the conditional relative frequency of metamerism is N_1 / N_0 [71].

6.1.1 Frequency of metamerism within CIECAM02

In a previous study of the frequency of metamerism [148], samples of 3,000 points were randomly selected for estimation. To obtain a more accurate estimate, 50,000 points (about 15% of the total available) were chosen according to a spatially uniform distribution on each scene here. The number of total pairs N = $50{,}000 \times 49{,}999/2 \approx 1.25 \times 10^9$ [88].

For compatibility with [153], the specification with default values for chromatic adaptation was used for calculating the CIECAM02 coordinates J, a_C, b_C as mentioned in Chapter 8, Section 8.1. Colour differences between samples within CIECAM02 were calculated according to the corresponding Euclidean distance [69, 154] because of the approximately perceptual uniformity of CIECAM02. Table 6.1 summarizes the estimates of the relative frequency and the conditional relative frequency of metamerism in the 50 natural scenes within CIECAM02.

As shown in Table 6.1, smaller changes in illuminant lead to lower relative frequencies and conditional relative frequencies of metamerism in natural scenes. This is because larger changes in illuminant produce more distinguishable pairs. When the degree of metamerism n = 1 or 2, the larger colour difference threshold of ΔE^{thr} = 1 resulted in a higher relative frequency of metamerism than the smaller threshold of ΔE^{thr} = 0.5. But when n = 3 or 4, the larger colour difference threshold resulted in a lower relative frequency. This result is a consequence of

the distribution of the colour difference between pairs. When ΔE^{thr} increases, the number of indistinguishable pairs N_0 under the first illuminant will increase. This may lead to an increase in the number of distinguishable pairs N_1 under the second illuminant. But when the degree of metamerism n increases, if ΔE^{thr} is too large, there will be fewer pairs with colour difference bigger than $n\Delta E^{thr}$, as explained in [71].

Table 6.1: Relative frequency and conditional relative frequency of metamerism in natural scenes, calculated with the Euclidean distances within CIECAM02. Entries show the means (SDs) of $\log_{10}$ frequency and conditional frequency.

Threshold ΔE^{thr}	Criterion degree [a] n	1st daylight CCT, K	2nd daylight CCT, K	log N_1/N	log N_1/N_0
0.5	1	4000	25000	−3.67 (0.45)	−0.11 (0.05)
		4000	6500	−3.85 (0.46)	−0.29 (0.11)
		6500	25000	−3.93 (0.40)	−0.24 (0.13)
	2	4000	25000	−4.04 (0.38)	−0.49 (0.26)
		4000	6500	−4.95 (0.54)	−1.29 (0.56)
		6500	25000	−4.74 (0.43)	−1.05 (0.50)
	3	4000	25000	−4.50 (0.41)	−0.94 (0.48)
		4000	6500	−5.82 (0.73)	−2.27 (0.87)
		6500	25000	−5.54 (0.64)	−1.85 (0.79)
	4	4000	25000	−4.92 (0.50)	−1.37 (0.64)
		4000	6500	−6.70 (0.98)	−3.14 (1.17)
		6500	25000	−6.25 (0.83)	−2.56 (1.01)
1.0	1	4000	25000	−2.90 (0.14)	−0.19 (0.07)
		4000	6500	−3.14 (0.44)	−0.42 (0.14)
		6500	25000	−3.19 (0.39)	−0.35 (0.16)
	2	4000	25000	−3.55 (0.39)	−0.83 (0.33)
		4000	6500	−4.78 (0.78)	−2.06 (0.80)
		6500	25000	−4.61 (0.60)	−1.77 (0.69)
	3 [b]	4000	25000	−4.41 (0.59)	−1.70 (0.71)
		6500	25000	−6.07 (1.04)	−3.24 (1.19)
	4 [b]	4000	25000	−5.18 (0.80)	−2.46 (0.96)

[a] Multiple of ΔE^{thr} for colour differences under second daylight, giving N_1 pairs out of N_0

[b] Results for other daylight pair or pairs omitted as $N_1 = 0$ for one or more scenes

As the criterion degree of metamerism increased, the variance of the relative frequency of metamerism over different scenes generally increased, which is consistent with previous findings [71]. To illustrate the variation over different scenes, the ranges defined by the logarithm of the ratio of the maximum to the minimum relative frequency are summarized in Table 6.2. For a criterion degree of metamerism of $n = 1$, the average log range over the 50 natural scenes was 1.73, which is greater than 50. For larger degrees of n, the ratios were even greater.

But notably the main cause of the variation in the observed frequency is different for different criterion degrees of metamerism. The observed frequency N_1/N can be decomposed to two factors: N_0/N and N_1/N_0. For degree of $n = 1$, the average range of log N_0/N was 1.84 and of log N_1/N_0 was 0.55, which means that the probability of finding indistinguishable pairs under the first daylight accounts for more variation in the relative frequency of metamerism than the conditional probability of these pairs becoming distinguishable under the second daylight [88]. Theoretically, if the probability of finding indistinguishable pairs under the first daylight can be described by one quantity, this quantity should have the power to predict the relative frequency of metamerism with $n = 1$. This predictive power will be discussed and explained in Chapter 6, Section 6.2.

Table 6.2: Difference between maximum and minimum of relative frequency and conditional relative frequency of metamerism in natural scenes within CIECAM02.

Threshold[a] ΔE^{thr}	Criterion degree[a] n	1st daylight CCT, K	2nd daylight CCT, K	Range[c] log N_0/N	Range[d] log N_1/N_0	Range[e] log N_1/N
0.5	1	4000	25000	1.94	0.24	1.81
		4000	6500	1.95	0.56	1.90
		6500	25000	1.90	0.68	1.71
	2	4000	25000	1.94	1.15	1.59
		4000	6500	1.94	3.17	2.40
		6500	25000	1.88	2.29	1.91
	3	4000	25000	1.94	2.35	2.05
		4000	6500	1.94	4.15	3.52
		6500	25000	1.90	3.45	2.88
	4	4000	25000	1.95	2.87	2.49
		4000	6500	1.95	4.88	4.66
		6500	25000	1.90	4.42	3.76
1.0	1	4000	25000	1.76	0.33	1.59
		4000	6500	1.77	0.68	1.80
		6500	25000	1.74	0.83	1.57
	2	4000	25000	1.76	1.51	1.77
		4000	6500	1.75	3.85	3.40
		6500	25000	1.72	2.95	2.85
	3[b]	4000	25000	1.76	3.14	2.84
		6500	25000	1.74	5.56	5.38
	4[b]	4000	25000	1.76	4.03	3.70

[a] Multiple of ΔE^{thr} for colour differences under second daylight, giving N_1 pairs out of N_0

[b] Results for other daylight pair or pairs omitted as $N_1 = 0$ for one or more scenes

[c] Difference between maximum and minimum of log N_0/N

[d] Difference between maximum and minimum of log N_1/N_0

[e] Difference between maximum and minimum of log N_1/N

6.1.2 Frequency of metamerism within CIELAB

To compare with previous estimates [148], smaller samples of 3,000 points were also taken for estimation within CIELAB. Because of the limited uniformity within CIELAB, the colour differences between samples were calculated according to CIEDE2000 [64, 150]. Table 6.3 summarizes the estimates of the relative frequency and the conditional relative frequency of metamerism in the 50 natural scenes within CIELAB. The results are consistent with both previous estimates [71] and showed a similar pattern as the estimates within CIECAM02.

Table 6.3: Relative frequency and conditional relative frequency of metamerism in natural scenes, calculated with the CIEDE2000 [91] within CIELAB. Entries show the means (SDs) of $\log_{10}$ frequency and conditional frequency.

Threshold ΔE^{thr}	Criterion degree n	1st daylight CCT, K	2nd daylight CCT, K	log N_0/N	log N_1/N_0
0.5	1	4000	25000	−3.47 (0.42)	−0.34 (0.16)
		4000	6500	−3.73 (0.41)	−0.60 (0.22)
		6500	25000	−3.65 (0.43)	−0.54 (0.19)
	2 [a]	4000	25000	−4.27 (0.50)	−1.14 (0.51)
		6500	25000	−5.07 (0.61)	−1.95 (0.78)
	3 [a]	4000	25000	−4.95 (0.55)	−1.82 (0.77)
1.0	1	4000	25000	−2.94 (0.34)	−0.58 (0.24)
		4000	6500	−3.25 (0.35)	−0.90 (0.26)
		6500	25000	−3.17 (0.35)	−0.82 (0.25)
	2 [a]	4000	25000	−4.35 (0.57)	−1.99 (0.66)

[a] Results for other daylight pair or pairs omitted as $N_1 = 0$ for one or more scenes

6.2 Predict metamerism

As mentioned in Chapter 6, Section 6.1.1, if one quantity can predict the probability of finding indistinguishable pairs under the first daylight, this quantity may have the power to predict the relative frequency of metamerism with $n = 1$. But to predict the relative frequency and conditional relative frequency of metamerism with different criterion degrees of metamerism, more comprehensive models are needed. In this section, models based on the

combinations of the estimated Shannon differential entropies of the colours of the scene under the same two daylights were used to predict the relative frequency and the conditional relative frequency of metamerism.

6.2.1 Predicting the frequency of metamerism

6.2.1.1 Models of prediction

For two continuous random variables, U_1 and U_2, let $h(U_1)$ and $h(U_2)$ be the differential entropies of the colours under the corresponding daylights, and let $h(U_2, U_1)$ be the joint differential entropy of the pair (U_2, U_1) [88]. In practice, the conditional entropy $h(U_2, U_1)$ was calculated by using $h(U_2 \mid U_1) = h(U_2, U_1) - h(U_1)$ [77].

The relationship between differential entropy and the relative frequency of metamerism depends on the decomposition $N_1/N = (N_0/N)(N_1/N_0)$. Because the more unpredictable U_1 is, the more likely that colour differences will be greater than ΔE^{thr}, and, therefore, the lower the value of N_0/N. Thus, the observed value of $\log N_0/N$ for each scene and pair of daylights might be modelled, to first order, by the estimate of $h(U_1)$, with a negative coefficient of proportionality, as shown in Equation 6.1.

$$\mathrm{E}\left[\log(N_0 / N)\right] = -\beta_1 h(U_1) + \alpha_1, \qquad 6.1$$

where E is the expectation, β_1 and α_1 are scalars, and $\beta_1 > 0$ [88].

Another factor N_1/N_0, which estimates the probability of indistinguishable pairs under the first daylight becoming distinguishable under the second daylight, has a certain dependence on the degree of uncertainty of U_2 given U_1, namely the conditional differential entropy $h(U_2, U_1)$. In other words, the more unpredictable U_2 is given U_1, the more likely that colour differences will be greater than $n\Delta E^{thr}$, and, therefore, the higher the value of N_1/N_0 [88]. Similarly, the observed value of $\log N_1/N_0$ for each scene and pair of daylights might be modelled, to first order,

by the estimate of $h(U_2 \mid U_1)$, with a positive coefficient of proportionality, as shown in Equation 6.2.

$$\mathrm{E}\left[\log(N_1 / N_0)\right] = \beta_2 h(U_2 \mid U_1) + \alpha_2, \qquad 6.2$$

where $\beta_2 > 0$ [88].

Because $\log N_1/N = \log N_0/N + \log N_1/N_0$, the observed value of $\log N_1/N$ for each scene and pair of daylights might be modelled, to first order, by the combination of Equation 6.1 and 6.2. That is,

$$\mathrm{E}\left[\log(N_1 / N)\right] = -\beta_1 h(U_1) + \beta_2 h(U_2 \mid U_1) + \alpha_0, \qquad 6.3$$

where β_1 and β_2 are same as those in Equation 6.1 and 6.2, and $\alpha_0 = \alpha_1 + \alpha_2$ [88].

The Equation 6.3 can be rewritten as

$$\mathrm{E}\left[\log(N_1 / N)\right] = -\beta_0 \left[\beta_1' h(U_1) - \beta_2' h(U_2 \mid U_1)\right] + \alpha_0, \qquad 6.4$$

where $\beta_1' = \beta_1 / (\beta_1^2 + \beta_2^2)^{1/2}$, $\beta_2' = \beta_2 / (\beta_1^2 + \beta_2^2)^{1/2}$ and $\beta_0 = (\beta_1^2 + \beta_2^2)^{1/2}$. When $\beta_2' = 0$, the full model defined by Equation 6.4 is reduced to a restricted model defined by Equation 6.5, that is,

$$\mathrm{E}\left[\log(N_1 / N)\right] = -\beta_1 h(U_1) + \alpha_1. \qquad 6.5$$

And when $\beta_1' = 0$, the full model is reduced to a model defined by Equation 6.6, that is,

$$\mathrm{E}\left[\log(N_1 / N)\right] = \beta_2 h(U_2 \mid U_1) + \alpha_2. \qquad 6.6$$

6.2.1.2 Prediction within CIECAM02

To test the predictive power of the full model and the two restricted models, the observed values of $\log N_1/N$ were regressed on the different combinations of estimates of $h(U_1)$ and $h(U_2 \mid U_1)$ over the 50 scenes, respectively [88]. Some regressions failed because the number of indistinguishable pairs under the second

illuminant $N_1 = 0$. The goodness of fit of the regression was described by R^2, unless the regression failed. All values of R^2 were adjusted for the degrees of freedom associated with different numbers of explanatory variables [110]. Estimates of the standard error (SE) for R^2 were obtained by a bootstrap with at least 1000 iterations [155].

The values of R^2 within CIECAM02 are summarized in Table 6.4. The results based on the full model defined by Equation 6.4 are shown in the last column of Table 6.4. For $n = 1$, the regression was very strong for all changes in illuminant and both thresholds, with mean $R^2 = 0.90$ (mean SE = 0.02). The regression was less strong for $n \geq 2$, with mean $R^2 = 0.66$ (mean SE = 0.09). When n increased, the regression became weaker. But the criterion degree of metamerism n is not the only predictor of the loss in dependence. The difference in the ranges of log N_0/N and log N_1/N_0 also indicate the loss. Figure 6.1 illustrates R^2 for the full model (last column in Table 6.4) plotted against the difference in ranges of log N_0/N (fifth column in Table 6.2) and log N_1/N_0 (sixth column in Table 6.2). The red line shows a linear regression with adjusted $R^2 = 0.74$ (SE = 0.08) [88].

Table 6.4: Regression over 50 scenes of log observed relative frequency of metamerism on estimated differential entropy within CIECAM02 [149] for various nominal colour difference thresholds, criterion degrees of metamerism, and daylights with different correlated colour temperatures [88].

Threshold[a] ΔE^{thr}	Criterion degree[b] n	1st daylight CCT, K	2nd daylight CCT, K	R^2 Eq. 6.5[c]	R^2 Eq. 6.6[d]	R^2 Eq. 6.4[e]
0.5	1	4000	25000	0.92	0.43	0.92
		4000	6500	0.86	0.31	0.88
		6500	25000	0.89	0.31	0.90
	2	4000	25000	0.74	0.10	0.90
		4000	6500	0.12	0.02	0.62
		6500	25000	0.17	0.03	0.64
	3	4000	25000	0.23	0.00	0.76
		4000	6500	0.00[g]	0.29	0.63
		6500	25000	0.00[g]	0.30	0.61
	4[f]	4000	25000	0.03	0.16	0.72
		4000	6500	0.04	0.45	0.60
		6500	25000	0.02[g]	0.44	0.61
1.0	1	4000	25000	0.93	0.35	0.94
		4000	6500	0.82	0.25	0.87
		6500	25000	0.84	0.22	0.86
	2	4000	25000	0.46	0.00[g]	0.84
		4000	6500	0.01	0.07	0.42
		6500	25000	0.01	0.18	0.57
	3[f]	4000	25000	0.01[g]	0.26	0.73
		6500	25000	0.01	0.44	0.59
	4[f]	4000	25000	0.01[g]	0.42	0.70

[a] Nominal threshold for colour differences under first daylight, giving N_0 pairs out of $N \approx 1.25\times10^9$ pairs chosen randomly from each of the 50 scenes

[b] Multiple of ΔE^{thr} for colour differences under second daylight, giving N_1 pairs out of N_0

[c] Proportion of variance accounted for by restricted linear model Equation 6.5.

[d] Proportion of variance accounted for by restricted linear model Equation 6.6.

[e] Proportion of variance accounted for by restricted linear model Equation 6.4.

[f] Results for other daylight pair or pairs omitted as $N_1 = 0$ for one or more scenes

[g] Adjustment for degrees of freedom omitted, as invalid

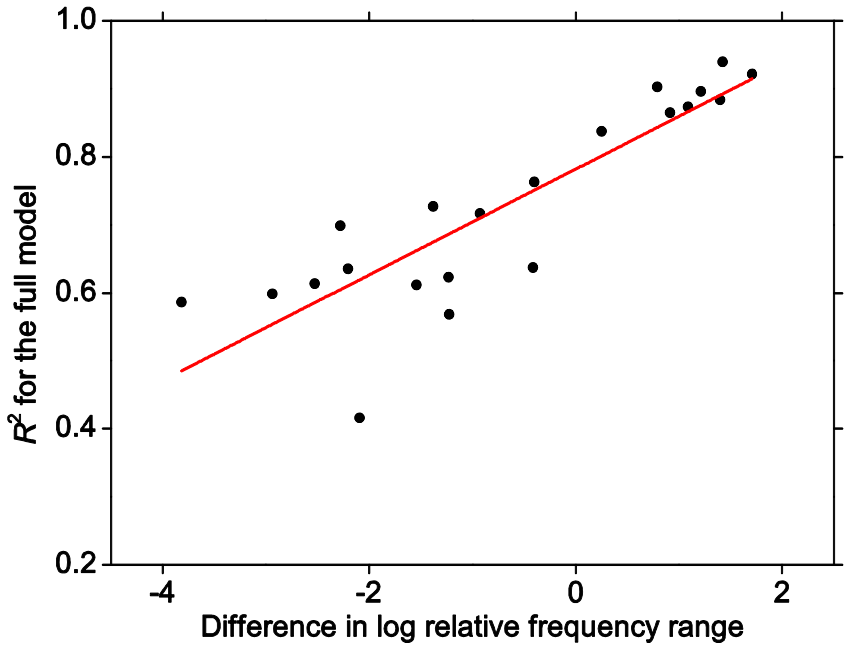

Figure 6.1: Dependence of goodness of fit of the full model on the difference in relative frequency ranges. Proportion R^2 of variance accounted for by Equation 6.4 is plotted against the difference in ranges of log N_0/N and log N_1/N_0. The red line over the ascending portion represents a linear regression.

As shown in the third column from last of Table 6.4, the regression based on the restricted model defined by Equation 6.5 was very strong with $n = 1$. For all changes in illumiannt and both thresholds, mean $R^2 = 0.88$ (mean SE = 0.03). But, by contrast with the full model, the strong regression of this restricted model disappeared for $n \geq 2$, with mean $R^2 = 0.12$ (mean SE = 0.06) [88].

For the restricted model defined by Equation 6.5, the difference in the ranges of log N_0/N and log N_1/N_0 also predicted the loss in dependence. Figure 6.2 illustrates R^2 for this restricted model plotted against the difference in ranges of log N_0/N and log N_1/N_0. A piecewise linear regression was shown in the red line with the first segment of the model forced to zero. For this regression, $R^2 = 0.98$ (SE = 0.01) [88].

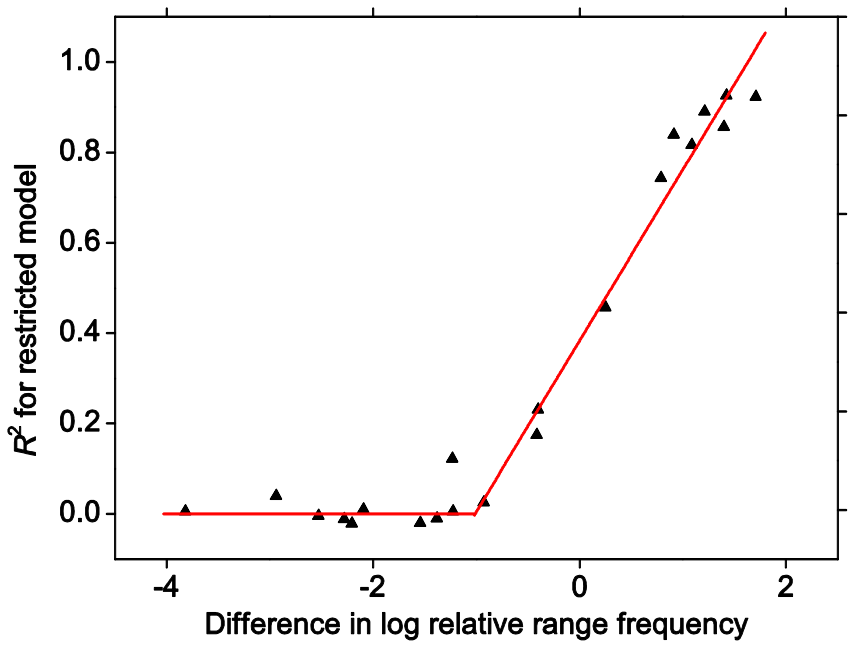

Figure 6.2: Dependence of goodness of fit of the restricted model on the difference in relative frequency ranges. Proportion R^2 of variance accounted for by Equation 6.5 is plotted against the difference in ranges of log N_0/N and log N_1/N_0. The red line represents a linear regression.

The regression based on another restricted model defined by Equation 6.6 was weak, as shown in the second column from last of Table 6.4. For all n, all three pairs of daylights, and both thresholds, mean $R^2 = 0.24$ (mean SE = 0.11) [88].

6.2.1.3 Prediction within CIELAB

The goodness of fit of the regression within CIELAB is summarized in Table 6.5. Due to the smaller number of samples (3000 points) selected for simulation, the probability of $N_1 = 0$ was higher. Therefore, there were fewer entries than in Table 6.4.

As expected, the performance within CIELAB is poorer than those within CIECAM02. For instance, with $n = 1$, mean $R^2 = 0.73$ (mean SE = 0.11) for the full model defined by Equation 6.4; for the restricted model defined by Equation 6.5, mean $R^2 = 0.62$ (mean SE = 0.11); and for the restricted model defined by Equation 6.6, mean $R^2 = 0.12$ (mean SE = 0.10).

Table 6.5: Regression over 50 scenes of log observed relative frequency of metamerism on estimated differential entropy within CILAB with colour-difference formula CIEDE2000 [150] for various nominal colour difference thresholds, criterion degrees of metamerism, and daylights with different CCTs [88].

Threshold[a] ΔE^{thr}	Criterion degree[b] n	1st daylight CCT, K	2nd daylight CCT, K	R^2 Eq. (7)[c]	R^2 Eq. (8)[d]	R^2 Eq. (6)[e]
0.5	1	4000	25000	0.75	0.24	0.78
		4000	6500	0.67	0.13	0.74
		6500	25000	0.77	0.22	0.82
	2[f]	4000	25000	0.34	0.00[g]	0.67
		4000	6500	0.03	0.08	0.51
	3[f]	4000	25000	0.01	0.10	0.47
1.0	1	4000	25000	0.54	0.05	0.68
		4000	6500	0.49	0.01	0.67
		6500	25000	0.53	0.04	0.71
	2[f]	4000	25000	0.01	0.12	0.49

[a] Nominal threshold for color differences under first daylight, giving N_0 pairs out of $N \approx 1.25\times10^9$ pairs chosen randomly from each of the 50 scenes

[b] Multiple of ΔE^{thr} for color differences under second daylight, giving N_1 pairs out of N_0

[c] Proportion of variance accounted for by restricted linear model Equation 6.5.

[d] Proportion of variance accounted for by restricted linear model Equation 6.6.

[e] Proportion of variance accounted for by restricted linear model Equation 6.4.

[f] Results for other daylight pair or pairs omitted as $N_1 = 0$ for one or more scenes

[g] Adjustment for degrees of freedom omitted, as invalid

There are two possible reasons behind this poorer performance. First, although the colour-difference formula CIEDE2000 helped improve the uniformity within CIELAB, the formula can only be used for estimating the relative frequency of metamerism, not for entropy. Second, the extent of the chromatic adaptation was different within two colour spaces [88].

6.2.2 Predicting the conditional frequency of metamerism

The logarithm of the observed conditional relative frequency of metamerism was also regressed on the different combinations of estimates of $h(U_1)$ and $h(U_2 \mid U_1)$ over the 50 scenes, respectively [156]. The goodness of fit of the regression is summarized in Table 6.6.

The results based on the full model defined by Equation 6.4 are shown in the last column of Table 6.6. For $n \geq 2$, the regression was strong for all changes in illuminant and both thresholds, with mean $R^2 = 0.70$ (mean SE = 0.20). The regression was less strong for $n = 1$, with mean $R^2 = 0.53$ (mean SE = 0.09). When n increased, the regression was slightly stronger.

As shown in the third column from last of Table 6.6, the regression based on the restricted model defined by Equation 6.5 was very weak. For all conditions, mean $R^2 = 0.18$ (mean SE = 0.09). This is unsurprising because a model based solely on $h(U_1)$ is not able to describe two random variables U_1 and U_2 that have some degree of independence.

By contrast, the regression based on another restricted model defined by Equation 6.6 was stronger, as shown in the second column from last of Table 6.6. For all conditions, mean $R^2 = 0.62$ (mean SE = 0.08).

The dependence between the conditional relative frequency of metamerism and the different combinations of entropies is as strong as the dependence between the relative frequency of metamerism and the different combinations of entropies. This is mainly because the conditional entropy $h(U_2 \mid U_1)$ describes the uncertainty of all colours under the second daylight given the knowledge of the colours under the first daylight, rather than of only those becoming distinguishable after a change in daylight.

Table 6.6: Regression over 50 scenes of log observed conditional relative frequency of metamerism on estimated differential entropy within CIECAM02 [149] for various nominal colour difference thresholds, criterion degrees of metamerism, and daylights with different correlated colour temperatures.

Threshold[a] ΔE^{thr}	Criterion degree[b] n	1st daylight CCT, K	2nd daylight CCT, K	R^2 Eq. 6.5[c]	R^2 Eq. 6.6[d]	R^2 Eq. 6.4[e]
0.5	1	4000	25000	0.15	0.64	0.69
		4000	6500	0.06	0.47	0.59
		6500	25000	0.06	0.41	0.43
	2	4000	25000	0.22	0.69	0.71
		4000	6500	0.19	0.63	0.67
		6500	25000	0.19	0.64	0.64
	3	4000	25000	0.26	0.71	0.72
		4000	6500	0.27	0.73	0.75
		6500	25000	0.23	0.71	0.71
	4[f]	4000	25000	0.28	0.75	0.76
		4000	6500	0.34	0.73	0.73
		6500	25000	0.25	0.72	0.72
1.0	1	4000	25000	0.15	0.64	0.69
		4000	6500	0.00	0.31	0.47
		6500	25000	0.03	0.27	0.29
	2	4000	25000	0.20	0.70	0.73
		4000	6500	0.11	0.44	0.48
		6500	25000	0.16	0.61	0.63
	3[f]	4000	25000	0.25	0.75	0.76
		6500	25000	0.21	0.66	0.67
	4[f]	4000	25000	0.26	0.74	0.76

[a] Nominal threshold for color differences under first daylight, giving N_0 pairs out of $N \approx 1.25 \times 10^9$ pairs chosen randomly from each of the 50 scenes

[b] Multiple of ΔE^{thr} for color differences under second daylight, giving N_1 pairs out of N_0

[c] Proportion of variance accounted for by restricted linear model Equation 6.5.

[d] Proportion of variance accounted for by restricted linear model Equation 6.6.

[e] Proportion of variance accounted for by restricted linear model Equation 6.4.

[f] Results for other daylight pair or pairs omitted as $N_1 = 0$ for one or more scenes

6.3 Discussion

It has been shown that the frequency and the conditional frequency of metamerism in natural scenes can be predicted. But the performance of prediction of the frequency of metamerism was much stronger than those of the conditional frequency of metamerism. In this section, two questions about the prediction of the frequency of metamerism are addressed. First, why does the combination of differential entropies of colours have such predictive power? Second, given a change in the procedure for obtaining a numerical specification of colours, how robust is this dependence between the frequency of metamerism and the different combinations of entropies?

6.3.1 Explanation of predictive power

Despite the fact that the full model defined by Equation 6.4 has only three explanatory variables, for $n = 1$, the mean proportion R^2 of variance accounted for by the full model was 0.90 within CIECAM02, and for $n \geq 2$, it was 0.66. The loss in dependence with larger n was expected. It is because as n increases, the frequency N_1/N became more and more influenced by the tails of the distribution of colours [88].

Nevertheless, it was unexpected that with even fewer explanatory variables, the restricted model defined by Equation 6.5 would retain such strong predictive power. For $n = 1$, the mean proportion R^2 of variance accounted for by this restricted model was 0.88, which was very close to that for the full model. But for $n \geq 2$, this restricted model failed completely, with mean R^2 falling to 0.12 [88].

As mentioned in Chapter 6, Section 6.1.1, for a criterion degree of metamerism of $n = 1$, most of the variation in the relative frequency of metamerism is determined by the probability of finding a pair of indistinguishable surfaces under the first daylight, rather than by the conditional probability of their becoming distinguishable under the second daylight. There was a high dependence between the differential entropy of colour $h(U_1)$ under the first

daylight and the number of indistinguishable pairs N_0 under the first daylight (explained in Chapter 6, Section 6.3.1.1). Therefore, for n = 1, when the variation of N_1/N was influenced mainly by the variation of N_0/N, the regression of the relative frequency was very strong. As n increased, the variation of N_0/N became less influential, and the regression became weaker [88].

6.3.1.1 Differential entropy and indistinguishable surfaces

Assume there are two random variables X and Y, both representing one colour attribute, such as hue. Suppose random variable X is uniformly distributed over the range $[-a, a]$, and zero elsewhere (i.e. all hue values equally likely in the scene). Suppose random variable Y is constant over a region of size Δa ($\Delta a \leq 2a$) centred at the origin, and zero elsewhere (i.e. only one hue value in the scene) [88].

For X, The relative frequency of finding two points at random within Δa is approximately $\Delta a/a$, which is the lowest for all distributions over the interval $[-a, a]$. For Y, the relative frequency of finding two points at random within Δa of each other is exactly 1, which is the highest.

On the contrary, the differential entropy $h(X) = \log 2a$, which is the highest over the interval $[-a, a]$, and the differential entropy $h(Y) = \log \Delta a$, which tends to minus infinity, as Δa tends to zero [77].

This inverse relationship was also true for the differential entropy of colours under the first daylight and the number of indistinguishable pairs under the first daylight. Figure 6.3 illustrated the dependence of the frequency of metamerism on the entropy of colours under the first illuminant within CIECAM02. The illuminant changed from daylights with CCTs 4000 K to 25,000 K. The nominal colour-difference threshold ΔE^{thr} was 0.5.

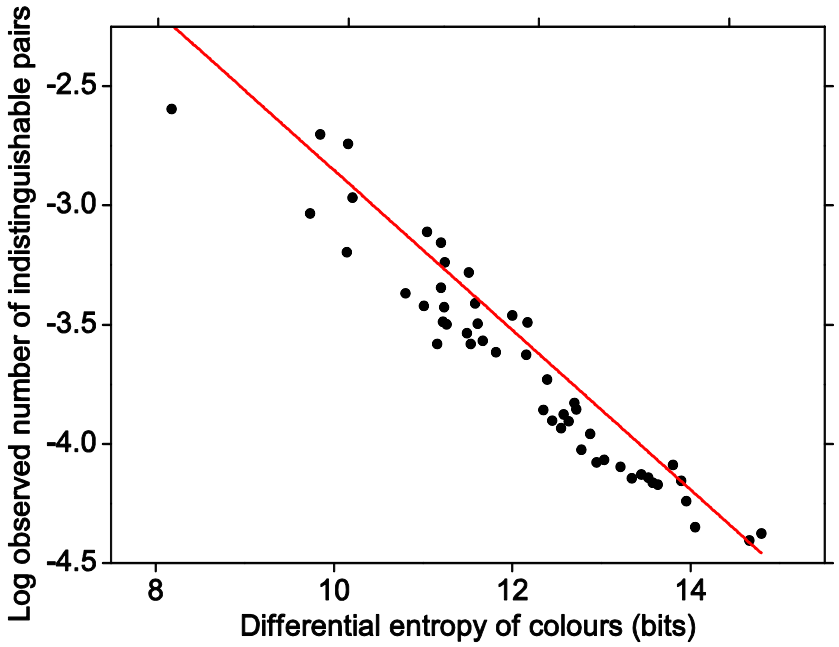

Figure 6.3: Regression of the number of indistinguishable pairs under the first daylight on the differential entropy of colours within CIECAM02.

6.3.1.2 Limitation of differential entropy

Although for present purposes differential entropy is a better description of the randomness of colour distributions than variance or colour gamut [88], the predictive power of the restricted models based on h(U_1) is inadequate with extreme criterion degrees of metamerism. Only the full model with the combination of entropies was able to reliably predict the frequency of metamerism. But there was still small proportion of the variation in the frequency of metamerism that could not be accounted for.

6.3.2 Robustness of strong dependence

Reversing the direction of illuminant changes resulted in small changes in relative frequency of metamerism [71]. But do these changes affect the strong relationship between the relative frequency and the combination of entropies? In

fact, the effects were small. Within CIECAM02, reversing the direction made the mean R^2 of the regression based on the full model fall by 0.08 for $n = 1$, and fall by 0.06 for $n \geq 2$. Within CIELAB, reversing the direction made mean R^2 rise by 0.07 for $n = 1$, and rise by 0.09 for $n \geq 2$.

It might be argued that if the observer does not adapt to D65, the effective colour distribution would be different, and consequently the differential entropy and the relative frequency of metamerism. To test the dependence under this condition, the coordinates J, a_C and b_C within CIECAM02 were obtained without chromatic adaptation at the reference illuminant D65. For $\Delta E^{thr} = 0.5$ with degree of metamerism of $n = 1$, the regression remained very strong for all three pairs of daylights, with mean $R^2 = 0.89$ (mean SE = 0.03). For $\Delta E^{thr} = 1$ with $n = 1$, mean $R^2 = 0.83$ (mean SE = 0.04).

If more scenes from other sources were included, would this affect the strong dependence? Two hyperspectral images from [157] were included to test the predictive power of different combination of differential entropies. Within CIECAM02, the goodness of fit of the full model defined by Equation 6.4 remained strong. For $n = 1$, the regression was very strong for all three pairs of daylights and both thresholds, with mean $R^2 = 0.89$ (mean SE = 0.02). The regression became less strong, for $n \geq 2$, with mean $R^2 = 0.65$ (mean SE = 0.09). The performance of the restricted model defined by Equation 6.5 was also consistent. For $n = 1$, mean $R^2 = 0.87$ (mean SE = 0.03), and for $n \geq 2$, mean $R^2 = 0.11$ (mean SE = 0.05).

Despite the technical changes made earlier, therefore, the different combinations of entropies of colours retain their predictive power of estimating the frequency of metamerism.

Chapter 7. Conclusion

There were three objectives of this thesis. The first was to construct models for predicting the frequency and the conditional frequency of metamerism in natural scenes, which was addressed in Chapter 6. The second was to determine whether colour gamut is a good description of the distribution of surface colours in natural scenes, which was addressed in Chapter 4. The third was to analyse the spectral reflectances of surfaces in natural scenes, which was addressed in Chapter 5.

The key results of this thesis and possible future work based on these results are described in this chapter.

7.1 Key results

The key findings of thesis were mainly obtained from the 50 natural scenes. Although the dataset is finite, it includes rural and urban images with different viewing distances, and different range of land-cover surfaces were represented in the data.

7.1.1 Predicting the frequency of metamerism

The frequency of metamerism offers a quantitative measurement of the reliability of material identity based on colours in natural scenes. More generally, it tells us whether the trichromacy is a good comprise for encoding the spectral reflectance in natural scenes. It was shown that the frequency of metamerism can be predicted. There was strong dependence of the frequency of metamerism on the combination of two entropies of colours: the differential entropy of the colours under one illuminant and the conditional differential entropy of those colours under another illuminant. It was found the differential entropy of colours alone has strong predictive power in estimating the frequency of metamerism when the criterion degree of metamerism was not extreme. There are two main possible contributory factors. First, when the criterion degree of metamerism was not

extreme, the most variation in the frequency of metamerism in natural scenes was determined by the probability of finding a pair of indistinguishable surfaces under the first daylight. Second, there was an inverse relationship between the differential entropy of colours and the number of indistinguishable colours under one illuminant. It means that when the criterion degree of metamerism is not extreme, higher uncertainty the colour has at a random point under one illuminant, less metamerism happens after a change in illuminant.

7.1.2 Using colour gamut as a description of colour information

Two different methods were used to estimate the volumes of the colour gamuts of natural scenes. The method based on convex-hull algorithms was not suited to estimating the volume accurately because colour distributions within a colour space of a natural scene can be concave. On the other hand, with certain colour difference thresholds, the logarithm of the volume of the colour gamut within CIECAM02 calculated by the cube-counting algorithm showed very strong linear dependence on the estimated differential entropy over 50 natural scenes. It is because these volumes can be treated as an approximation of the discrete entropy, apart from a scaling factor, that they have a strong dependence on the corresponding differential entropy. This result means that given a reasonable colour difference threshold for the colour cubes, and within an approximately perceptually uniform colour space, the gamut volume can provide a good description of the uncertainty of colour appearance in natural scenes. It must fail, however, when the distribution of colours with the gamut is very non-uniform.

7.1.3 Analysis of reflectances in natural scenes

The spectral the reflectances of the surfaces with relevance to human vision in natural scenes were analysed to determine the minimum number of basis functions needed for an accurate approximation of spectral reflectances in natural scenes. The accuracy of the approximations was measured by mathematical quantities and colorimetric differences between the original and the

approximated reflectances. For colour vision, the results from PCA mean that a three-dimensional linear model is unlikely to recover most of the spectral information in natural scenes. In addition, the basis functions revealed by PCA cannot be related to real pigments because PCA is intended to explain the largest global variance.

The reflectances of the surfaces underlying metamerism in natural scenes were found to be similar. It may indicate that the majority of metamerism comes from surfaces which consist of the same material, such as grasses and leaves.

7.2 Future work

7.2.1 More comprehensive model for predicting frequency of metamerism

The models for predicting the frequency of metamerism in natural scenes are imperfect. Even based on the full model, some of the variation in the frequency of metamerism was not accounted for. Furthermore, the proportion of the variation in the conditional frequency of metamerism which cannot be accounted for by the models was even larger. More explanatory variables or higher orders might be needed in order to predict the frequency and the conditional frequency of metamerism more accurately.

7.2.2 Threshold of distinguishability in colour spaces

The threshold of visual distinguishability between different colours played an important role both in the estimation of the volume of colour gamut and the estimation of the frequency of metamerism in natural scenes. Although a range of thresholds were used in this thesis, a more precise definition of the distinguishability in different colour spaces will make the estimation of gamut volumes and frequency of metamerism more relevant to human vision.

7.2.3 Non-linear model for approximations of reflectances

As mentioned in Chapter 5, independent component analysis was used to analyse the spectral reflectances because, unlike principal component analysis, it does not require orthogonality between basis functions. But there are practical difficulties about ranking the significance of independent components from ICA. If a criterion related to distinguishability of human vision can be used for ranking the significance, it might help reduce the dimensionality of accurately approximating the spectral reflectances in natural scenes.

7.2.4 More accurate estimator of differential entropy

Although the robustness of the application of the offset version of Kozachenko-Leonenko estimator on colour appearance was examined in this thesis, this estimator is still imperfect, especially for the samples with small size. The accuracy might be improved if the bias introduced by the nearest-neighbours algorithm can be reduced.

Chapter 8. Appendix

8.1 Parameters of transformation from CIEXYZ to CIECAM02

There were three different settings for transformation from CIEXYZ to CIECAM02 [65] in this thesis. The main differences were the degree of adaptation and the choice of the reference daylight for adaptation.

The values of the three adopted white [67] are [99.5972, 100.0000, 60.8812] for the daylight with CCT of 4,000 K, [95.0470, 100.0000, 108.8830] for the daylight with CCT of 6,500 K, and [97.9655,100.0000, 194.0558] for the daylight with CCT of 25,000 K.

According to the specification of CIECAM02 [65], the luminance of adapting field L_A was set to 20 cd/m^2; background luminance Y_b was set to be equal to the mean of the luminance component of the tristimulus values over a scene under a certain illuminant; and the surround was assumed to be 'average'. If the observer was assumed to be fully adapted to the illuminant, the degree of adaptation was kept to 1.

References

1. CIE, "History of the CIE," (International Commision on Illumination, Vienna, 1990).
2. S. K. Shevell, *The science of color* (Elsevier Science, 2003).
3. G. Wyszecki and W. S. Stiles, *Color Science: Concepts and Methods, Quantitative Data and Formulae,* 2nd ed. (Wiley-Interscience 1982).
4. K. R. Gegenfurtner and D. C. Kiper, "Color Vision," Annu. Rev. Neurosci. **26**, 181-206 (2003).
5. S. G. Solomon and P. Lennie, "The machinery of colour vision," Nat Rev Neurosci **8**, 276-286 (2007).
6. W. S. Geisler and M. S. Banks, "Visual performance," in *Handbook of optics*, M. Bass, ed. (McGraw-Hill, 2010).
7. J. B. R. Hammond, B. R. Wooten, and D. M. Snodderly, "Individual variations in the spatial profile of human macular pigment," J. Opt. Soc. Am. A **14**, 1187-1196 (1997).
8. J. Jonas, U. Schneider, and G. H. Naumann, "Count and density of human retinal photoreceptors," Graefe's Arch Clin Exp Ophthalmol **230**, 505-510 (1992).
9. J. B. Jonas, A. M. Schmidt, J. A. Mullerbergh, U. M. Schlotzerschrehardt, and G. O. H. Naumann, "Human optic-berve fiber count and optic disk size," Investigative ophthalmology & visual science **33**, 2012-2018 (1992).
10. X. Pitkow and M. Meister, "Decorrelation and efficient coding by retinal ganglion cells," Nat Neurosci **15**, 628-635 (2012).
11. M. A. Webster and D. I. A. MacLeod, "Factors underlying individual differences in the color matches of normal observers," J. Opt. Soc. Am. A **5**, 1722-1735 (1988).
12. CIE/ISO, "CIE Colorimetry - Part 1: Standard Colorimetric Observers " (CIE/ISO, Vienna, 2006).
13. P. Cornelissen, A. Richardson, A. Mason, S. Fowler, and J. Stein, "Contrast sensitivity and coherent motion detection measured at photopic

luminance levels in dyslexics and controls," Vision Res. **35**, 1483-1494 (1995).

14. A. Augustin and Augustin, "The physiology of scotopic vision, contrast vision, color vision, and circadian rhythmicity: can these parameters be influenced by blue-light-filter lenses?," Retina **28**, 1179-1187 (2008).
15. A. Stockman and L. T. Sharpe, "The spectral sensitivities of the middle- and long-wavelength-sensitive cones derived from measurements in observers of known genotype," Vision Res. **40**, 1711-1737 (2000).
16. A. Stockman, L. T. Sharpe, and C. Fach, "The spectral sensitivity of the human short-wavelength sensitive cones derived from thresholds and color matches," Vision Res. **39**, 2901-2927 (1999).
17. A. Stockman, C. Ripamonti, B. Henning, and D. Petrova, "Colour & Vision Research Laboratory."
18. W. S. Geisler, "Visual Perception and the Statistical Properties of Natural Scenes," Annual Review of Psychology **59**, 167-192 (2008).
19. L. T. Sharpe, A. Stockman, W. Jagla, and H. Jägle, "A luminous efficiency function, V*(λ), for daylight adaptation," J. Vision **5**(2005).
20. A. Stockman, H. Jägle, M. Pirzer, and L. T. Sharpe, "The dependence of luminous efficiency on chromatic adaptation," J. Vision **8**(2008).
21. P. K. Kaiser and R. M. Boynton, *Human Color Vision*, 2nd ed. (Optical Society of America, Washington, DC, 1996).
22. T. Young, "The Bakerian Lecture: Experiments and Calculations Relative to Physical Optics," Phil. Trans. R. Soc. Lond. **94**, 1-16 (1804).
23. W. B. Marks, W. H. Dobelle, and E. F. MacNichol, "Visual Pigments of Single Primate Cones," Science **143**, 1181-1182 (1964).
24. R. L. De Valois, I. Abramov, and G. H. Jacobs, "Analysis of Response Patterns of LGN Cells," J. Opt. Soc. Am. **56**, 966-977 (1966).
25. A. M. Derrington, J. Krauskopf, and P. Lennie, "Chromatic mechanisms in lateral geniculate nucleus of macaque," The Journal of physiology **357**, 241-265 (1984).
26. L. M. Hurvich and D. Jameson, "An opponent-process theory of color-vision," Psychological review **64**, 384-404 (1957).

27. J. Krauskopf, D. R. Williams, and D. W. Heeley, "Cardinal directions of color space," Vision Res. **22**, 1123-1131 (1982).
28. C. R. Ingling Jr and B. H.-P. Tsou, "Orthogonal combination of the three visual channels," Vision Res. **17**, 1075-1082 (1977).
29. A. Stockman and D. H. & Brainard, *Color vision mechanisms,* 3rd ed., The Optical Society of America Handbook of Optics (McGraw Hill, New York, 2009), Vol. III: Vision and Vision Optics.
30. G. W. Larson, H. Rushmeier, and C. Piatko, "A visibility matching tone reproduction operator for high dynamic range scenes," Visualization and Computer Graphics, IEEE Transactions on **3**, 291-306 (1997).
31. R. Rodieck, *The First Steps in Seeing* (Sinauer Associates, 1998).
32. M. A. Webster and J. D. Mollon, "Adaptation and the color statistics of natural images," Vision Res. **37**, 3283-3298 (1997).
33. M. A. Webster, "Adaptation and visual coding," J. Vision **11**(2011).
34. T. D. Lamb and E. N. Pugh, "Phototransduction, Dark Adaptation, and Rhodopsin Regeneration The Proctor Lecture," Investigative ophthalmology & visual science **47**, 5138-5152 (2006).
35. M. D. Fairchild and L. Reniff, "Time course of chromatic adaptation for color-appearance judgments," J. Opt. Soc. Am. A **12**, 824-833 (1995).
36. B. J. Craven and D. H. Foster, "An operational approach to colour constancy," Vision Res. **32**, 1359-1366 (1992).
37. O. Rinner and K. R. Gegenfurtner, "Time course of chromatic adaptation for color appearance and discrimination," Vision Res. **40**, 1813-1826 (2000).
38. D. G. Pelli and B. Farell, "Psychophysical methods," in *Handbook of optics*, M. Bass, ed. (McGraw-Hill, 2010).
39. M. A. Georgeson and G. D. Sullivan, "Contrast constancy: deblurring in human vision by spatial frequency channels," The Journal of physiology **252**, 627-656 (1975).
40. G. S. Brindley, *Physiology of the retina and the visual pathway,* 2nd ed. (Edward Arnold Ltd., London, 1960).
41. W. S. Stiles and J. M. Burch, "Interim Report to the Commission Internationale de l'Eclairage, Zurich, 1955, on the National Physical

Laboratory's Investigation of Colour-matching (1955)," Optica Acta: International Journal of Optics **2**, 168 - 181 (1955).

42. W. D. Wright, "A re-determination of the trichromatic coefficients of the spectral colours," Trans. Opt. Soc. **30**, 141 (1929).
43. J. Guild, "The colorimetric properties of the spectrum," Phil. Trans. R. Soc. A **A 230**, 149–187 (1931).
44. H. S. Fairman, M. H. Brill, and H. Hemmendinger, "How the CIE 1931 color-matching functions were derived from Wright-Guild data," Color Res. Appl. **22**, 11-23 (1997).
45. CIE, "Fundamental chromaticity diagram with physiological axes – Parts 1," 170-1 (Central Bureau of the Commission Internationale de l' Éclairage, Vienna, 2006).
46. CIE/ISO, "CIE Colorimetry - Part 2: CIE standard illuminants," (CIE/ISO, Vienna, 2006).
47. D. H. Foster, "Color constancy," Vision Res. **51**, 674-700 (2011).
48. D. H. Brainard and B. A. Wandell, "Analysis of the retinex theory of color vision," J. Opt. Soc. Am. A **3**, 1651-1661 (1986).
49. E. H. Land and J. J. McCann, "Lightness and Retinex Theory," J. Opt. Soc. Am. **61**, 1-11 (1971).
50. G. D. Finlayson, M. S. Drew, and B. V. Funt, "Spectral sharpening: sensor transformations for improved color constancy," J. Opt. Soc. Am. A **11**, 1553-1563 (1994).
51. G. D. Finlayson, M. S. Drew, and B. V. Funt, "Color constancy: generalized diagonal transforms suffice," J. Opt. Soc. Am. A **11**, 3011-3019 (1994).
52. Y. Nayatani, "A simple estimation method for effective adaptation coefficient," Color Res. Appl. **22**, 259-268 (1997).
53. Y. Nayatani, "Revision of the chroma and hue scales of a nonlinear color-appearance model," Color Res. Appl. **20**, 143-155 (1995).
54. CIE, "Colorimetry," 15:2004 (CIE Central Bureau, Vienna, 2004a).
55. Y. Liu, J. Shigley, E. Fritsch, and S. Hemphill, "Abnormal Hue-Angle change of the gemstone tanzanite between CIE illuminants d65 and a in CIELAB color space," Color Res. Appl. **20**, 245-250 (1995).

56. N. Moroney, "A hypothesis regarding the poor blue constancy of CIELAB," Color Res. Appl. **28**, 371-378 (2003).
57. D. L. MacAdam, "Colorimetric data for samples of OSA uniform color scales," J. Opt. Soc. Am. **68**, 121-130 (1978).
58. D. L. MacAdam, "Uniform color scales," J. Opt. Soc. Am. **64**, 1691-1702 (1974).
59. M. Melgosa, J. J. Quesada, and E. Hita, "Uniformity of some recent color metrics tested with an accurate color-difference tolerance dataset," Appl. Opt. **33**, 8069-8077 (1994).
60. F. J. J. Clarke, R. McDonald, and B. Rigg, "Modification to the JPC79 Colour–difference Formula," J. Soc. Dyers Colour. **100**, 128-132 (1984).
61. M. R. Luo and B. Rigg, "BFD (l:c) colour-difference formula Part 2-Performance of the formula," J. Soc. Dyers Colour. **103**, 126-132 (1987).
62. M. R. Luo and B. Rigg, "BFD (l:c) colour-difference formula Part 1-Development of the formula," J. Soc. Dyers Colour. **103**, 86-94 (1987).
63. CIE, "Industrial Color Difference Evaluation," 116 (Central Bureau of the CIE, Vienna, 1995).
64. M. R. Luo, G. Cui, and B. Rigg, "The development of the CIE 2000 colour-difference formula: CIEDE2000," Color Res. Appl. **26**, 340-350 (2001).
65. CIE, "A colour appearance model for colour management system: CIECAM02," 159:2004 (CIE Central Bureau, Vienna, 2004b).
66. CIE, "The CIE 1997 interim colour appearance model (simple version), CIECAM97s, CIE 131-1998," 1520-6378 (Wiley Subscription Services, Inc., A Wiley Company, 1998).
67. S. Westland and C. Ripamonti, *Computational Colour Science Using MATLAB* (Wiley-Blackwell 2004).
68. N. Moroney and H. Zeng, "Field trials of the CIECAM02 color appearance model," (Hewlett-Packard Laboratories, 2003).
69. M. R. Luo, G. Cui, and C. Li, "Uniform colour spaces based on CIECAM02 colour appearance model," Color Res. Appl. **31**, 320-330 (2006).

70. G. Cui, M. R. Luo, B. Rigg, G. Roesler, and K. Witt, "Uniform colour spaces based on the DIN99 colour-difference formula," Color Res. Appl. **27**, 282-290 (2002).
71. D. H. Foster, K. Amano, S. M. C. Nascimento, and M. J. Foster, "Frequency of metamerism in natural scenes," J. Opt. Soc. Am. A **23**, 2359-2372 (2006).
72. D. H. Foster, S. Nascimento, Eacute, M. C. Rgio, and K. Amano, "Information limits on neural identification of colored surfaces in natural scenes," Visual Neurosci. **21**, 331-336 (2004).
73. FGDC, "National Vegetation Classification Standard (Version 2)," (Federal Geographic Data Committee, U.S. Geological Survey, Reston, Virginia, 2008).
74. UNESCO, "International classification and mapping of vegetation," (UNESCO standing Committee on Classification and Mapping of Vegetation on a World Basis, Paris, 1973).
75. R. G. W. Hunt, *Measuring Colour*, 3rd ed. (Fountain Press, Kingston-upon-Thames, England, 1998).
76. C. E. Shannon, "A mathematical theory of communication," Bell Syst. Tech. J. **27**, 379-423 and 623-656 (1948).
77. T. M. Cover and J. A. Thomas, *Elements of Information Theory*, 2nd ed. (Wiley-Interscience, 2006).
78. T. Troscianko, C. P. Benton, P. G. Lovell, D. J. Tolhurst, and Z. Pizlo, "Camouflage and visual perception," Philos. Trans. R. Soc. B-Biol. Sci. **364**, 449-461 (2009).
79. Z. Li and R. S. Berns, "Comparison of methods of parameric correction for evaluating metamerism," Color Res. Appl. **32**, 293-303 (2007).
80. G. Wyszecki, "Evaluation of Metameric Colors," J. Opt. Soc. Am. **48**, 451-452 (1958).
81. J. B. Cohen and W. E. Kappauf, "Metameric Color Stimuli, Fundamental Metamers, and Wyszecki's Metameric Blacks," The American Journal of Psychology **95**, 537-564 (1982).
82. R. S. Berns and F. W. Billmeyer, "Proposed indices of metamerism with constant chromatic adaptation," Color Res. Appl. **8**, 186-189 (1983).

83. M. J. Garrett and D. F. Mark, "A top down description of S-CIELAB and CIEDE2000," Color Res. Appl. **28**, 425-435 (2003).
84. M. R. Luo, B. Rigg, and K. J. Smith, "CMC 2002 colour inconstancy index; CMCCON02," Color. Technol. **119**, 280-285 (2003).
85. D. B. Judd, D. L. Macadam, G. Wyszecki, H. W. Budde, H. R. Condit, S. T. Henderson, and J. L. Simonds, "Spectral distribution of typical daylight as a function of correlated color temperature," J. Opt. Soc. Am. **54**, 1031-1036 (1964).
86. IEC, "Multimedia systems and equipment–colour measurement and management–part 2-1: Colour management–default RGB colour space–sRGB," (International Electrotechnical Commission Brussels, 1999).
87. S. M. C. Nascimento, F. P. Ferreira, and D. H. Foster, "Statistics of spatial cone-excitation ratios in natural scenes," J. Opt. Soc. Am. A **19**, 1484-1490 (2002).
88. G. Feng and D. H. Foster, "Predicting frequency of metamerism in natural scenes by entropy of colors," J. Opt. Soc. Am. A **29**, A200-A208 (2012).
89. P. Sun and P. Morovic, "Inter-relating colour difference metrics," in *IS&T/SID Tenth Color Imaging Conference: Color Science and Engineering Systems, Technologies, and Applications*, (Society for Imaging Science and Technology, 2002), 55-60.
90. S. M. Nascimento, D. H. Foster, and K. Amano, "Psychophysical estimates of the number of spectral-reflectance basis functions needed to reproduce natural scenes," J. Opt. Soc. Am. A **22**, 1017-1022 (2005).
91. G. Sharma, W. Wu, and E. N. Dalal, "The CIEDE2000 color-difference formula: Implementation notes, supplementary test data, and mathematical observations," Color Res. Appl. **30**, 21-30 (2005).
92. D. H. Foster, I. Marín-Franch, K. Amano, and S. M. C. Nascimento, "Approaching ideal observer efficiency in using color to retrieve information from natural scenes," J. Opt. Soc. Am. A **26**, B14-B24 (2009).
93. G. Buchsbaum and A. Gottschalk, "Trichromacy, Opponent Colours Coding and Optimum Colour Information Transmission in the Retina,"

Proceedings of the Royal Society of London. Series B. Biological Sciences **220**, 89-113 (1983).

94. A. Kraskov, H. Stögbauer, and P. Grassberger, "Estimating mutual information," Phys. Rev. E **69**, 066138 (2004).
95. P. Grassberger, "Entropy Estimates from Insufficient Samplings," http://arxiv.org/abs/physics/0307138 (2003).
96. G. A. Darbellay and I. Vajda, "Estimation of the Information by an Adaptive Partitioning of the Observation Space," IEEE Trans. Inf. Theory **45**, 1315 (1999).
97. T. Hastie, R. Tibshirani, and J. Friedman, *The Elements of Statistical Learning*, 2nd ed., Springer Series in Statistics (Springer, 2009).
98. B. W. Silverman, *Density Estimation for Statistics and Data Analysis (Monographs on Statistics and Applied Probability)*, 1 ed. (CRC Press, London, 1986).
99. L. F. Kozachenko and N. N. Leonenko, "Sample estimate of the entropy of a random vector," Problems of Information Transmision **23**, 95-101 (1987).
100. M. N. Goria, N. N. Leonenko, V. V. Mergel, and P. L. N. Inverardi, "A new class of random vector entropy estimators and its applications in testing statistical hypotheses," J. Nonparametr. Stat. **17**, 277 - 297 (2005).
101. I. Marín-Franch, "Information-theoretic analysis of trichromatic images of natural scenes under different phases of daylight," PhD Thesis (University of Manchester, Manchester, 2009).
102. R. Luther, "Aus dem Gebiet der Farbreizmetrik (On color stimulus metrics)," Zeitschrift für technische Physik **8**, 540-558 (1927).
103. J. M. M. Linhares, P. D. Pinto, and S. M. C. Nascimento, "The number of discernible colors in natural scenes," J. Opt. Soc. Am. A **25**, 2918-2924 (2008).
104. R. G. Kuehni, "The early development of the Munsell system," Color Res. Appl. **27**, 20-27 (2002).
105. J. Morovic and M. R. Luo, "The fundamentals of gamut mapping: A survey," J. Imaging Sci. Technol. **45**, 283-290 (2001).

106. C. Li, M. R. Luo, B. Rigg, and R. W. G. Hunt, "CMC 2000 chromatic adaptation transform: CMCCAT2000," Color Res. Appl. **27**, 49-58 (2002).
107. A. M. Bakke, I. Farup, and J. Y. Hardeberg, "Evaluation of algorithms for the determination of color gamut boundaries," J. Imaging Sci. Technol. **54**, 050502 (2010).
108. R. Balasubramanian and E. Dalal, "A method for quantifying the color gamut of an output device," Proc. SPIE **3018**, 110–116 (1997).
109. M. R. Pointer and G. G. Attridge, "The number of discernible colours," Color Res. Appl. **23**, 52-54 (1998).
110. D. B. Montgomery and D. G. Morrison, "A Note on Adjusting R^2," The Journal of Finance **28**, 1009-1013 (1973).
111. M. Melgosa, R. Huertas, and R. S. Berns, "Performance of recent advanced color-difference formulas using the standardized residual sum of squares index," J. Opt. Soc. Am. A **25**, 1828-1834 (2008).
112. H. S. Fairman and M. H. Brill, "The principal components of reflectances," Color Res. Appl. **29**, 104-110 (2004).
113. L. T. Maloney, "Evaluation of linear models of surface spectral reflectance with small numbers of parameters," J. Opt. Soc. Am. A **3**, 1673-1683 (1986).
114. L. T. Maloney and B. A. Wandell, "Color constancy: a method for recovering surface spectral reflectance," J. Opt. Soc. Am. A **3**, 29-33 (1986).
115. A. Mansouri, T. Sliwa, J. Y. Hardeberg, and Y. Voisin, "Representation and estimation of spectral reflectances using projection on PCA and wavelet bases," Color Res. Appl. **33**, 485-493 (2008).
116. E. K. Oxtoby and D. H. Foster, "Perceptual limits on low-dimensional models of Munsell reflectance spectra," Perception **34**, 961-966 (2005).
117. A. K. Romney, "Relating reflectance spectra space to Munsell color appearance space," J. Opt. Soc. Am. A **25**, 658-666 (2008).
118. J. L. Dannemiller, "Spectral reflectance of natural objects: how many basis functions are necessary?," J. Opt. Soc. Am. A **9**, 507-515 (1992).

119. C.-C. Chiao, T. W. Cronin, and D. Osorio, "Color signals in natural scenes: characteristics of reflectance spectra and effects of natural illuminants," J. Opt. Soc. Am. A **17**, 218-224 (2000).
120. D.-Y. Tzeng and R. S. Berns, "A review of principal component analysis and its applications to color technology," Color Res. Appl. **30**, 84-98 (2005).
121. J. P. S. Parkkinen, J. Hallikainen, and T. Jaaskelainen, "Characteristic spectra of Munsell colors," J. Opt. Soc. Am. A **6**, 318-322 (1989).
122. J. Cohen, "Dependency of the spectral reflectance curves of the Munsell color chips," Psychonomic Science **1**, 369-370 (1964).
123. M. H. Brill, "A non-PC look at principal components," Color Res. Appl. **28**, 69-71 (2003).
124. Q. Chen, L. J. Wang, and S. Westland, "Analysis of Hyperspectral Images Based on PCA," Adv. Mater. Res. **187**, 641-646 (2011).
125. K. Mantere, J. Parkkinen, M. Mäntyjärvi, and T. Jaaskelainen, "Eigenvector interpretation of the Farnsworth-Munsell 100-hue test," J. Opt. Soc. Am. A **12**, 2237-2243 (1995).
126. H. K. Lichtenthaler, A. Gitelson, and M. Lang, "Non-Destructive Determination of Chlorophyll Content of Leaves of a Green and an Aurea Mutant of Tobacco by Reflectance Measurements," Journal of Plant Physiology **148**, 483-493 (1996).
127. D. A. Sims and J. A. Gamon, "Relationships between leaf pigment content and spectral reflectance across a wide range of species, leaf structures and developmental stages," Remote Sens. Environ. **81**, 337-354 (2002).
128. A. Hyvärinen and E. Oja, "Independent component analysis: algorithms and applications," Neural Netw. **13**, 411-430 (2000).
129. O. Kohonen, J. Parkkinen, and T. Jääskeläinen, "Databases for spectral color science," Color Res. Appl. **31**, 381-390 (2006).
130. J. Wang and C.-I. Chang, "Independent component analysis-based dimensionality reduction with applications in hyperspectral image analysis," Geoscience and Remote Sensing, IEEE Transactions on **44**, 1586-1600 (2006).

131. Z. Yang, S. LaConte, X. Weng, and X. Hu, "Ranking and averaging independent component analysis by reproducibility (RAICAR)," Human Brain Mapping **29**, 711-725 (2008).
132. D. D. Lee and H. S. Seung, "Algorithms for non-negative matrix factorization," Adv. Neural Inform. Process. Systems **13**, 556-562 (2001).
133. D. D. Lee and H. S. Seung, "Learning the parts of objects by non-negative matrix factorization," Nature **401**, 788-791 (1999).
134. G. Buchsbaum and O. Bloch, "Color categories revealed by non-negative matrix factorization of Munsell color spectra," Vision Res. **42**, 559-563 (2002).
135. M. W. Berry, M. Browne, A. N. Langville, V. P. Pauca, and R. J. Plemmons, "Algorithms and applications for approximate nonnegative matrix factorization," Comput. Stat. Data Anal. **52**, 155-173 (2007).
136. A. K. Romney and T. Indow, "Munsell reflectance spectra represented in three-dimensional Euclidean space," Color Res. Appl. **28**, 182-196 (2003).
137. S. Amirshahi and S. Amirhahi, "Adaptive non-negative bases for reconstruction of spectral data from colorimetric information," Opt. Rev. **17**, 562-569 (2010).
138. F. J. M. Schmitt, "A method for the treatment of metamerism in colorimetry," J. Opt. Soc. Am. **66**, 601-608 (1976).
139. K. Takahama and Y. Nayatani, "New Method for Generating Metameric Stimuli of Object Colors," J. Opt. Soc. Am. **62**, 1516-1520 (1972).
140. G. D. Finlayson and P. Morovic, "Metamer sets," J. Opt. Soc. Am. A **22**, 810-819 (2005).
141. S. G. Kandi and M. A. Tehran, "Applying metamer sets to investigate data dependency of principal component analysis method in recovery of spectral data," Color Res. Appl. **36**, 349-354 (2011).
142. S. Bianco, "Reflectance spectra recovery from tristimulus values by adaptive estimation with metameric shape correction," J. Opt. Soc. Am. A **27**, 1868-1877 (2010).
143. G. D. Finlayson and P. M. Morovic, *Metamer crossovers of infinite metamer sets*, Eighth Color Imaging Conference: Color Science and

Engineering Systems, Technologies, Applications (Soc Imaging Science & Technology, Springfield, 2000), pp. 13-17.

144. W. S. Stiles and G. Wyszecki, "Intersections of the Spectral Reflectance Curves of Metameric Object Colors," J. Opt. Soc. Am. **58**, 32-38 (1968).

145. Y. Mizokami and M. Webster, "Are Gaussian spectra a viable perceptual assumption in color appearance?," J. Vision **10**, 399 (2010).

146. S. Westland and C. Ripamonti, "Invariant cone-excitation ratios may predict transparency," J. Opt. Soc. Am. A **17**, 255-264 (2000).

147. S. M. C. Nascimento, F. P. Ferreira, and D. H. Foster, "Statistics of spatial cone-excitation ratios in natural scenes," J. Opt. Soc. Am. A - Opt. Image Sci. Vis. **19**, 1484-1490 (2002).

148. D. H. Foster, K. Amano, S. M. C. Nascimento, and M. J. Foster, "Frequency of metamerism in natural scenes," J. Opt. Soc. Am. A - Opt. Image Sci. Vis. **23**, 2359-2372 (2006).

149. CIE, "A colour appearance model for colour management systems: CIECAM02," CIE Publication 159:2004 (CIE Central Bureau, Vienna, 2004).

150. CIE, "Colorimetry, 3rd Edition," CIE Publication 15:2004 (CIE Central Bureau, Vienna, 2004).

151. P.-L. Sun and J. Morovic, "Inter-relating colour difference metrics," in *Tenth Color Imaging Conference: Color Science and Engineering Systems, Technologies, Applications*, (Society for Imaging Science and Technology, 2002), 55-60.

152. S. M. C. Nascimento, D. H. Foster, and K. Amano, "Psychophysical estimates of the number of spectral-reflectance basis functions needed to reproduce natural scenes," J. Opt. Soc. Am. A - Opt. Image Sci. Vis. **22**, 1017-1022 (2005).

153. I. Marín-Franch and D. H. Foster, "Number of perceptually distinct surface colors in natural scenes," J Vision **10(9):9**, 1-7 (2010).

154. M. Melgosa, R. Huertas, and R. S. Berns, "Performance of recent advanced color-difference formulas using the standardized residual sum of squares index," J. Opt. Soc. Am. A - Opt. Image Sci. Vis. **25**, 1828-1834 (2008).

155. B. Efron and R. J. Tibshirani, *An Introduction to the Bootstrap* (Chapman & Hall/, 1994).

156. D. H. Foster and G. Feng, "Visual and Material Identity in Natural Scenes: Predicting How Often Indistinguishable Surfaces Become Distinguishable," in *Predicting Perceptions: Proceedings of the 3rd International Conference on Appearance* (Lulu Press, 2012), 79-81.

157. A. Chakrabarti and T. Zickler, "Statistics of real-world hyperspectral images," in *Computer Vision and Pattern Recognition (CVPR), 2011 IEEE Conference on*, 2011), 193-200.